Tunable Band Pass Filters for Communication Systems

by

Gowrish Basavarajappa

A thesis
presented to the University of Waterloo
in fulfillment of the
thesis requirement for the degree of
Doctor of Philosophy
in
Electrical and Computer Engineering

Waterloo, Ontario, Canada, 2021

Examining Committee Membership

The following served on the Examining Committee for this thesis. The decision of the Examining Committee is by majority vote.

External Examiner	Hjalti H. Sigmarsson Associate Professor, School of Electrical and Computer Engineering, University of Oklahoma
Supervisor	Raafat R. Mansour Professor, Department of Electrical and Computer Engineering, University of Waterloo
Internal Member	Safieddin Safavi-Naeini Professor, Department of Electrical and Computer Engineering, University of Waterloo
Internal Member	Slim Boumaiza Professor, Department of Electrical and Computer Engineering, University of Waterloo
Internal-external Member	Carolyn Ren Professor, Department of Mechanical and Mechatronics Engineering, University of Waterloo

AUTHOR'S DECLARATION

I hereby declare that I am the sole author of this thesis. This is a true copy of the thesis, including any required final revisions, as accepted by my examiners.

I understand that my thesis may be made electronically available to the public.

Abstract

The ever-increasing demand for high communication data rate and high-quality multi-media services; over past few decades, has ignited new avenues in radio architectures. Frequency reconfigurable (or frequency agile) communication systems are among the key architectures for efficient and cost-effective utilization of the allotted frequency spectrum. The emerging concept of on-orbit flexible payload (or programmable payload) in satellite communication is another encouraging development on the horizon. In-addition, tunability in filters used for remote radio unit (RRU) is highly preferred by network operators owing to the high cost of installing RRU both in low density remotely accessed locations and in high density expensive urban locations. Such frequency reconfigurable radio architectures typically demand reconfigurability (tunability) of components within the physical layer as well. Hence, tunable filters play a vital role in realization of frequency reconfigurable communication systems.

In general, any fixed frequency filter can be transformed into a tunable filter by introducing tuning elements dedicated to tuning the resonators and the coupling structures. Thus, a tunable filter of order *N* would require *2N+1* tuning elements to maintain a constant absolute bandwidth (BW) over the tuning range. This use of large number of tuning elements not only increases size and cost, but also adds to the complexity of the tuning control mechanism, particularly when configured in a closed loop system. Over the past decade, a significant research has been carried out to reduce the number of tuning elements by roughly 50% (i.e. with only *N* tuning elements). The coupling structures are suitably designed to maintain their performance over the tuning range, eliminating *N+1*, while only *N* tuning elements are used for tuning the *N* resonators. The goal here is to further reduce the number of tuning elements to a 'single tuning element'.

The thesis presents several novel configurations for a high-Q tunable band pass filter employing a single tuning element, while maintaining a constant BW, return loss performance and location of the transmission zeros over a wide tuning range. Advanced filter synthesis techniques for both tunable filter and fixed filters are also proposed.

A tunable double-septa waveguide (WG) filter is presented employing a single tuning element. The theory of coupling behavior of single septum and double septa to achieve constant absolute BW is explored. The tuning mechanism of the proposed filter is explained with measurement results presented for a Ku-band tunable WG filter designed at 15 GHz with a 2% fractional BW to achieve 15% tuning

range. BW variation is observed to be within ±5% while the center frequency is tuned from 14.65 to 17.15 GHz. The filter promises to be useful in emerging 5G millimeter-wave applications, where the filter size is very small to accommodate multiple mechanical tuning elements. Furthermore, the proposed design methodology is scalable, i.e., the tuning mechanism is independent of the filter order.

A frequency reconfigurable dual-mode WG filter having an elliptic response is presented. The proposed filter maintains a constant absolute BW and a constant rejection BW (i.e. constant frequency spacing between transmission zeros) over the tuning range. Furthermore, the filter can be tuned using a single tuning mechanism. A 4^{th} order prototype filter at 11.5 GHz with 50 MHz bandwidth and 2 symmetric transmission zeros (± 45 MHz) is fabricated and measured.

A novel configuration of a BW reconfigurable WG filter that uses only two tuning elements irrespective of the filter order is proposed. The proposed filter configuration demonstrates that it can achieve a relatively wide BW variations without deviating the center frequency. A 4 pole prototype filter is designed, fabricated and tested at Ku-band. The measured BW tunability of the filter is nearly 35 % from 225 to 320 MHz at 13.375 GHz. To the author's knowledge, this is the only BW reconfigurable filter that can be tuned with only two tuning elements regardless of the filter order.

The thesis also demonstrates the feasibility of realizing a high-Q λ/2 resonator based tunable coaxial filter, which is tuned by a single rotational tuning element irrespective of the filter order. The proposed filter has low variations in the absolute BW and insertion loss (IL) over a relatively wide tuning range. A prototype four-pole filter is developed at 2.5 GHz with a fractional BW of 4% to verify the concept. The measured tuning range of the filter is 20%, within which the BW variation is better than ±10% and IL variation is better than 0.05 dB. The proposed concept is easily expandable to filters with higher order. Furthermore, the concept is adopted to design a tunable diplexer using only a single tuning mechanism while maintaining the frequency performance of each channel and the frequency spacing between the two channels over the tuning range. The proposed high-Q tunable filter is promising for use in the frequency-agile communication architecture at the cellular base-station and aerospace applications.

A novel configuration of a High-Q coaxial tunable filter which employs a single rotational mechanism to tune the filter, while using fixed λ/4 resonators is also presented. The rotational tuning concept is different from that proposed for the tunable coaxial λ/2 resonators. A prototype filter is designed for the proof of concept, which has a tuning range of 11.6% from 685 MHz to 770 MHz, over which bandwidth variation is within 10.5±0.7 MHz.. In-addition, the proposed design methodology can

be scaled to realize higher order filters. The proposed filter promises to be useful in a wide range of telecommunication applications including flexible payload in aerospace applications.

Acknowledgements

First and foremost, I am grateful and thankful to my supervisor, Professor Raafat Mansour without whose fatherly professional and personal guidance this would not have been possible. I learnt many life lessons in-addition to technical and professional expertise from him.

My deepest gratitude goes to all the members of my family, for the wonderful support they all provided; specially, my mother, Sukanya C. M., my father, Basavarajappa C., for their endless love and support.

I like to thank my committee members, Professor Safieddin Safavi-Naeini, Professor Slim Boumaiza and Professor Carolyn Ren for their support and guidance throughout the duration of the Ph.D. programme.

My sincere thanks to my external examiner, Professor Hjalti H. Sigmarsson for reading my thesis and providing valuable feedback.

I would also like to thank all my friends in CIRFE laboratory at the University of Waterloo and all those who contributed to my learning experience. I like to specially thank Dr. Tejinder Singh, Navjot Khaira, Hassan Kianmehr, Dr. Junwen Jiang, Huayong Jia, Farzad Yazdani, Arash Fouladi Azarnaminy and Dr. Luis Enrique Gutierrez for all their help during my years of graduate studies.

I like to thank the entire staff at Electrical and Computer Engineering for their continuous support and encouragement during my years of graduate studies.

Finally, my thanks go to all my dear friends and relatives who have enriched my life, and who helped me overcome the difficult times and made this journey enjoyable.

Dedication

To my parents, who gave me life and nurtured it;

To my supervisor and teachers, who gave me knowledge and nurtured it;

To my friends and relatives, who gave me their time and nurtured it;

To God Almighty, who sent such wonderful people into my life . . .

Table of Contents

AUTHOR'S DECLARATION iii
Abstract iv
Acknowledgements vii
Dedication viii
List of Figures xi
List of Tables xiv
Chapter 1 Introduction 1
1.1 Motivation 1
1.2 Research Objectives 4
1.3 Thesis Outline 4
Chapter 2 Literature Survey 5
2.1 Tunable BPF with constant absolute BW 5
2.2 Tunable BPF with single tuning element 9
Chapter 3 Filter Design Methodology 13
3.1 Introduction 13
3.2 Coupled Resonator 13
3.3 Fictitious IO Coupling 16
3.4 Conclusion 24
Chapter 4 Tunable Waveguide Filters 25
4.1 Introduction 25
4.2 Frequency Reconfigurable Single Mode Filter 26
4.3 Bandwidth Reconfigurable Filter 36
4.4 Frequency Reconfigurable Dual Mode Filter 42
4.5 Conclusion 48
Chapter 5 Tunable Coaxial Filters 50
5.1 Introduction 50
5.2 Frequency Reconfigurable λ/2 Resonator Filter 50
5.3 Frequency Reconfigurable λ/4 Resonator Filter 61
5.4 Conclusion 70
Chapter 6 Conclusion and Future Work 71
6.1 Conclusion 71

6.2 Future Work 72
Bibliography 73
Appendix A Publications 78

List of Figures

Fig. 1.1: Spacecraft SES-12 and SES-14 from Airbus which employ electric propulsion, 2018 1

Fig. 1.2: Robotic refueling mission from NASA and Orbit Fab, 2019 2

Fig. 1.3: Front End Receiver Architecture 3

Fig. 1.4: Front End Transmitter Architecture 3

Fig. 2.1: High-Q Tunable Coaxial BPF [9], [12], 2014 6

Fig. 2.2: High-Q Tunable Coaxial BPF [9], [13], 2014 6

Fig. 2.3: High-Q Tunable Cavity BPF [14], 2014 7

Fig. 2.4: High-Q Tunable Cavity BPF [15], 2018 8

Fig. 2.5: High-Q Tunable Cavity BPF [16], 2019 8

Fig. 2.6: High-Q Tunable Dielectric Resonator BPF [17], 2007 9

Fig. 2.7: High-Q Tunable Cavity BPF [22], 1989 10

Fig. 2.8: High-Q Tun. Cav. BPF with Dielectric Perturber [23], 2017 10

Fig. 2.9: High-Q Tun. WG BPF with 3D Printed Ribbon [24], 2018 11

Fig. 2.10: High-Q Tunable Coaxial Filter [25], 2008 11

Fig. 3.1: Four Step Filter Design Procedure 14

Fig. 3.2: Major Modules in Filter Synthesis 15

Fig. 3.3: N^{th} order filter configuration with cross couplings is divided into N/2 sections 17

Fig. 3.4: Section equivalence requires IR - IO coupling equivalence 17

Fig. 3.5: 6^{th} order filter with 4 TZ 17

Fig. 3.6: IR and IO couplings of the inductive iris coupling structure 18

Fig. 3.7: IR-IO coupling equivalence chart 18

Fig. 3.8: Design of section 1: IR-IO coupling transformation 19

Fig. 3.9: Design of section 1: 3D EM design 19

Fig. 3.10: Design of section 2 : IR-IO coupling transformation 20

Fig. 3.11: Design of section 2 : 3D EM design 20

Fig. 3.12: Design of section 3 : No coupling transformation required 21

Fig. 3.13: Design of section 3 : 3D EM design 21

Fig. 3.14: Synthesized 6^{th} order WG filter with 4 TZ 22

Fig. 3.15: Synthesis of 6^{th} order WG filter with 4 TZ 22

Fig. 3.16: 9^{th} order trisection filter with 3 asymmetric TZ 23

Fig. 3.17: Synthesis of 9^{th} order filter with 3 asymmetric TZ 24

Fig. 4.1: Assembly View of the Proposed Tunable WG Filter 28
Fig. 4.2: 3D Schematic of the Proposed Tunable WG Filter 28
Fig. 4.3: Single and Double Septa Coupling 29
Fig. 4.4: IR Coupling using Double Septa 30
Fig. 4.5: IR Coupling with Constant $k_{ij}*f_r$ product 30
Fig. 4.6: IO Coupling with Constant Peak Group Delay w.r.t f_r 31
Fig. 4.7: Movable Metal Insert (a) without pattern, (b) with pattern 32
Fig. 4.8: Resonator Loading : Metal Septum and Iris Coupled Resonators 32
Fig. 4.9: EM Simulated Response : S_{11} and S_{21} 33
Fig. 4.10: EM Simulated Response : BW and IL Variation 33
Fig. 4.11: Fabricated Prototype Unit 34
Fig. 4.12: Measured Filter Response: S_{11} and S_{21} 35
Fig. 4.13: Measured BW and IL Variation over the Tuning Range 35
Fig. 4.14(a): Measured Spurious Response of the Tunable Filter at 15.6 GHz 35
Fig. 4.14(b): Measured Group Delay of the Tunable Filter at 15.6 GHz 36
Fig. 4.15: Schematic of the proposed High-Q BW reconfigurable WG filter 37
Fig. 4.16: Impact of septum position on the coupling value 38
Fig. 4.17: Resonator Loading: Impact of coupling structure on the res. frequency 38
Fig. 4.18: Simulated S_{11} and S_{21} 39
Fig. 4.19: Photograph of the prototype filter 40
Fig. 4.20: Measured results: S_{11} and S_{21} 41
Fig. 4.21(a): Measured results: spurious response 41
Fig. 4.21(b): Measured results: group delay response 41
Fig. 4.22: Schematic: Proposed frequency reconfigurable waveguide filter with elliptic response 43
Fig. 4.23: Schematic: Internal dimensions and coupling configuration 44
Fig. 4.24: Simulated transmission co-efficient 45
Fig. 4.25: Simulated reflection co-efficient 45
Fig. 4.26: Simulated absolute BW and rejection BW 45
Fig. 4.27: Photograph of prototype filter - fabricated parts and assembled filter 46
Fig. 4.28: Measured transmission co-efficient 46
Fig. 4.29: Measured reflection co-efficient 47
Fig. 4.30: Measured absolute BW and rejection BW 47

Fig. 4.31: Measured spurious performance 47
Fig. 5.1: Coaxial Resonator (λ/2 Resonator) 51
Fig. 5.2: Proposed λ/2 Resonator 51
Fig. 5.3: IR coupling with Elliptic Iris 52
Fig. 5.4: IO Coupling with Shaped Probe 53
Fig. 5.5: Resonator Loading: Generic Polygon and Fixed Screw 54
Fig. 5.6: Tunable Coaxial Filter Prototype 55
Fig. 5.7: Resonator Loading 55
Fig. 5.8: EM Simulated Response 56
Fig. 5.9: Simulated BW and IL over the Tuning Range 56
Fig. 5.10: Fabricated Prototype 57
Fig. 5.11: Measurement Setup 58
Fig. 5.12: Measured Response: (a) S_{21} (b) S_{11} 58
Fig. 5.13: Measured results (a) BW and IL (b) Spurious Performance 59
Fig. 5.14: Enhancing Return Loss 60
Fig. 5.15: 3-D model of a tunable diplexer using dedicated filters at each frequency band 60
Fig. 5.16: Simulated results of the tunable diplexer: tuning rod is at 25 degrees. 60
Fig. 5.17: Simulated results of the tunable diplexer: tuning rod is at 75 degrees. 63
Fig. 5.18: Schematic: Proposed Coaxial Tunable Filter (λ/4 Resonator) 64
Fig. 5.19: Schematic: Front View of the Proposed Coaxial Tunable Filter 64
Fig. 5.20: Resonant Frequency and Unloaded Quality Factor 65
Fig. 5.21: Inter-Resonator Couplings over the Tuning Range 65
Fig. 5.22: Input-Output Couplings over the Tuning Range 66
Fig. 5.23: Simulation: Transmission Co-efficient 66
Fig. 5.24: Simulation: Reflection Co-efficient 67
Fig. 5.25: Simulation: Bandwidth and Insertion Loss 67
Fig. 5.26: Fabrication - Photograph of the Tunable Filter 68
Fig. 5.27: Measurement - Transmission Co-efficient 68
Fig. 5.28: Measurement - Reflection Co-efficient 69
Fig. 5.29: Measurement - Bandwidth and Insertion Loss 69

List of Tables

Table 1.1: High Level Features of a Tunable BPF 4
Table 2.1: Summary of Literature Survey: High-Q Tunable Filters 12
Table 3.1: Comparison of WG filter synthesis techniques 23
Table 4.1: Comparison of Proposed Tunable WG BPF with Existing WG Solutions 36
Table 4.2: Comparison of BW Reconfigurable High-Q Filters 42
Table 5.1: Comparison of Proposed Tunable Coaxial BPF with Existing Coaxial Solutions 60
Table 5.2: Comparison of High-Q Tunable Coaxial Filters 69

Chapter 1
Introduction

1.1 Motivation

The ever-increasing demand for high communication data rate and high-quality multi-media services; over past few decades, has ignited new avenues in radio architectures. Frequency reconfigurable (or frequency agile) communication systems are among the key architectures for efficient and cost-effective utilization of the allotted frequency spectrum [1]-[2]. The emerging concept of on-orbit flexible payload (or programmable payload) in satellite communication is another such encouraging development on the horizon [3]-[5]. Typically, a communication satellite has a lifespan of 15 years which is largely due to the exhaustion of satellite fuel (liquid propellants used for on-orbit drift corrections). There have been significant developments in recent past to enhance the lifespan of a communication satellite using innovative mechanisms like on-orbit satellite refueling, electric propulsion systems [6]-[8]. For example, Fig. 1.1 depicts the spacecraft missions SES-12 and SES-14 from Airbus, which employ electric propulsion systems for orbit raising, successfully launched in 2018 [8]. Fig. 1.2 depicts the demonstration of robotic refueling mission from NASA and Orbit Fab in International Space Station in 2019 [6].

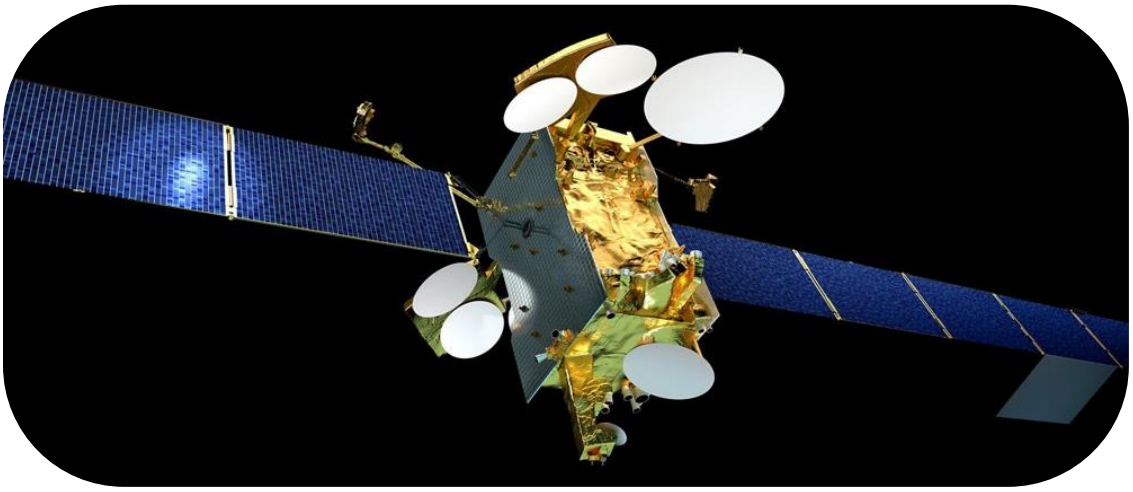

Fig. 1.1: Spacecraft missions SES-12 and SES-14 from Airbus employing electric propulsion, 2018

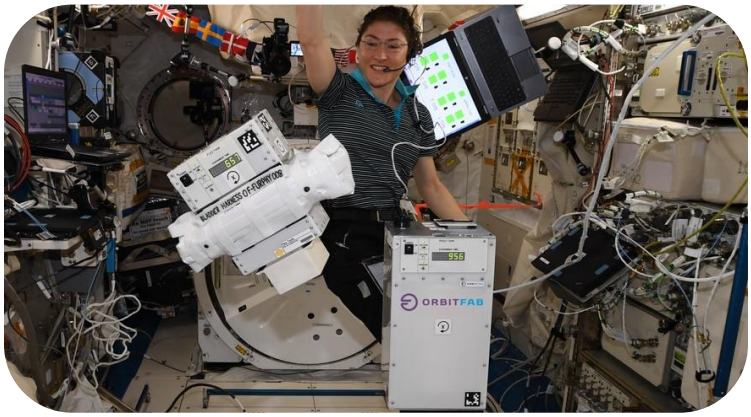

Fig. 1.2: Robotic refueling mission from NASA and Orbit Fab, 2019

Hence, a communication satellite with longer lifespan inevitably demands a flexible payload to satisfy the requirements of a rapidly transforming scenario of communication requirements and standards. A flexible payload incorporates the feature of re-configurability in both radiation coverage as well as frequency allocation [4]. Tunable filters offer the flexibility in terms of frequency selection and bandwidth allocations to the transponders. Hence, a tunable filter is a vital component in flexible payload of emerging satellite communication architecture.

In-addition to reconfigurable systems, tunable filter technologies also add value in wireless systems that usually use identical filters with the exception of center frequency by reducing the production cost and delivery schedule. The production cost can be significantly reduced by fabricating identical filter units ahead of time that can be easily reconfigured during the final production phase to fit the required frequency plan, thus offering a competitive delivery schedule. Furthermore, tunability in filters used for remote radio unit (RRU) is highly preferred by network operators owing to expensive affair of installing RRU both in low density remotely accessed locations and in high density expensive urban locations.

In a typical wireless radio architecture tunable BPFs have been proposed in front-end receivers to suppress image and other interfering signals as depicted in Fig. 1.3. BPF-1 shown in the block diagram is expected to be tunable in a reconfigurable architecture. Tunable filters have been proposed in transmitter architecture as well for high power applications as depicted in Fig. 1.4. Typically, LO and BPF are the narrow band components in radio architecture and a reconfigurable system predominantly depends on the tunability of these two components. Reconfigurable phase locked loop based LO can be tuned over a wide range of frequencies. Hence, high performance tunable BPF is one of the important requirements in successful realization of reconfigurable communication systems.

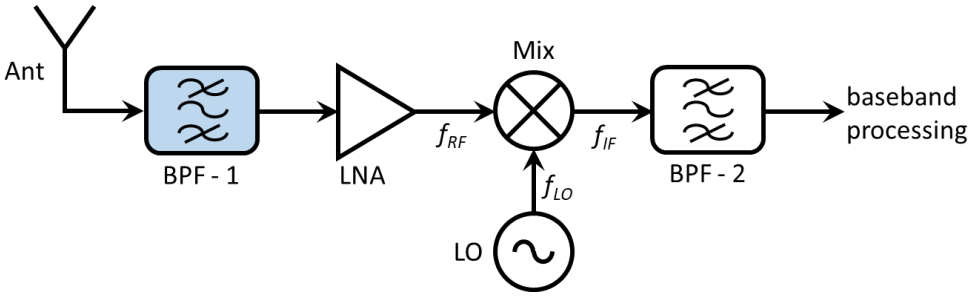

Fig. 1.3: Front End Receiver Architecture (BPF – band pass filter, LNA – low noise amplifier, LO – local oscillator, Mix – mixer, Ant – antenna)

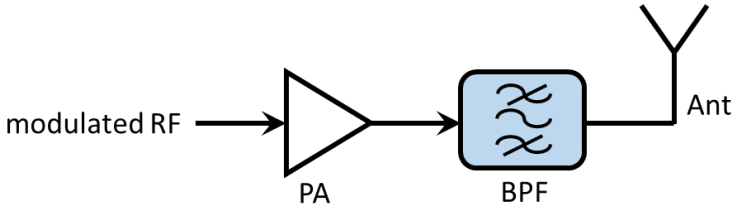

Fig. 1.4: Front End Transmitter Architecture (PA – power amplifier)

High performance tunable BPF plays a vital role in a frequency reconfigurable communication system. One of the important requirements for such tunable filters in most applications is to maintain constant absolute BW over the tuning range. The data rate is BW dependent thus maintaining the same date rate over the tuning range requires maintaining the same BW. In addition, most of communication system applications require maintaining certain isolation requirements at fixed frequency offsets, which cannot be satisfied if the BW is changed. Thus, by maintaining a constant absolute BW over the tuning range, the achievable data rate and the filter isolation requirements remain the same over the entire tuning range, which is highly desirable.

Typically, such radio architectures require high-Q (Quality factor) tunable filters with a constant absolute bandwidth (BW) over the tuning range. Filters for space applications are required to have BW reconfigurability as well. As is well known, any filter of order *N* can be readily reconfigured by using *2N +1* independent tuning elements. This significantly increases size and cost, and also adds to the complexity of the tuning control mechanism. Hence, in order to reduce the cost and for enhanced reliability, it is desirable to reduce the number of tuning elements to minimum possible without compromising the performance. Table 1.1 summarizes the high-level desirable features of a tunable BPF used in front end architecture.

Table 1.1: High Level Features of a High Performance Tunable BPF

Feature	Requirement
Insertion Loss / Quality Factor	Low / High
Tunability	Centre Frequency and / or Bandwidth
Tuning Range	Large (> 10 %)
Number of Tuning Elements	Minimum Possible

1.2 Research Objective

The overall objective of this research is to develop frequency reconfigurable filters that employ a minimum number of tuning elements (ideally one), while maintaining an absolute constant bandwidth, the return loss performance and spacing between transmission zeros, over relatively wide tuning range (at least 10%). Majority of today's wireless and satellite applications employ 3D high-Q filters, therefore the focus of the research is also on developing 3D tunable filters with a minimum degradation of insertion loss over the tuning range. It is worth mentioning here that a considerable amount of research has been carried on planar microstrip tunable filters, however the work on 3D tunable filters is very limited.

1.3 Thesis Outline

The motivation and objectives of the thesis are described in Chapter 1. Chapter 2 presents the existing solutions for tunable filters under literature survey and identifies the research opportunities. Chapter 3 presents the design methodology adopted in designing waveguide and coaxial filter. It also presents a novel design methodology developed during the research which is applicable for designing waveguide filters with transmission zeros. Chapter 4 describes the research activities of the proposed tunable filter solutions in waveguide technology for reconfigurable communication system that are tunable in both center frequency and bandwidth. Chapter 5 describes the research activities of the proposed tunable filter solutions in coaxial technology for reconfigurable communication system. Chapter 6 describes a novel configuration of non-magnetic isolator and circulator using BPF. Chapter 7 concludes the thesis by summarizing the results achieved, followed by proposals for future research.

Chapter 2
Literature Survey

Typically, high-Q filters are tuned mechanically to achieve minimum insertion loss (IL) over the tuning range. In such filters, it is highly desirable to realize filter tuning with minimum number of tuning elements (or mechanisms). This not only reduces the complexity of control system, cost and size of the filter but is a highly desirable feature in millimeter wave applications where the filter size is in itself too small to accommodate multiple mechanical tuning elements. Hence, the two key requirements of High-Q tunable filters are; maintaining constant absolute BW and keep the number of tuning elements to a minimum.

2.1 Tunable BPF with constant absolute BW

In general, any filter of order '*N*' can be readily tuned for constant absolute BW using '*2N + 1*' independent tuning elements. Over the past years, significant research has resulted in reducing the number of tuning elements [9], [10] to 50% by using tuning elements only for *N*-resonators. One of such recent inventions reported as in [9], [11] and [12] (shown in Fig. 2.1) is a tunable coaxial BPF, which achieves High-Q and constant absolute BW over the tuning range. This structure utilizes mechanism to change the gap between resonator post and tuning disk, thus changing the frequency response of the filter. The technique is used to realize tunable filters at 2 GHz with a tuning range of 400 MHz and at 5 GHz with a tuning range of 1 GHz. A tunable coaxial filter with constant Q and absolute BW over the tuning range with innovative angular tuning technique is also reported in [9] and [13] (shown in Fig. 2.2). The filter has a tuning range of 430 MHz centered at 3.6 GHz.

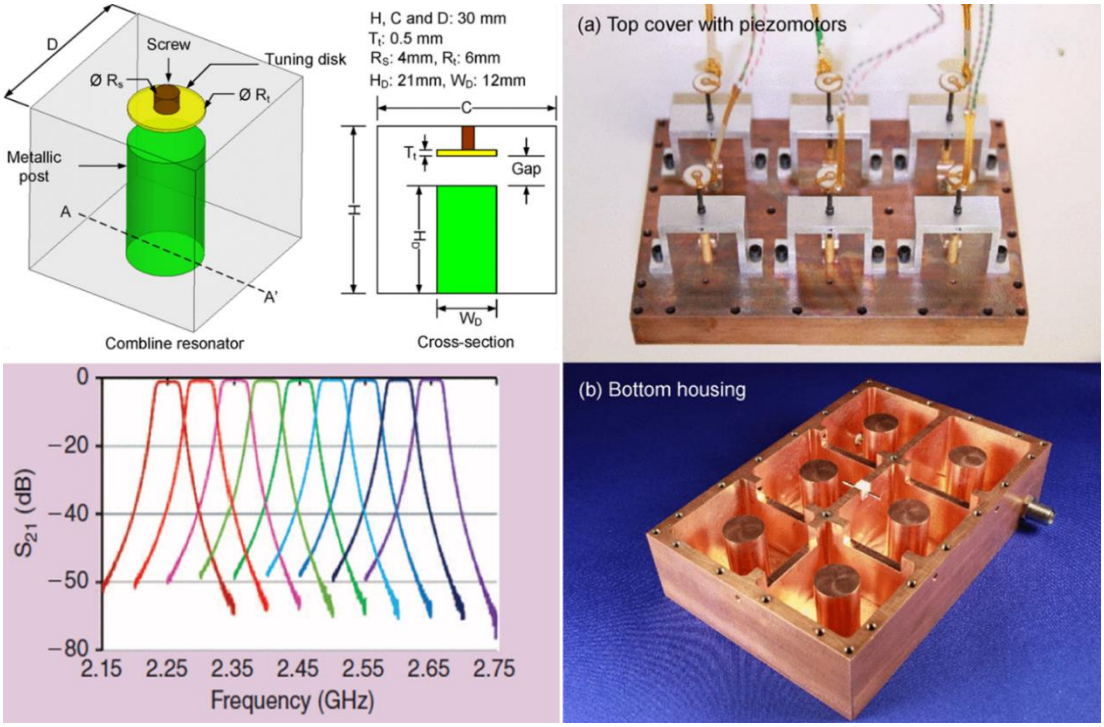

Fig. 2.1: High-Q Tunable Coaxial BPF [9], [12], 2014

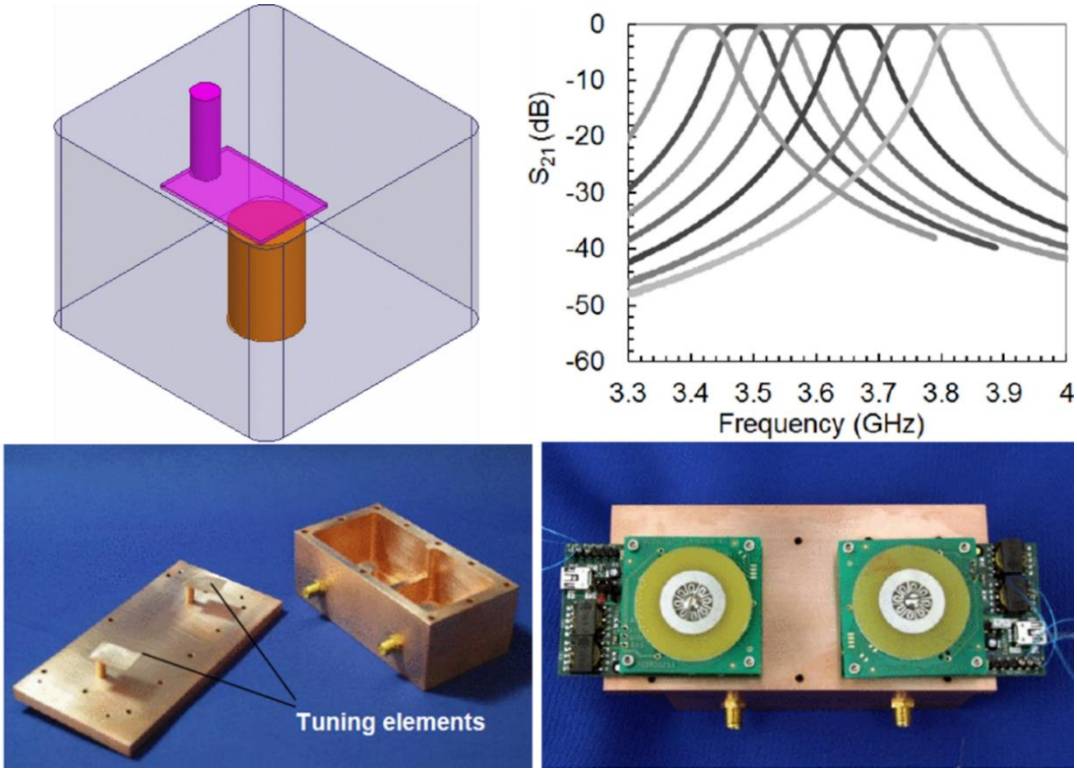

Fig. 2.2: High-Q Tunable Coaxial BPF [9], [13], 2014

A tunable BPF using circular waveguide (WG) cavity resonators at K-band with 200 MHz tuning range is demonstrated for aerospace applications [14] (shown in Fig. 2.3). Resonant frequency is tuned by moving one of the side walls of the cavity. A tunable cavity filter with rotating dielectric plates has been recently demonstrated at K–band [15] (shown in Fig. 2.4). A dielectric plate is inserted in each resonator, and it's rotation leads to the frequency tuning. The filter is demonstrated at 19.5 GHz with a tuning range of 300 MHz and it maintains a constant absolute BW over the tuning range. A tunable cavity filter using contactless tuning plunger is demonstrated at K-band [16] (shown in Fig. 2.5). The filter maintains a constant absolute BW when tuned from 19 GHz to 19.5 GHz. High-Q tunable dielectric resonator filter using MEMS actuation has been demonstrated at Ku-band [17]-[18] (shown in Fig. 2.6). The filter has a tuning range of 400 MHz at 15.6 GHz and maintains a constant absolute BW over the tuning range. On similar lines, MEMS based tunable filters have been developed at C and Ka-band as well [19]-[21].

While these filter designs ([9]-[21]) are able to realize a constant absolute BW over a reasonably wide tuning range, these filters however require the use of a number of independent tuning elements that is equal to the number of resonators. In other words, the number of independent tuning elements is equal to the filter order. This increases the size and cost, and also adds to the complexity of tuning control mechanism. In order to circumvent these issues and to enhance design reliability through minimization of parts count, it is desirable to reduce the number of tuning elements to minimum possible without compromising the performance; High-Q, constant absolute BW and tuning range.

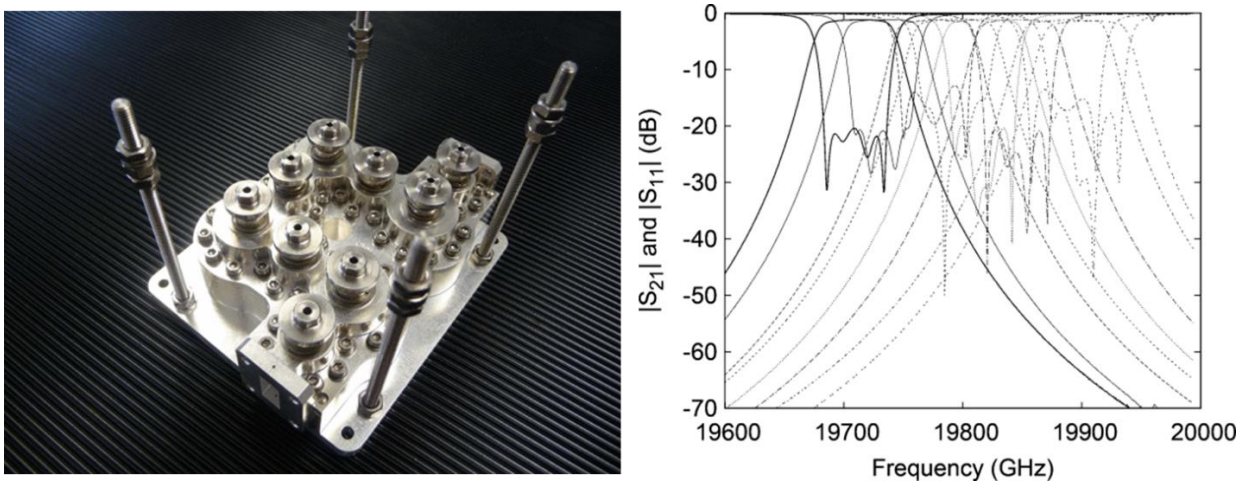

Fig. 2.3: High-Q Tunable Cavity BPF [14], 2014

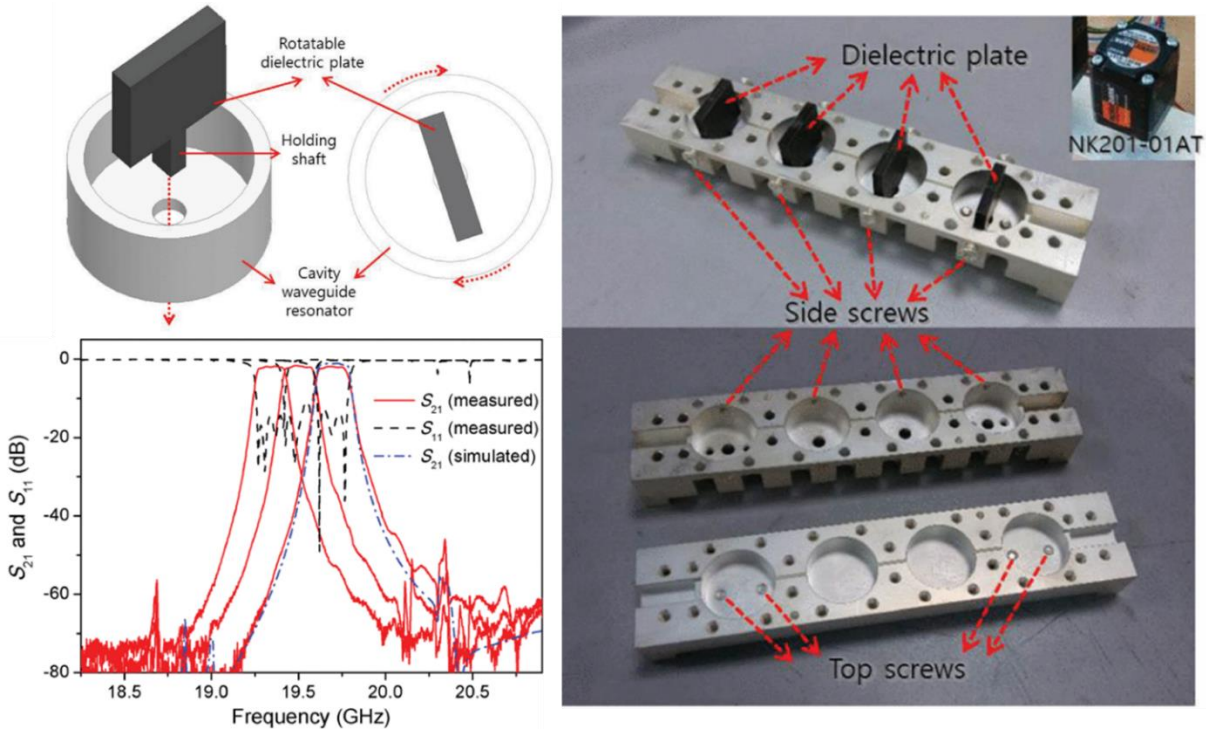

Fig. 2.4: High-Q Tunable Cavity BPF [15], 2018

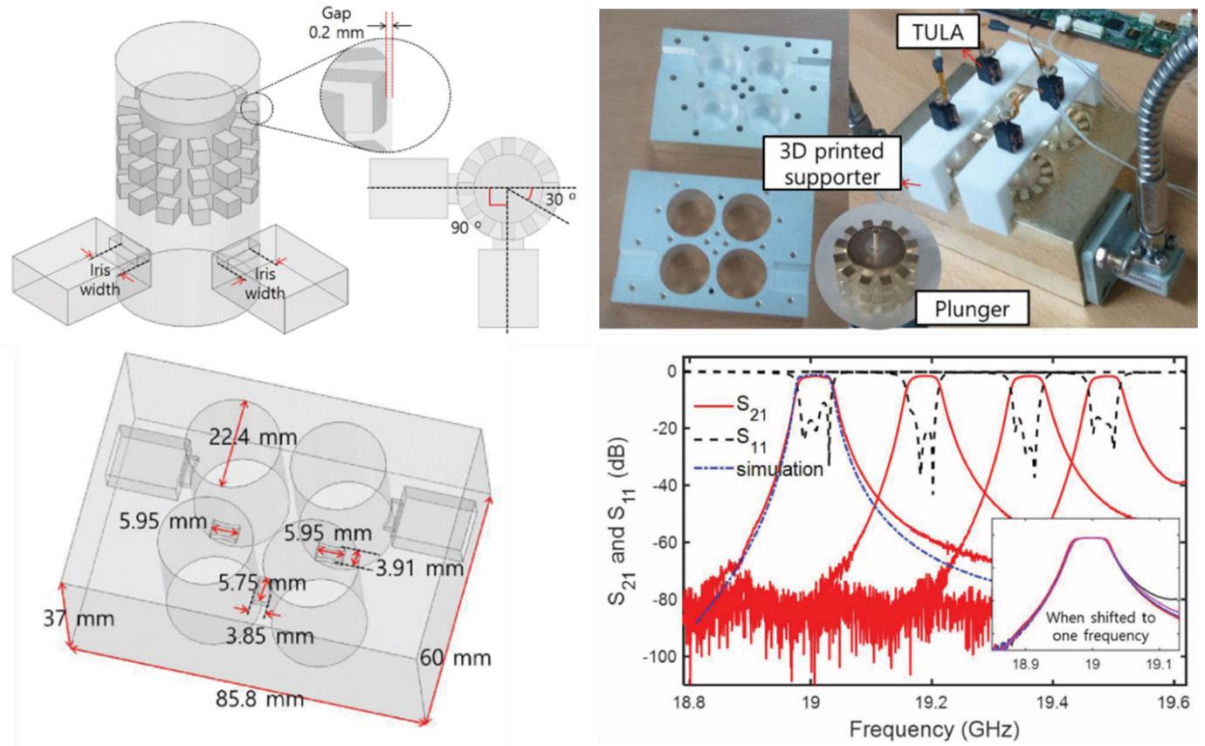

Fig. 2.5: High-Q Tunable Cavity BPF [16], 2019

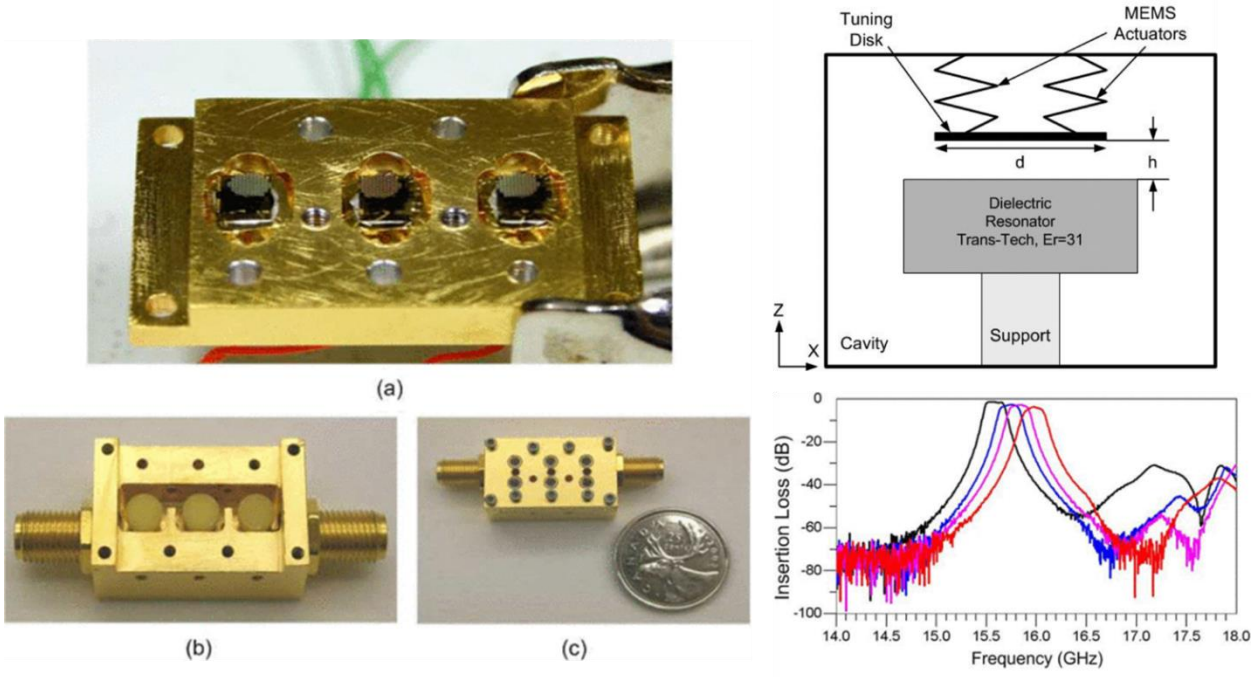

Fig. 2.6: High-Q Tunable Dielectric Resonator BPF [17], 2007

2.2 Tunable BPF with single tuning element

One of the early developments in this regard is a 4-pole tunable WG cavity filter at X-band [22] (shown in Fig. 2.7). The filter tuning is achieved by linearly moving one of the end plates of each cavity by means of a common stepper motor. However, the tuning range achieved is quite low around 200 MHz at 12 GHz. Furthermore, the filter does not maintain constant absolute BW over the tuning range. A 3rd order tunable WG cavity filter presented in [23] (shown in Fig. 2.8) aims to achieve a wider tuning range of around 2.2 GHz at 11 GHz. The filter utilizes dielectric perturber within each resonating cavity, which on rotation tunes the cavity filter while maintaining constant absolute BW over the tuning range. Though the filter utilizes a system of rack to mechanically couple the rotation of all dielectric perturbers, however such a tuning mechanism becomes quite complicated for practical applications as the filter order increases. Furthermore, the filter suffers from significant Q reduction due to dielectric perturbers. Reference [24] proposes an X-band WG cavity filter (shown in Fig. 2.9) which is tuned by rotating a spiral ribbon. The filter achieves a tuning range of 700 MHz at 12 GHz with constant absolute BW within the tuning range. However, the proposed structure involves complicated tuning mechanism and suffers from degraded Q as a result of involved tuning mechanism. To serve applications at lower end of the spectrum, a tunable coaxial filter is proposed in reference [25] (shown in Fig. 2.10) which has a

tuning range of 360 MHz at 2GHz. Though the filter is claimed to be tuned using a single tuning mechanism, however, the filter utilizes (2N-1) spring supported tuning elements. The filter is tuned by using a metallic plate with properly designed ramps for each of the tuning elements. During the operation, each tuning element is pushed by its corresponding ramp. Due to the physical contact between the tuning elements and the ramps, the filter is exposed to wear and tear effects and undesired lateral stress between tuning elements and the ramp.

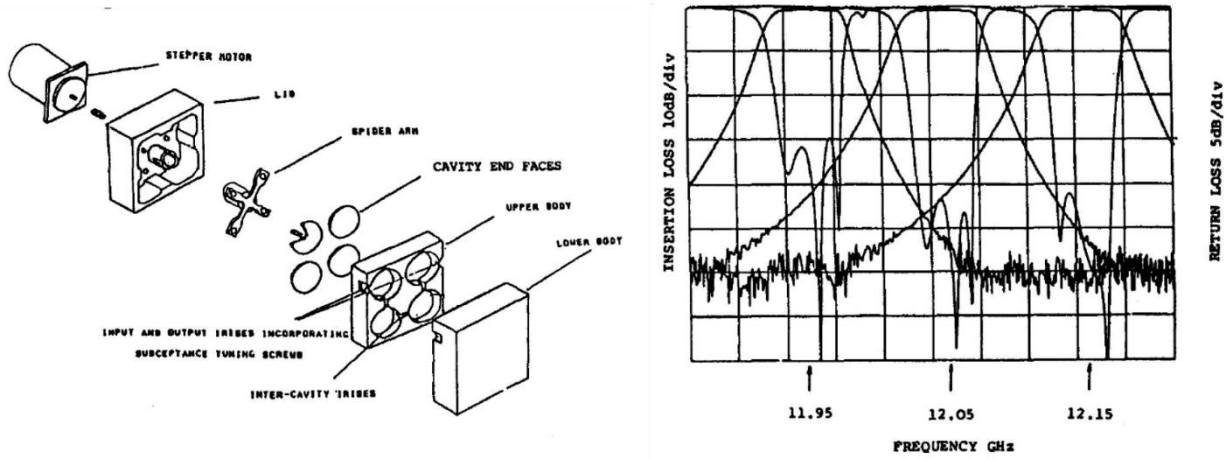

Fig. 2.7 High-Q Tunable Cavity BPF [22], 1989

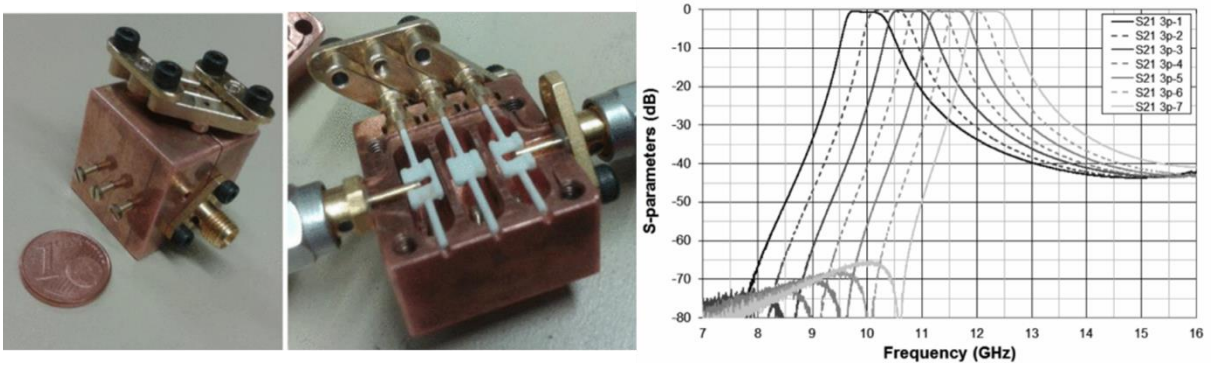

Fig. 2.8 High-Q Tunable Cavity Filter with Dielectric Perturber [23], 2017

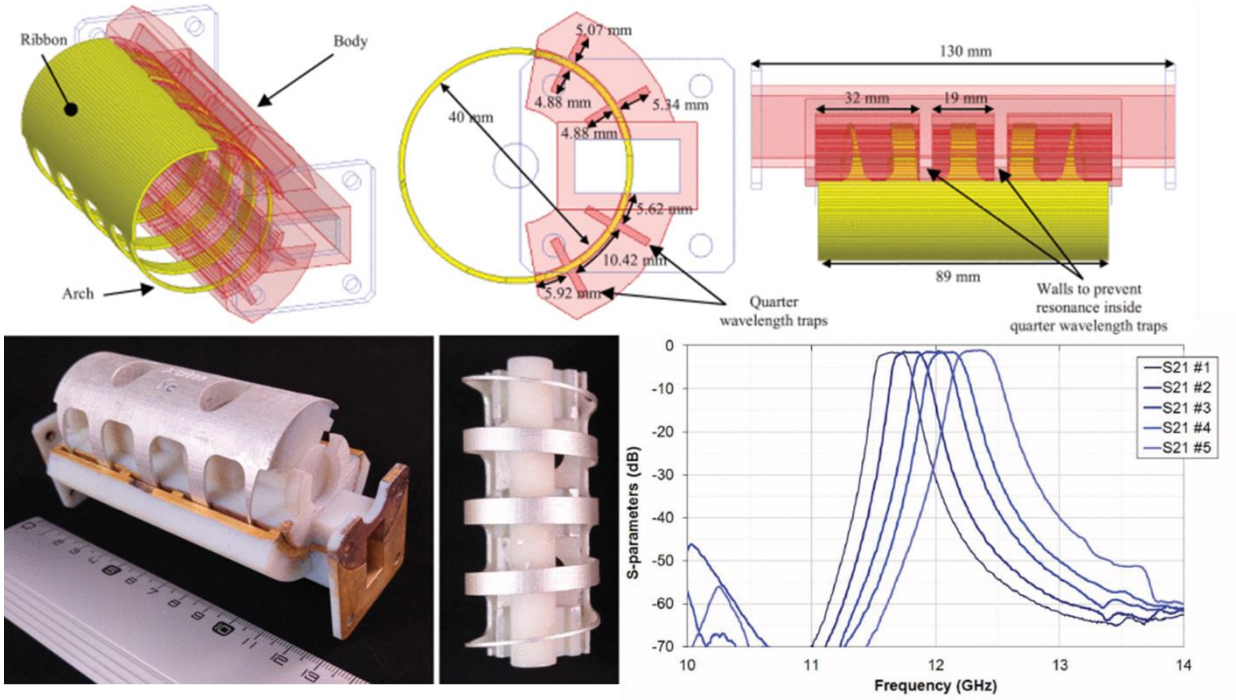

Fig. 2.9 High-Q Tunable WG Filter with 3D Printed Ribbon [24], 2018

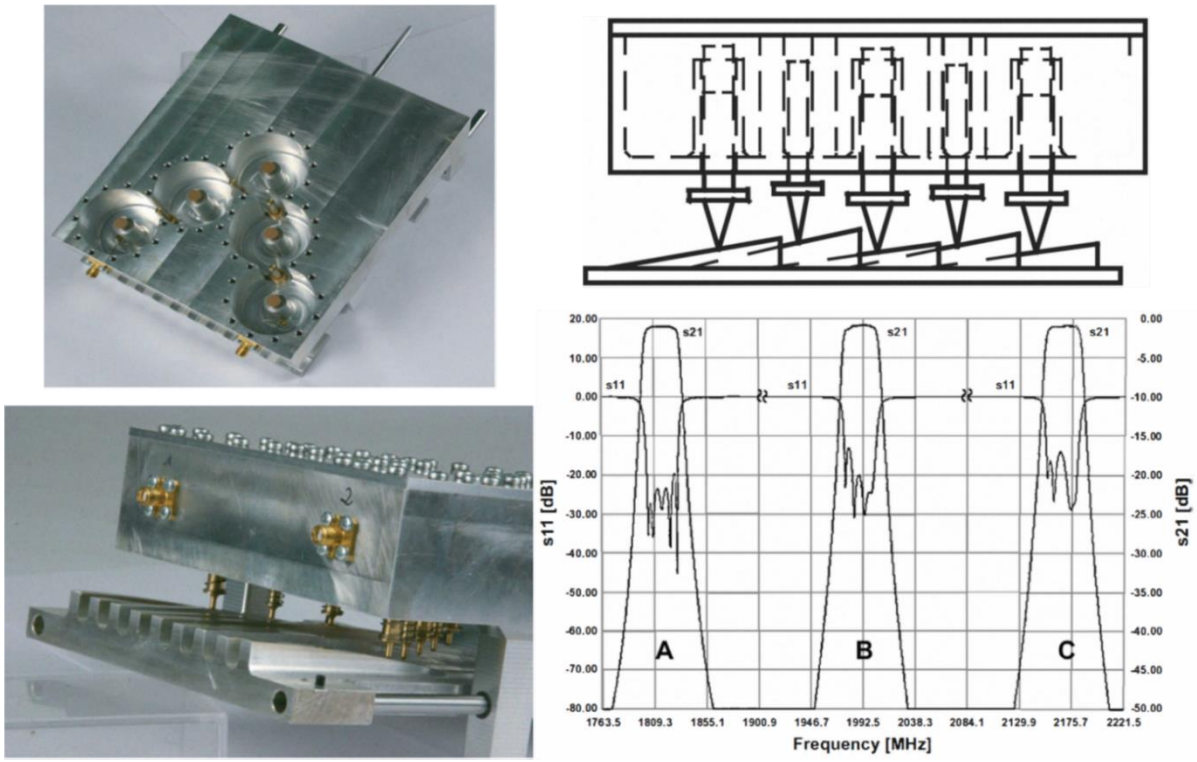

Fig. 2.10 High-Q Tunable Coaxial Filter [25], 2008

While these filter designs ([22]-[25]) have made attempts to realize High-Q tunable filters which can be tuned by using a single tuning element and yet maintain a constant absolute BW, however they all (except [22]) utilize quite complicated tuning mechanisms which is a detrimental factor for reliable operation especially in aerospace and backhaul applications. With regards to [22], the tuning range achieved is quite low around 200 MHz at 12 GHz and the absolute BW variation in such designs increases as the tuning range increases. Table 2.1 summarizes all the existing solutions.

Table 2.1: Summary of Literature Survey: High-Q Tunable Filters

Ref.	Tech.	Freq.	Q	Tun. Range	BW and Var.	Tun. Elem. and Mech.
[12]	coaxial	2.5 GHz	> 2250	400 MHz / (16%)	30 MHz / <±5%	N / robust
[13]	coaxial	3.6 GHz	> 5650	430 MHz / (12%)	75 MHz / <±5%	N / robust
[14]	WG	19.8 GHz	> 6700	200 MHz / (1%)	54 MHz / <±5%	2*N+1 / complex
[15]	WG	19.5 GHz	> 4500	340 MHz / (2%)	180 MHz / <±5%	N / robust
[16]	WG	19.5 GHz	> 9000	500 MHz / (3%)	54 MHz / <±5%	N / complex
[17]	DR	15.6 GHz	> 1300	400 MHz / (3%)	150 MHz / <±5%	N / complex
[18]	DR	4.7 GHz	> 510	160 MHz / (4%)	21 MHz / <±5%	N / robust
[19]	coaxial	4.8 GHz	> 460	2.8 GHz /(1.8:1)	not constant	N / complex
[20]	coaxial	4.8 GHz	> 300	1.5 GHz /(1.4:1)	not constant	N / complex
[21]	WG	21.5 GHz	> 1000	725 MHz / (3%)	350 MHz / <±5%	N / robust
[22]	WG	12 GHz	> 9000	200 MHz / (2%)	60 MHz / <±10%	1 / robust
[23]	WG	11 GHz	> 1400	2.2 GHz / (21%)	516 MHz /<±10%	1 / complex
[24]	WG	12 GHz	> 850	700 MHz / (6%)	200 MHz / <±5%	1 / complex
[25]	coaxial	2 GHz	> 2000	360 MHz / (18%)	25 MHz / <±5%	2*N-1 / complex

Hence, one of the research objectives in this research is to develop High-Q tunable BPFs in coaxial and WG technologies with following features:

- Tuning range between 10 % to 20 %
- Absolute BW variation < 10 %
- Tuning elements – minimum possible (ideally 1)
- Tuning mechanism – robust and simple

Chapter 3
Filter Design Methodology

3.1 Introduction

This chapter provides a brief outline of the filter design methodology used in this thesis. It also presents a novel, systematic and an efficient synthesis technique for designing waveguide filters with transmission zeros. The proposed EM-based synthesis technique directly results in a filter design with an RF performance that is in excellent agreement with the ideal filter performance, thus significantly reducing the post fine optimization effort. Furthermore, the proposed technique also reduces the EM simulation resources required for the filter synthesis. The synthesis technique is lucidly explained by designing a symmetrical 6^{th} order waveguide filter with 4 transmission zeros. To the best of author's knowledge, this is the first filter synthesis technique, which can be adopted to design waveguide filters including transmission zeros with minimum or no post fine optimization.

3.2 Coupled Resonator Filters

Fig. 3.1 summarizes the design methodology beginning with specifications and ending with the synthesis of physical structure of a BPF. Once the required filter function is obtained (to meet the desired specifications), the next step is to create a circuit model which can realize the filter function. Such a circuit model will also be beneficial in optimizing 3D EM simulations of the filter using Space Mapping techniques. Three circuit models predominantly used at RF and Microwave frequencies are Coupling Matrix (CM) model, K-inverter model and J-inverter model. These filter circuit models are well described in [2]. At the end of this step, one will have either CM values (or K-inverter / J-inverter values) that are derived from the filter function.

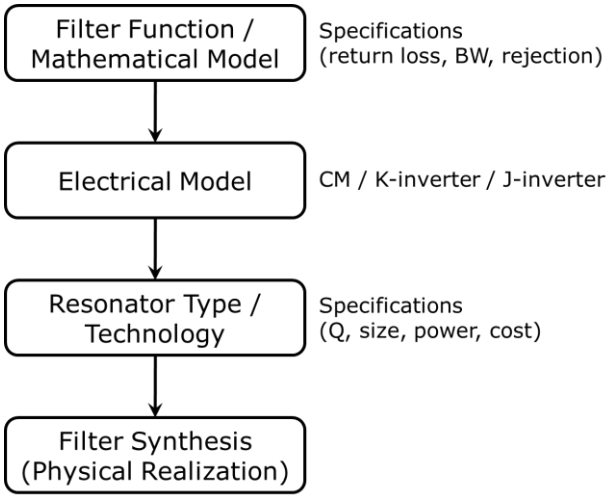

Fig. 3.1: Four Step Filter Design Procedure

The physical filter synthesis in itself involves three major modules: inter-resonator (IR) couplings, input-output (IO) couplings and resonator loading. The IR couplings can be calculated either using analytical approach (including simulation) or using empirical approach (measurement). For synchronous design (identical resonators i.e. same frequency), widely used analytical approach is to use Electric Wall and Magnetic Wall conditions and relate the physical dimensions to the coupling values using following equations:

$$k = \frac{{f_e}^2 - {f_m}^2}{{f_e}^2 + {f_m}^2} \tag{3.1}$$

$$M = \frac{f_0}{BW} * k \tag{3.2}$$

where, f_e is resonant frequency with Electric wall, f_m is resonant frequency with Magnetic wall, f_0 is filter centre frequency, BW is filter bandwidth, k is physical coupling co-efficient and M is normalized coupling co-efficient (from CM). For asynchronous design, the generic equations can be found at [26]. One of the empirical method involves weak excitation of two resonators with coupling structure and determining f_e and f_m from the reflection co-efficient plot (two sharp peaks in S_{21} plot). Nature of coupling itself can be distinguished using the phase of S_{11} [26]. At the end of this step, the physical dimensions of the IR coupling structures are determined.

For IO coupling, reflection group delay is predominantly used both in analytical approach and empirical approach. The feed structure is varied until following condition is satisfied:

$$\tau_{max} = \frac{4*Q_e}{\omega_0} \qquad \textit{and occurs at } f_0 \tag{3.3}$$

where, τ_{max} is group delay of the reflection co-efficient (S_{11}), Q_e is the loaded Quality factor at input (or output) resonator given by :

$$Q_e = \frac{f_0}{BW*R_{in}} \tag{3.4}$$

where R_{in} (or R_{out}) is obtained from CM as M_{S1}^2 (or M_{NL}^2). At the end of this step, the physical dimensions of structures which can realize the required input and output couplings are determined. Finally, all the resonators need to be tuned to absorb the loading due to the coupling structures or apertures. This step though not emphasized very often in fixed filter designs (as it can be absorbed during optimization), however the impact of resonator loading becomes a critical aspect in designing tunable filters using single tuning element. Finally, by combining all the loaded resonators with IO coupling structures and IR coupling structures, one can obtain an initial filter; which closely approaches the desired filtering operation. Fine tuning (optimization) of this initial structure yields the desired filter ready for application at hand. Fig. 3.2 summarizes filter design methodology adopted [2].

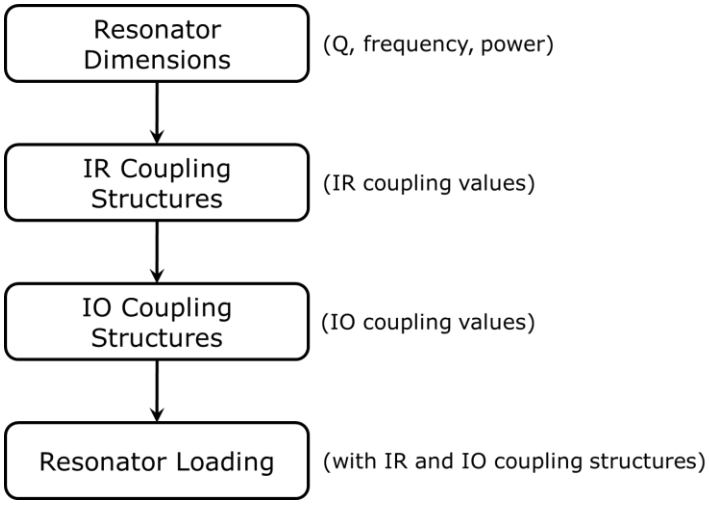

Fig. 3.2: Major Modules in Filter Synthesis

During the course of the research a MATLAB code is developed to generate transversal and folded Coupling Matrices. The Coupling Matrix based design methodology is not elaborated further in this thesis, since it is well documented in the text book “Microwave Filters for Communication Systems: Fundamentals, Design, and application” by Richard J. Cameron, Chandra Kudsia and Raafat R. Mansour [2].

3.3 A Novel Approach for EM Design of Filters Using Fictitious IO Coupling

Though the collection of filter synthesis technique is rich with diverse methodologies, a majority of these methodologies lead to a design that requires post optimization to realize the ideal design response. Especially so, for designing waveguide (WG) filters with several transmission zeros (TZ). Such filters are widely used in telecommunication applications at microwave and millimetre wave frequencies [2]. Traditionally, K-impedance (or J-admittance) inverter model based synthesis techniques have been successfully utilized for designing all-pole WG filters (without TZ) [2], [27]. For designing filters with TZ, the Coupling Matrix (CM) based filter model has become almost ubiquitous [2], [28]. Electro-Magnetic (EM) based single resonator synthesis technique utilizes the CM, however the synthesis result is not sufficiently close to the ideal filter response [2], [26]. As a result, a significant effort is required in post synthesis optimization. Ness has presented a unified sequential approach to design all-pole filters by adopting reflection group delay [29]. Another sequential technique utilizing reflection impedance (or admittance) phase has also been developed for designing all-pole filters [30]. However, both these techniques ([29], [30]) cannot be adopted for designing WG filters with TZ.

In this section, we present a systematic and an efficient EM-based synthesis technique for designing WG filters with TZ. The proposed technique yields result that is very close to the ideal response, thus significantly reducing post fine optimization that are typically needed when implementing EM-based synthesis techniques [2]. Furthermore, the proposed technique also significantly reduces the simulation resources (simulation time and computation resource) since the filter is divided into small sections consisting of two or three resonators and each section is dealt with independently. The idea of the proposed concept is to devise an approach to accurately account for the loading from adjacent sections.

Fig. 3.3 depicts an N^{th} order folded filter configuration incorporating cross couplings essential for realizing TZ. The proposed synthesis technique divides the filter into "N/2" sections, where each section is composed of 2 resonators terminated with WG ports, where we replace the inter-resonator (IR) couplings with input-output (IO) coupling as shown in Fig. 3.4. The goal is to design each section that is composed of 2 resonators independently. This requires that the intermediate WG source-load terminals (Fig. 3.4b) provide an identical IO couplings to the 2 resonators as that provided by the IR couplings in the filter (Fig. 3.4a). Hence, by developing a simple mapping chart between IR coupling and IO coupling, the entire filter can be synthesized with remarkable simplicity yet accurately and efficiently. The approach adopted in the proposed filter synthesis technique also eliminates the associated synthesis complexity, which is directly proportional to the filter order encountered by

sequential synthesis techniques [29], [30]. As a result, a WG filter of any order can be seamlessly designed by adopting the proposed synthesis technique as will be described in the following section

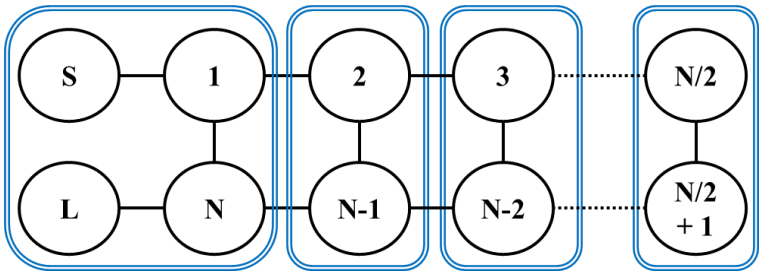

Fig. 3.3: N^{th} order filter configuration with cross couplings is divided into N/2 sections. Each section is composed of 2 resonators.

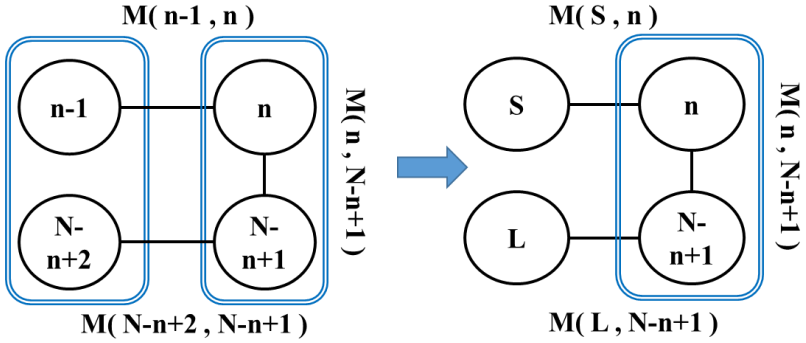

Fig. 3.4: Section equivalence requires IR - IO coupling equivalence

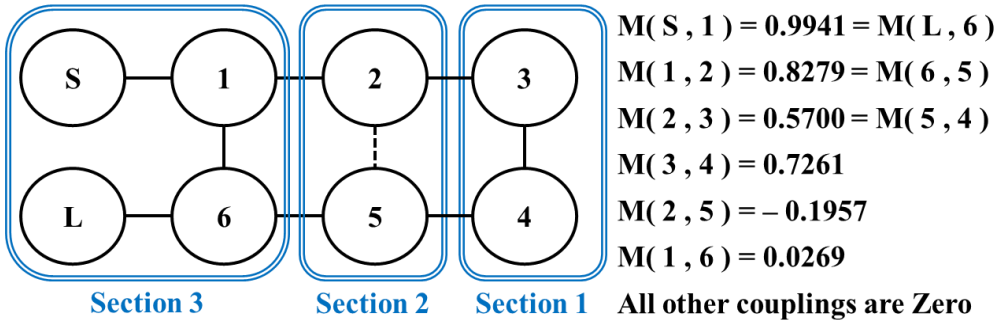

Fig. 3.5: 6^{th} order filter with 4 TZ

A 6^{th} order WG filter with stringent specifications (i.e. center frequency = 10 GHz, bandwidth = 100 MHz, return loss over the bandwidth > 20 dB, 4 TZ at 10 GHz ± 75 MHz and 10 GHz ± 125 MHz) is adopted to describe the step by step procedure of the proposed synthesis technique. WR 90 rectangular WG cavity resonator operating in TE_{101} mode is used [31]. The filter configuration and the associated CM is depicted in Fig. 3.5. The entire filter can be seamlessly designed using following 4 steps:

Establishing IR – IO equivalence

The first step in the proposed synthesis technique is to establish the IR-IO coupling equivalence, which will enable each section to be designed independently. For a given physical coupling structure, the corresponding IR coupling can be determined by using Eigen mode technique [2]. For the same physical coupling structure, the corresponding IO coupling can be determined by using reflection group delay technique [2]. Hence, by relating the IR and IO couplings for the same iris width 'w', the required IR-IO coupling equivalence is established. Fig. 3.6 depicts the IR and IO couplings of an inductive iris coupling structure where the iris width 'w' is parametrically varied. Fig. 3.7 depicts the IR-IO coupling equivalence which is derived from Fig. 3.6.

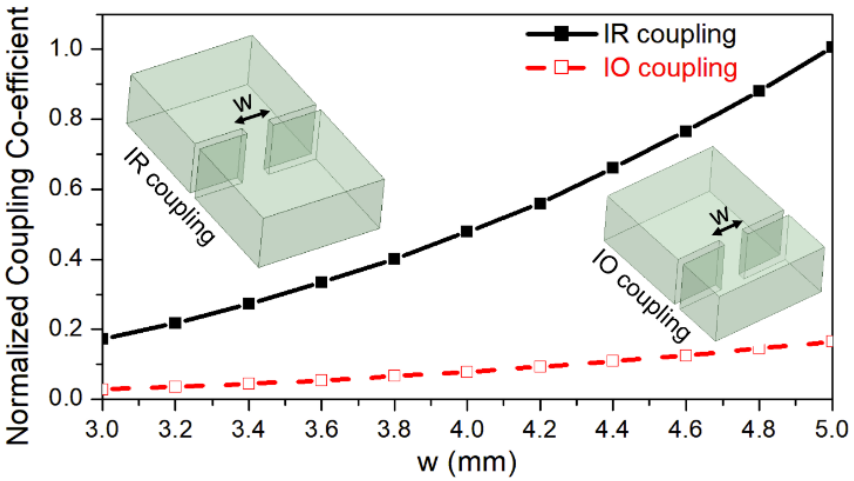

Fig. 3.6: IR and IO couplings of the inductive iris coupling structure [iris thickness = 1.5 mm, waveguide dimensions: WR 90]

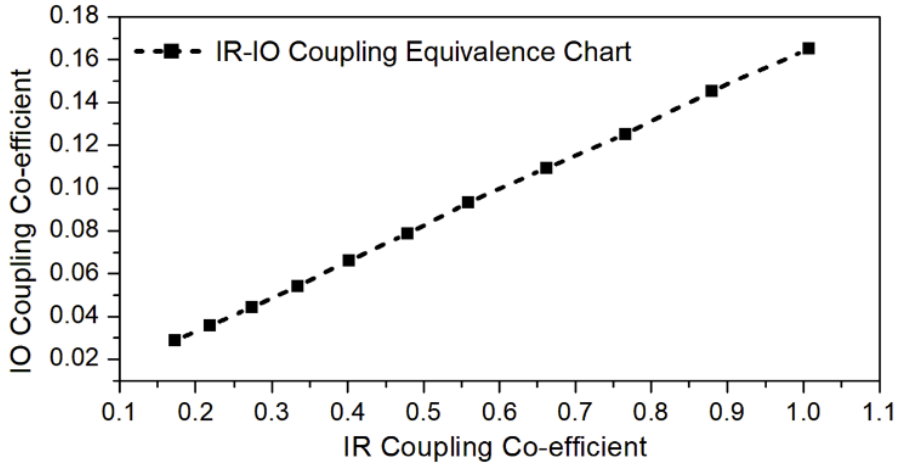

Fig. 3.7: IR-IO coupling equivalence chart (normalized coupling co-efficient)

Design of Section 1

Referring to Fig. 3.5, the section 1 comprises of resonators 3 and 4. In order to independently design this section, it is essential to determine the intermediate IO couplings corresponding to IR couplings M(2,3) and M(5,4) by using the IR-IO coupling equivalence chart depicted in Fig. 3.7. The transformation of IR couplings to intermediate IO couplings for the section 1 is shown in Fig. 3.8. The 3D EM design of section 1 is depicted in Fig. 3.9. It comprises of only 2 resonators with 3 irises (only three physical parameters for symmetrical filter structures). Space mapping is adopted on this reduced structure where the transformed coupling matrix model is used as the coarse model [2], [32]. ANSYS HFSS is used for the 3D EM simulation [33].

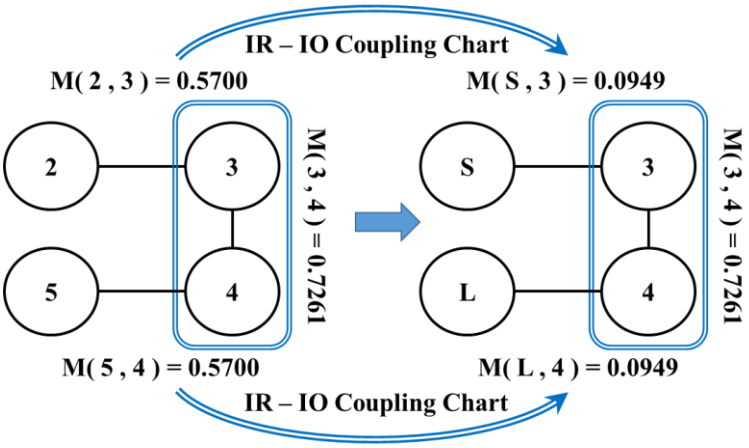

Fig. 3.8: Design of section 1: IR-IO coupling transformation

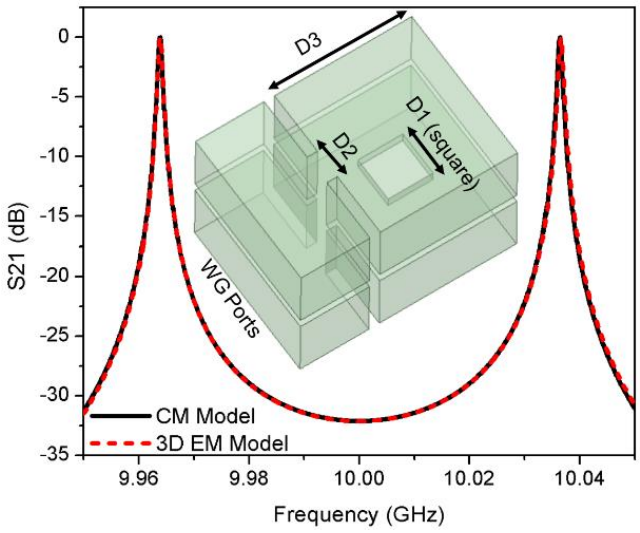

Fig. 3.9: Design of section 1: 3D EM design [D1 = 6.5491, D2 = 4.2634, D3 = 19.9306, iris thickness = 1.5, all dimensions are in mm, WR 90 waveguide]

Design of Section 2

For the design of section 2 comprising of resonators 2 and 5, the IR couplings M(1,2) and M(6,5) are transformed into IO couplings as shown in Fig. 3.10 by using the IR-IO coupling equivalence chart. Fig. 3.11 depicts the 3D EM design for the section 2. To account for the resonator loading, the iris coupling structures corresponding to M(2,3) and M(5,4) are incorporated in the 3D model with detuned resonators. However, it is worth mentioning here that these coupling structures (i.e. corresponding to M(2,3) and M(5,4)) are fixed dimensions (obtained from section 1) and are not included as variables in the design of section 2. Thus, the design of section 2 also involves 3D EM simulation of only 2 resonators with 3 physical parameters.

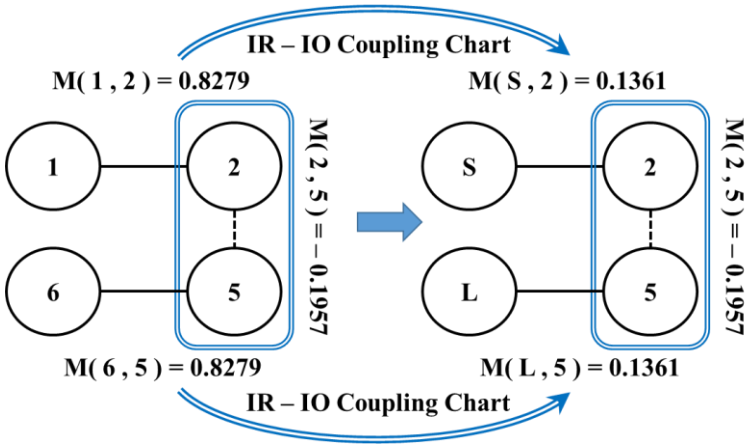

Fig. 3.10: Design of section 2 : IR-IO coupling transformation

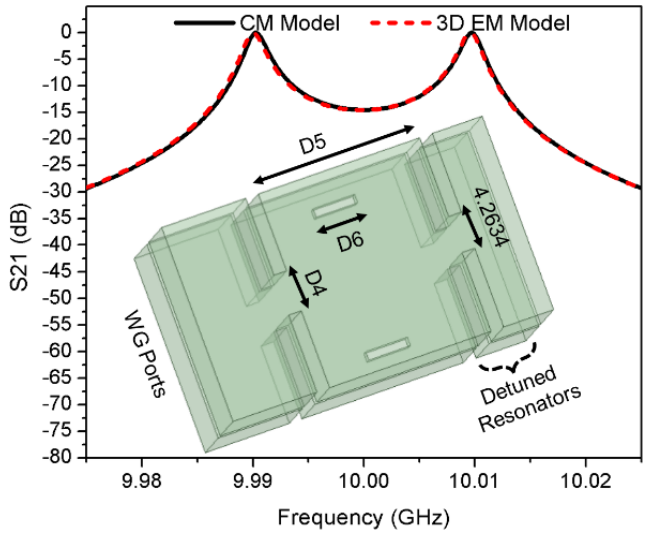

Fig. 3.11: Design of section 2 : 3D EM design [D4 = 4.7087, D5 = 19.189, D6 = 4.93, D6 iris width = 1, D6 position from side wall = 2.5, all dimensions are in mm]

Design of Section 3

Finally, for the design of section 3 comprising of resonators 1 and 6, no additional coupling transformation is required as they are inherently coupled to source-load terminals as shown in Fig. 3.12. The 3D EM design for the section 3 involving only 2 resonators with 3 physical parameters is depicted in Fig. 3.13. As expected, the iris coupling structures corresponding to M(1,2) and M(6,5) with detuned resonators are incorporated in the 3D model to account for the resonator loading as fixed parameters.

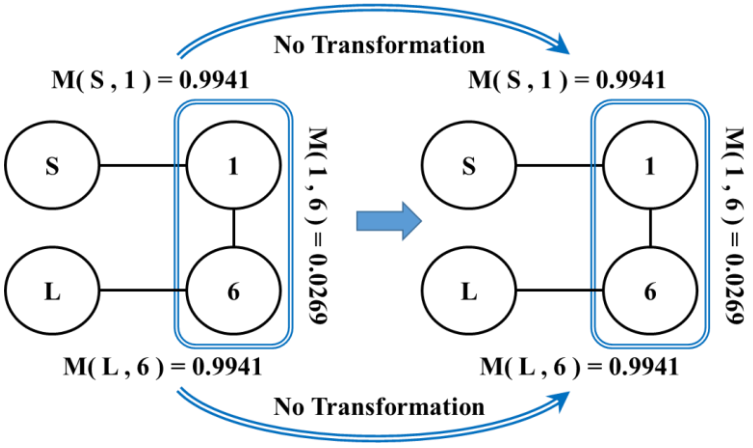

Fig. 3.12: Design of section 3 : No coupling transformation required

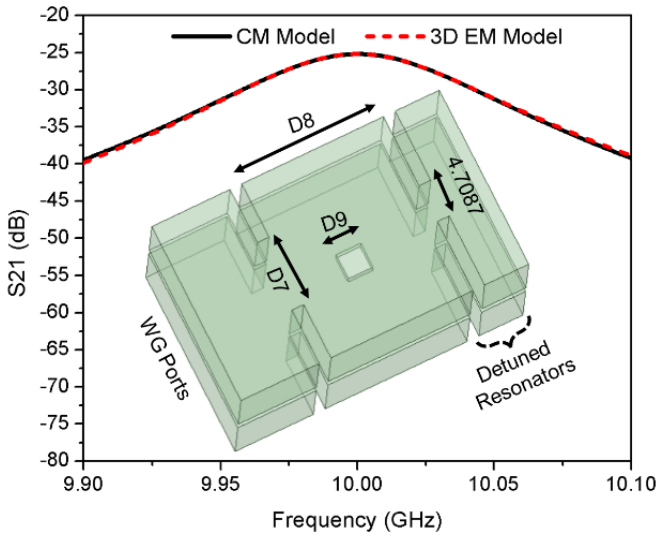

Fig. 3.13: Design of section 3 : 3D EM design [D7=8.86, D8=18.095, D9=3.14, all dimensions are in mm]

Now, by combining the dimensions obtained from all 3 sections, which have been independently designed, the required 6th order filter is obtained as shown in Fig. 3.14. The 3D EM simulation of the synthesized filter is depicted in Fig. 3.15 in comparison with the optimum filter obtained using the coupling matrix given in Fig. 3.5. It can be observed that the synthesized filter is in excellent agreement with the optimum filter and hence is a good starting point for post synthesis filter optimization techniques, if required. The proposed synthesis technique is very efficient, since each section comprising of only 2 coupled resonators is independently designed. This approach is vital especially when designing higher order WG filters. Table 1 compares the proposed synthesis technique with other techniques available in the literature for designing of WG filters.

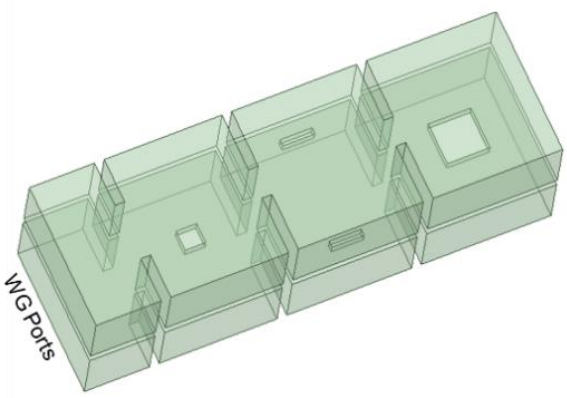

Fig. 3.14: Synthesized 6th order WG filter with 4 TZ (combining the dimensions obtained from all 3 sections each designed independently)

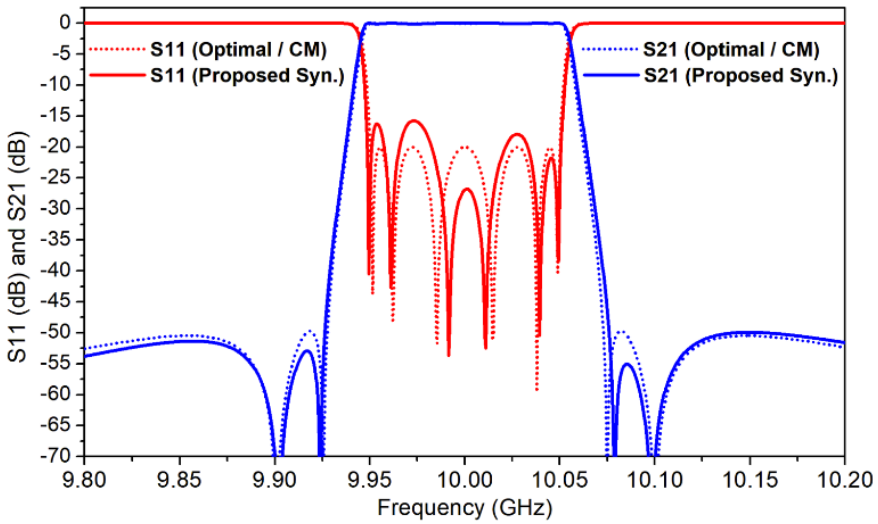

Fig. 3.15: Synthesis of 6th order WG filter with 4 TZ [optimal filter from CM : dotted curves, synthesized filter from proposed technique : solid curves]

Table 3.1: Comparison of WG filter synthesis techniques

Synthesis Technique	All-Pole Filter	Filter with TZ	Design Stages	Resonators per Stage
Imp. Invertor	Yes	No	2	NA
EM-based SR	Partial	Partial	N/2	1
Ref. Group Delay	Yes	No	N/2	1, 2, 3, . , N/2
Ref. Imp. Phase	Yes	No	N/2	1, 2, 3, . ,N/2
Proposed	**Yes**	**Yes**	N/2	**2**

SR : single resonator, Ref. : reflection, Imp. : impedance (or admittance), NA : not applicable

As a value addition, the proposed WG filter synthesis technique can also be embraced in designing filters with advanced filter configurations as well. Fig. 3.16 shows one such 9th order filter with 3 asymmetric TZ in Trisection configuration [2]. The entire filter design requires 19 independent variables. By dividing the filter configuration into 3 sections and by transforming IR to IO couplings between the sections, the filter can be synthesized in 3 sections. Where, each section comprises only 3 resonators and at-most 7 variables. Fig. 3.17 depicts the synthesized filter using the proposed technique and the 3D EM simulation in comparison with the optimum filter. It is observed that the synthesized filter response is in excellent agreement with the optimum filter response, thus significantly reducing the post synthesis optimization effort. The mismatch in the 3rd TZ at 10.15 GHz is attributed to the dispersion effect of the coupling structure.

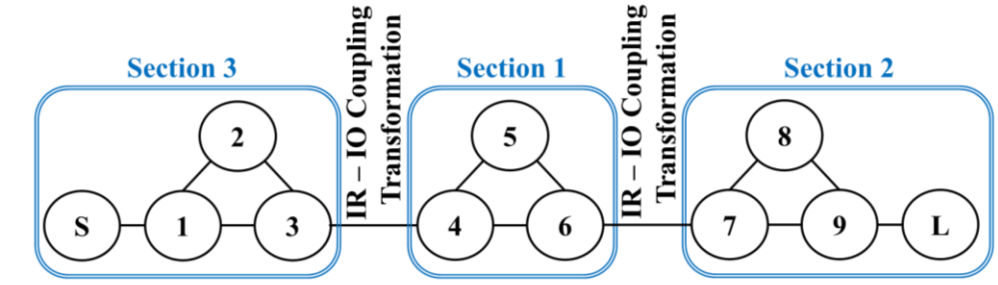

M(S , 1) = 0.9875 M(3 , 4) = 0.5484 M(6 , 7) = 0.5484 M(L , 9) = 0.9875
M(1 , 2) = 0.7278 M(1 , 3) = 0.3704 M(2 , 3) = 0.4988 M(1 , 1) = 0.0092
M(4 , 5) = 0.5140 M(4 , 6) = 0.1547 M(5 , 6) = 0.5140 M(2 , 2) = – 0.5143
M(7 , 8) = 0.5697 M(7 , 9) = 0.1656 M(8 , 9) = 0.7997 M(3 , 3) = 0.0750
M(4 , 4) = 0.0350 M(5 , 5) = – 0.2813 M(6 , 6) = 0.0254 M(7 , 7) = 0.0426
M(8 , 8) = – 0.2272 M(9 , 9) = 0.0092 All other couplings are Zero

Fig. 3.16: 9th order trisection filter with 3 asymmetric TZ

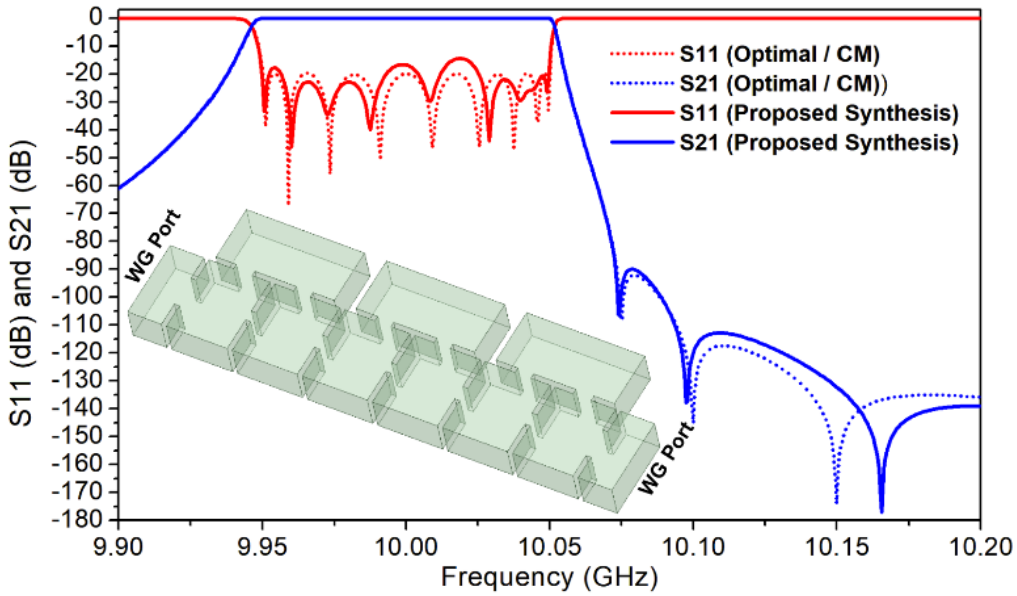

Fig. 3.17: Synthesis of 9th order filter with 3 asymmetric TZ [optimal filter from CM: dotted curves, synthesized filter from prop. technique: solid curves]

3.4 Conclusion

This chapter has presented a systematic and an efficient synthesis technique for designing WG filters including transmission zeros. The proposed technique is adopted to synthesize multiple WG filters; a 6th order filter with 4 symmetric TZ and a 9th order filter with 3 asymmetric TZ. The proposed synthesis technique directly results in a filter with an RF performance that is in excellent agreement with the ideal filter, thus significantly reducing the post fine optimization effort. Furthermore, the proposed technique also significantly reduces the computation resources, since the filter is divided into small sections consisting of two or three resonators and each section is dealt with independently. To the best of author's knowledge, this is the first filter synthesis technique, which can be efficiently adopted to design waveguide filters including transmission zeros, with synthesized results that are in excellent agreement with the ideal filter response.

Chapter 4
Tunable Waveguide Filters

4.1 Introduction

This chapter presents three novel filter configurations:

- A novel configuration for a high-Q tunable waveguide (WG) filter with a constant absolute bandwidth (BW). The key feature of this filter is that it is tuned by a single tuning element. This chapter investigates the theory of coupling behavior of single septum and double septa to achieve constant absolute BW. The filter design methodology is lucidly presented covering the design strategy adopted for inter-resonator coupling, input–output coupling and tuning element. The tuning mechanism of the proposed filter is explained with measurement results presented for a Ku-band tunable WG filter designed at 15 GHz with a 2% BW to achieve 15% tuning range. The filter promises to be useful in emerging 5G millimeter-wave applications, where the filter size is very small to accommodate multiple mechanical tuning elements. Furthermore, the proposed design methodology is scalable, i.e., the tuning mechanism is independent of the filter order.
- The concept was extended to implement a novel configuration of a High-Q bandwidth reconfigurable WG filter tuned with only two tuning elements regardless of the filter order. The filter is realized in rectangular WG technology and is capable to tune the BW without deviating the center frequency. Furthermore, the configuration is scalable to higher order filters without the need for additional tuning mechanisms. For the proof of concept, a four-pole prototype filter is designed, fabricated, and tested at the Ku-band. The measured BW tunability of the filter is nearly 35% from 225 to 320 MHz. The center frequency remains unaltered at 13.375 GHz over the BW range.
- A novel frequency reconfigurable dual-mode WG filter with elliptic response. The proposed filter maintains a constant absolute BW and a constant rejection BW (frequency spacing between transmission zeros) over the tuning range. Furthermore, the filter can be tuned using a single tuning mechanism. A 4th order prototype filter at 11.5 GHz with 50 MHz bandwidth and 2 symmetric transmission zeros (± 45 MHz) is fabricated and measured. The measured tuning range of the filter is 390 MHz within which the absolute BW variation is within ±1 MHz. In-addition, the measured frequency spacing between the transmission zeros varies well within ±2 MHz over the entire tuning range.

4.2 Frequency Reconfigurable Single Mode Filter

Extending the CM design methodology of fixed frequency filters to tunable filters, we observe (from eq. 4.1 and eq. 4.2) that to maintain constant absolute BW, following two conditions need to be satisfied [2],[34].

$$k_{ij} * f_r = M_{ij} * BW \tag{4.1}$$

$$\tau_{s11\_max} = 4 / \left(2\pi * BW * {M_{s1}}^2\right) \tag{4.2}$$

- A constant $k_{ij} * f_r$ product over the tuning range
- A constant peak input/output reflection group delay w.r.t to center frequency over the tuning range

where, k_{ij} is the physical coupling co-efficient between the resonators, f_r is the resonant frequency, M_{ij} is the normalized coupling co-efficient between the resonators, BW is the bandwidth, M_{s1} is the normalized coupling co-efficient at input and τ_{s11_max} is the peak input (or output) reflection group delay. The normalized coupling co-efficients in the CM depend only on the filter type and its order, and not on center frequency and BW.

In general, any fixed filter can be transformed into a tunable filter by introducing tuning elements each dedicated for resonator and coupling structures. Thus, such a tunable filter of order *N* would require *2*N+1* tuning elements to maintain constant absolute BW over the tuning range. A significant research effort to reduce the number of tuning elements by 50% (i.e. with only *N* tuning elements) has been carried out in references [9]-[10], where the coupling structures are suitably designed such that the required conditions eq. 4.1 and eq. 4.2 are satisfied without the need of any tuning mechanism for couplings. Hence, such a filter does not require tuning elements for IR and IO couplings, and utilizes *N* tuning elements for *N* resonators.

The goal here is to further reduce this to 'single tuning element' !

The next immediate question one naturally encounters is that, "*why are N tuning elements required, when in-fact all the resonators are supposed to resonate at the same frequency? Hence, a single common tuning mechanism should have been sufficient ?!*". The reason is hidden in the minute aspect of resonator loading discussed in section 3.1. It is very important to observe that each resonator experiences different amount of loading (due to different coupling values). A widely adopted approach is to re-adjust the resonator dimensions such that all of the loaded resonators resonate at the same

frequency [2]. Such an approach can be effectively utilized for a fixed frequency design but very often cannot absorb the loading impact on the resonators over the entire tuning range using single tuning mechanism. This is one of the primary reasons which mandates the requirement of an independent tuning mechanism for each resonator in the reported High-Q tunable filters [12]-[21]. In other words, the tuning elements for the resonators have to be adjusted by different amount for each resonator at each frequency. This is also the primary reason for using different ramp (or slope) for each of the resonator tuning element in the reported tunable coaxial filter [25].

Furthermore, the impact of resonator loading becomes even more prominent as the tuning range increases. Resonator loading has been the major impediment in successful realization of tunable filters with single tuning element maintaining constant absolute BW. Any such tunable filter design using a single tuning mechanism should ensure that the loading impact of all the resonators are absorbed in the common tuning mechanism in-addition to satisfying the constant absolute BW conditions (eq. 4.1 and eq. 4.2).

For applications requiring tunable filters using WG technology, the solution of realizing tunable filters using single tuning mechanism is hidden in the details of E-plane metal septum filter. Interestingly, E-plane metal septum fixed frequency filters are also widely used in aerospace applications due to superior performance like low insertion loss, high power handling capacity and higher fabrication yield [35]. Furthermore, E-plane septum is physically isolated from the tuning element (side wall movement) and hence significantly simplifies the tuning mechanism. A 5th order Chebyshev all pole filter is designed for the proof of the proposed concept. The filter is designed at 15 GHz with a fractional BW of 2%. Fig. 4.1 depicts the assembly view of the proposed tunable WG double septum filter with WG dimensions of '*a=13 mm*' and '*b=6.5 mm*'. The filter is tuned using a metal insert moving inside one of the body halves. Fig. 4.2 depicts the internal 3D schematic of the filter.

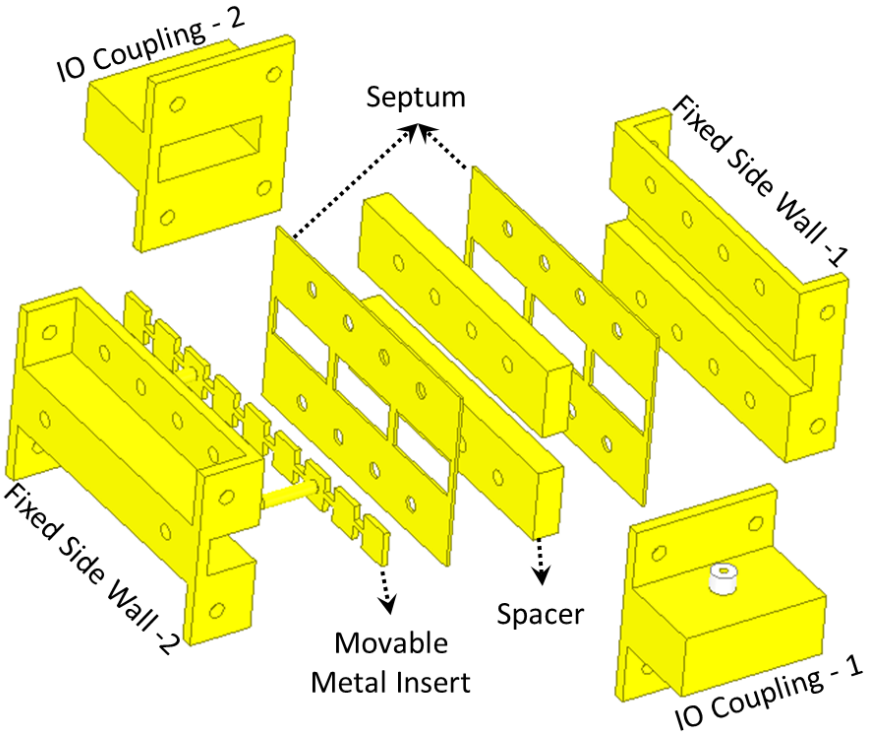

Fig. 4.1: Assembly View of the Proposed Tunable WG Filter

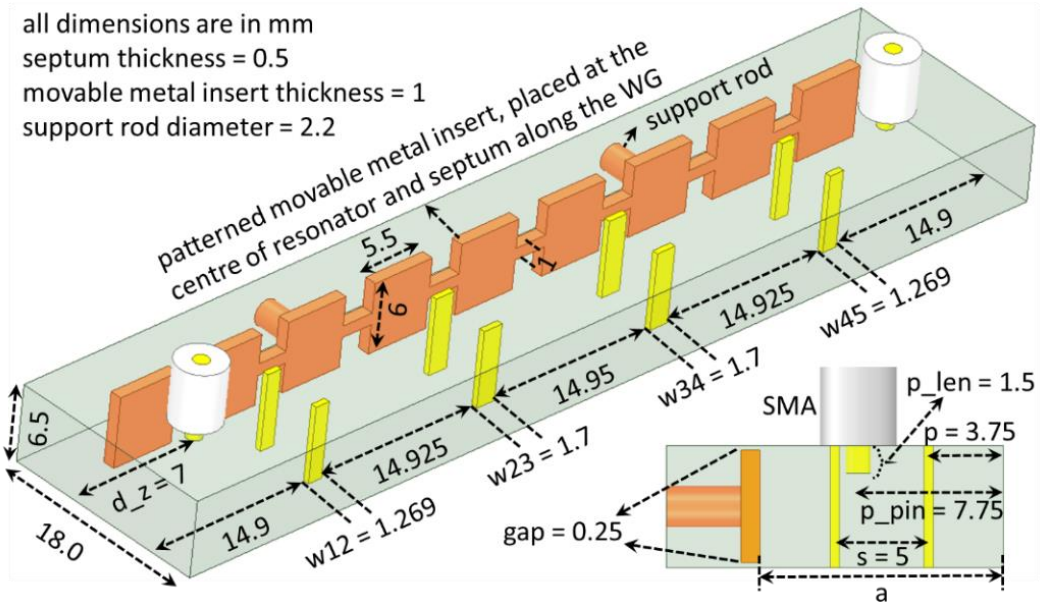

Fig. 4.2: 3D Schematic of the Proposed Tunable WG Filter

IR Coupling

To start with, IR coupling is implemented using metal septum between the resonators. Fig. 4.3(a) shows a schematic of two WG resonators coupled by a single septum and double septa. As the resonator frequency is tuned, ANSYS HFSS is used to extract coupling values from the 3D structure [2], [33]. Fig. 4.3(b) depicts the $k_{ij}f_r$ product for the single septum and double septa over the tuning range. The resonant frequency is tuned by varying the width of cavity i.e. *'a'* dimension as shown in Fig. 4.3(b). It can be observed that the double septa has a significantly wider tuning range, where $k_{ij}f_r$ product is constant. The double septa offers wider tuning range compared to single septum, since it has an additional degree of freedom. The single septum coupling structure has only two variables: width and position of the septum, whereas the double septa has three variables: width, position (*'p'*) and spacing between the septa (*'s'*). This provides flexibility in optimizing the structure to realize the coupling behavior shown in Fig 4.3(b). It is worth mentioning here that, following a similar argument, metallic septa higher than two are expected to provide further wider tuning range for IR coupling.

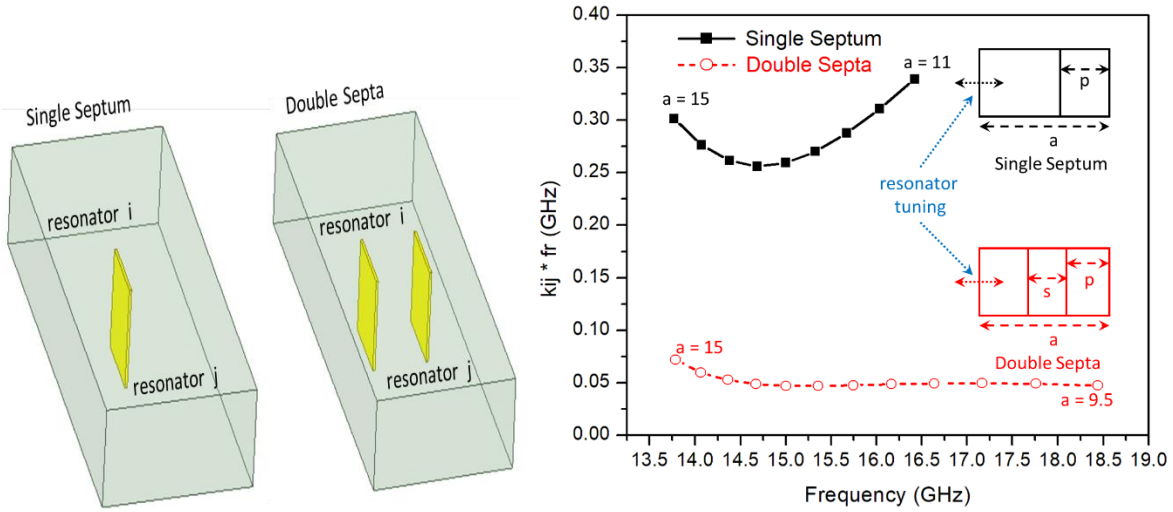

(a) (b)

Fig. 4.3: Single and Double Septa Coupling (a) Schematic, (b) IR coupling (s=5 mm, p=3.75 mm)

For the double septa IR coupling, it is observed that the width of the septa determines the coupling value whereas position and spacing determine the tuning range. Fig. 4.4 depicts the impact of position and spacing on the tuning range. Thus, the design of IR coupling is performed in two sequential steps: to start with, suitable values of position and spacing of the double septa are searched to maximize the tuning range over the band of interest. Once the position and spacing are finalized ($s = 5\ mm$ and $p = 3.75\ mm$ for the particular design), the width of septa is determined based on the desired coupling values

of the filter. From Fig. 4.5 it can be observed that the $k_{ij}f_r$ product is nearly constant from 14.7 GHz to 17.7 GHz. The desired $k_{ij}f_r$ values are 0.2596 GHz (M_{12} and M_{45}) and 0.1907 GHz (M_{23} and M_{34}).

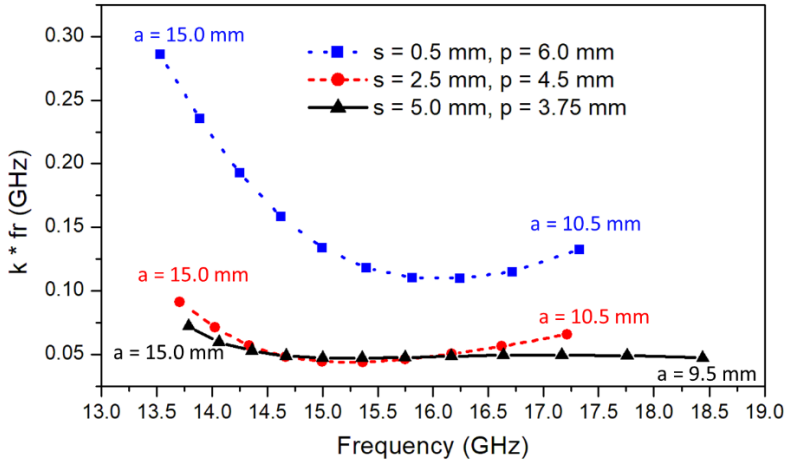

Fig. 4.4: IR Coupling using Double Septa: 's' and 'p' effect on Tuning Range

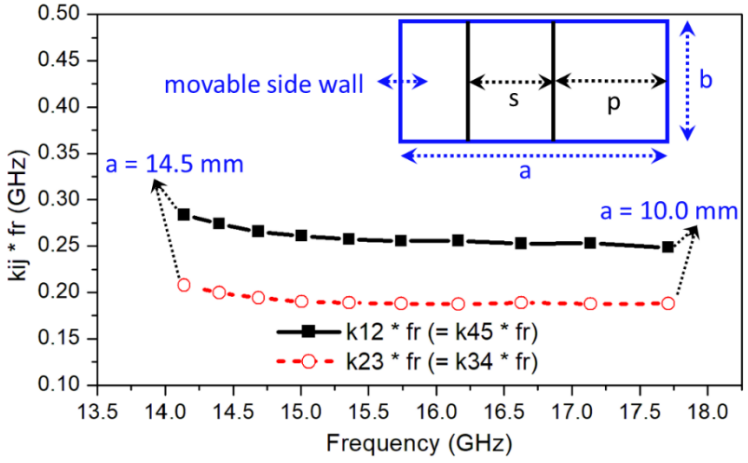

Fig. 4.5: IR Coupling with Constant $k_{ij}f_r$ product : s = 5 mm and p = 3.75 mm

IO Coupling

The IO coupling is realized using an SMA probe shown in Fig. 4.2. Fig. 4.6 depicts the peak group delay, which is nearly constant from 14.6 to 16.6 GHz. Referring to Fig. 4.2, it can be observed that the IO coupling also has 3 degrees of freedom : '*p_len*' (pin length), '*d_z*' (distance from shorting wall) and '*p_pin*' (position within the WG). It is observed that the pin length determines the IO coupling value whereas distance ('*d_z*') and position ('*p_pin*') determine the tuning range. To start with, the distance and position are tuned to maximize the tuning range. Following which, the pin length is altered to obtain the required IO coupling.

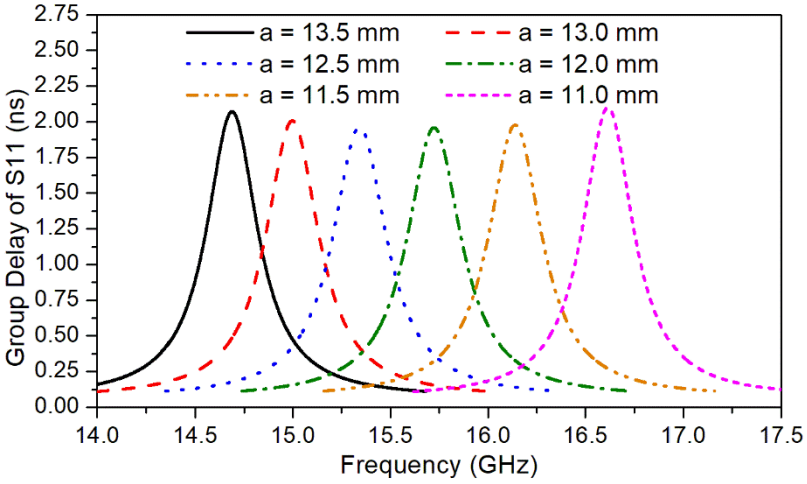

Fig. 4.6 IO Coupling with Constant Peak Group Delay w.r.t f_r

Tunability

Tunability of the filter is achieved by moving the sidewall of the WG filter i.e. by changing the '*a*' dimension. In the proposed filter, this is achieved by linearly moving the patterned single-metal insert in proximity of one the septa as shown in Fig. 4.2. The metal insert is designed to have a gap of 0.25 mm on both sides (top and bottom) to facilitate friction free movement. The shape of the metal insert tuning element is selected to eliminate undesired modes resulting from having a gap between metal insert and the WG wall. Fig. 4.7(a) shows the undesired mode generated when the movable metal insert has no pattern. It can be observed from Fig. 4.7(b) that suitable patterning of movable metal insert helps to eliminate these modes from the band of interest. Two support rods are used to minimize skewing of the metal insert tuning element within WG. A single motor is used to drive the two supporting rods.

Resonator Loading

The most important feature of the E-plane metal septum filter which enables for single tuning mechanism is that inherently, the metallic septum filter has a low resonator loading impact. This can be observed in Fig. 4.8, which depicts the resonator loading impact of a septum coupled resonator in-comparison to an iris (inductive) coupled resonator. Fig. 4.8 plots the change in resonant frequency of the resonator as the coupling is increased. One can arrive at this observation from intuition as well. The boundary condition in case of septum coupled resonator varies significantly less over the coupling values as compared to iris coupled resonator.

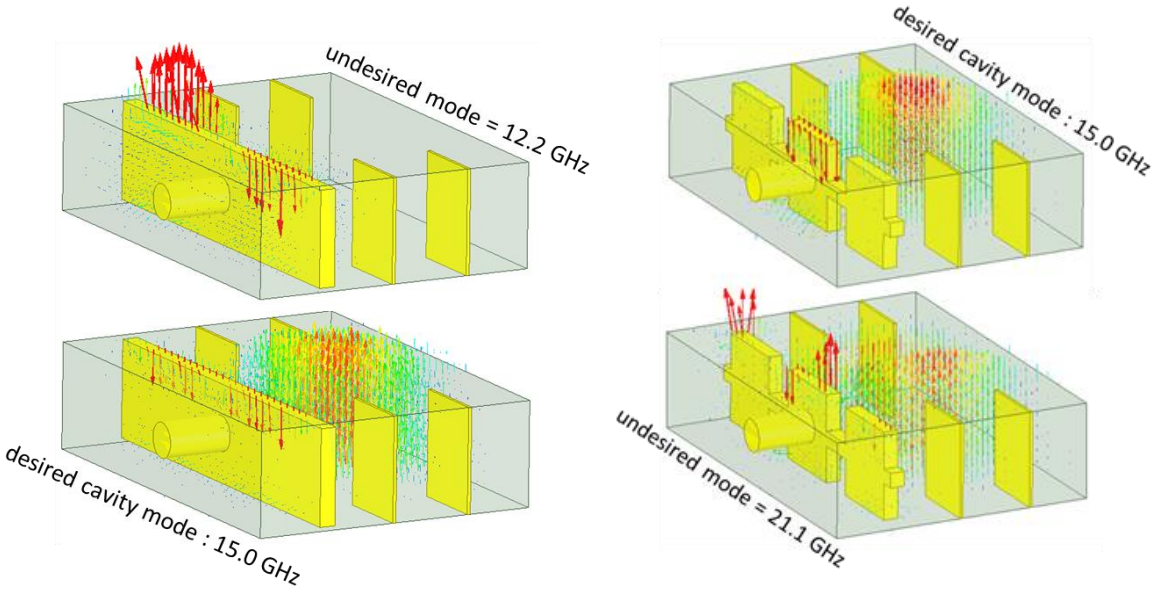

(a) (b)

Fig. 4.7: Movable Metal Insert (a) without pattern, (b) with pattern

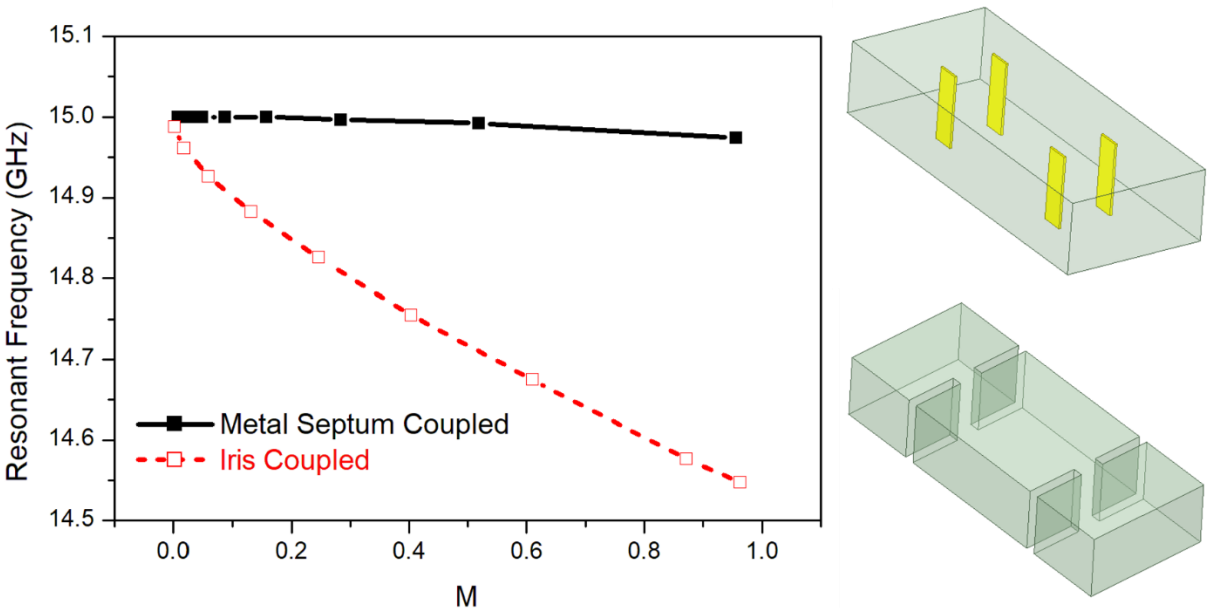

Fig. 4.8 Resonator Loading : Metal Septum and Iris Coupled Resonators

Fig. 4.9 depicts the EM-simulated response of the proposed tunable filter obtained by varying the position of metal insert tuning element. Fig. 4.10 illustrates the variation of BW and insertion loss (IL) over the tuning range. BW variation is observed to be within ±5% while the center frequency is tuned from 14.65 GHz to 17.15 GHz corresponding to the tuning range of 15.7%. IL of the filter is around

0.3 dB over the entire tuning range. The philosophy adopted in the present work is rapid prototyping for the proof of concept. Certainly, the filter return loss can be improved by rigorous optimization of the parameters *'s', 'p'* and *'w'*. The simulated unloaded Quality factor of the resonator is around 5000 at 15 GHz.

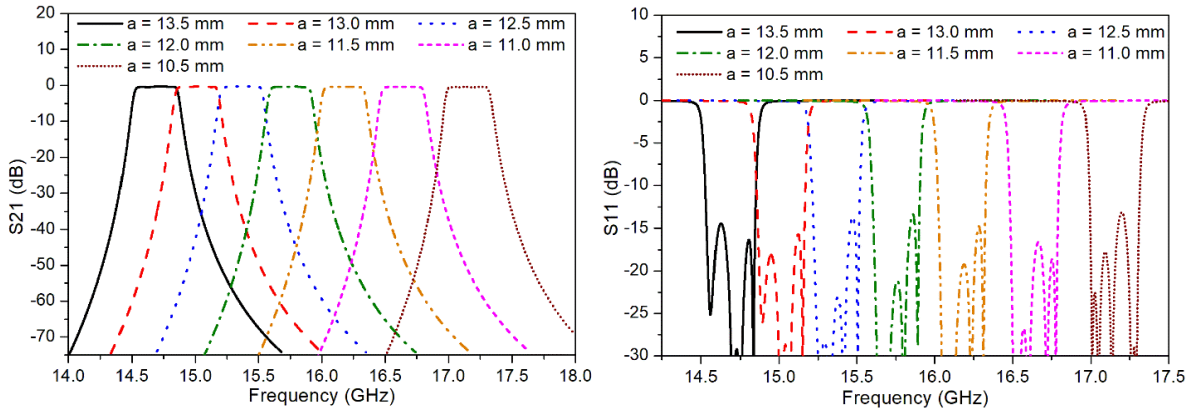

Fig. 4.9: EM Simulated Response : S_{11} and S_{21}

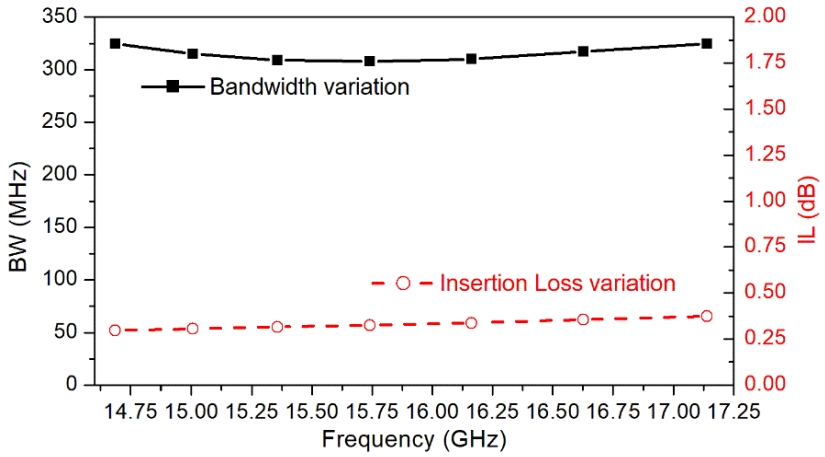

Fig. 4.10: EM Simulated Response : BW and IL

Fig. 4.11(a) shows the photograph of individual WG components of the prototype unit developed as a proof of concept prior to assembly. Copper is used for the two WG halves, two septa, and for the tuning element. The input and output resonators are realized using a single metallic piece. Aluminum rather than copper is used for these single metallic pieces since it is easier to minimize the corner radius during machining. Fig. 4.11(b) shows the photograph of the motor based tuning station with the assembled tunable filter. The mechanism allows changing the penetration of the metal insert inside the filter. It should be noted that the tuning station employs only one motor. It is built as a generic tuning

station for testing prototype tunable filters. The unit is interfaced to a computer that controls the linear movement. In an actual application, a similar miniature mechanism can be connected directly to the metal insert and integrated with the filter housing to realize an overall compact tunable filter.

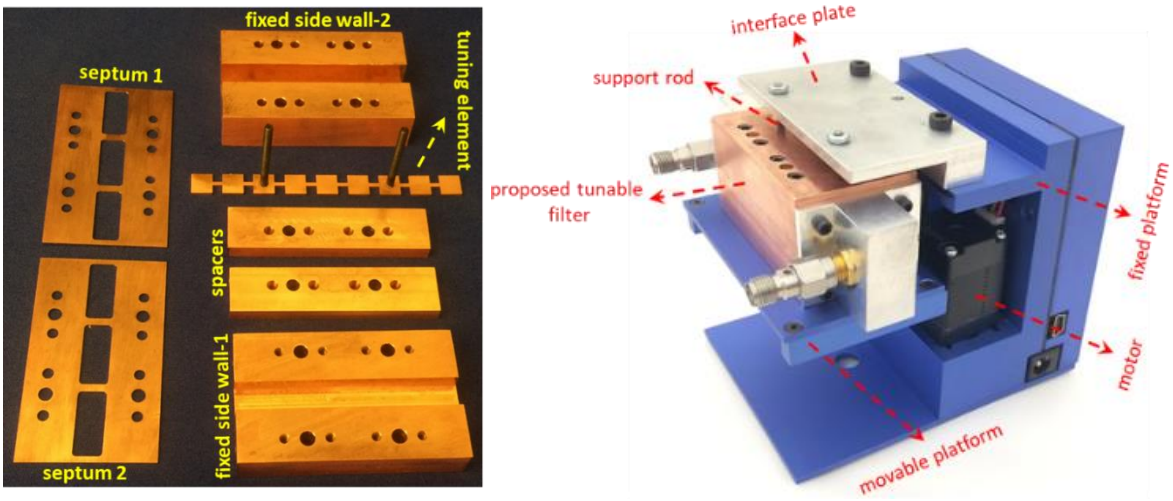

Fig. 4.11 Fabricated Prototype Unit (a) Dis-assembled, (b)Tunable Filter with Tuning Station

Fig. 4.12 depicts the measured response of the filter. Tuning range of the filter is 1.4 GHz (from 14.8 GHz to 16.2 GHz) where the BW variation is within 5%. The measured variations of BW and IL over the tuning range are shown in Fig 4.13. The increase in the measured IL of around 0.6 dB is attributed predominantly to the fact that the first and last cavities are made of aluminum and to the use of Kapton tape to ensure the 0.25 mm gap between the metal insert tuning element and the WG walls. Silver plating the whole filter will certainly help in improving the IL. The spurious performance of the filter is shown in Fig. 4.14(a). The measured group delay at 15.6 GHz is shown in Fig. 4.14(b). The filter has a spurious free response until 20 GHz. It is important to note that the methodology used for the design of proposed tunable filter is easily scalable, i.e., the tuning mechanism is independent of the order of filter. This is one of the key features of the proposed tunable filter. Table 1 compares the proposed tunable WG BPF with existing WG BPF solutions.

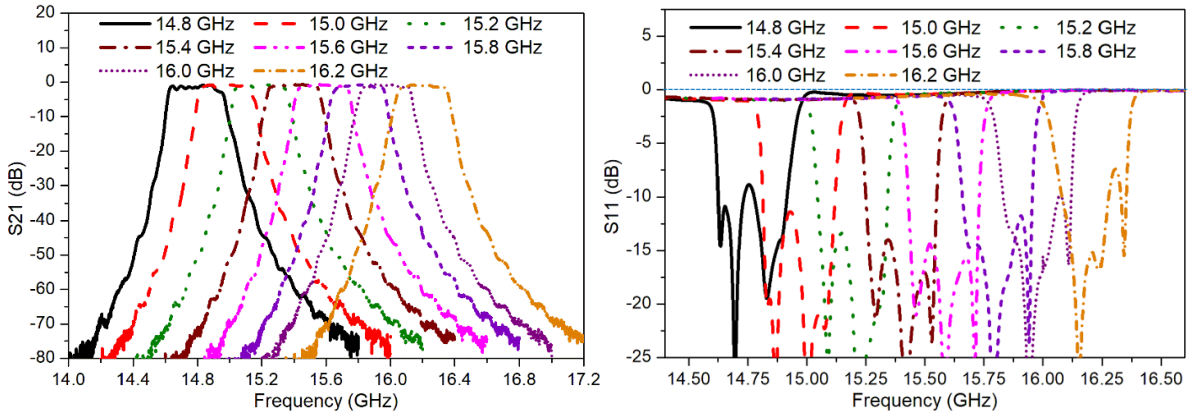

Fig. 4.12: Measured Filter Response: S_{11} and S_{21}

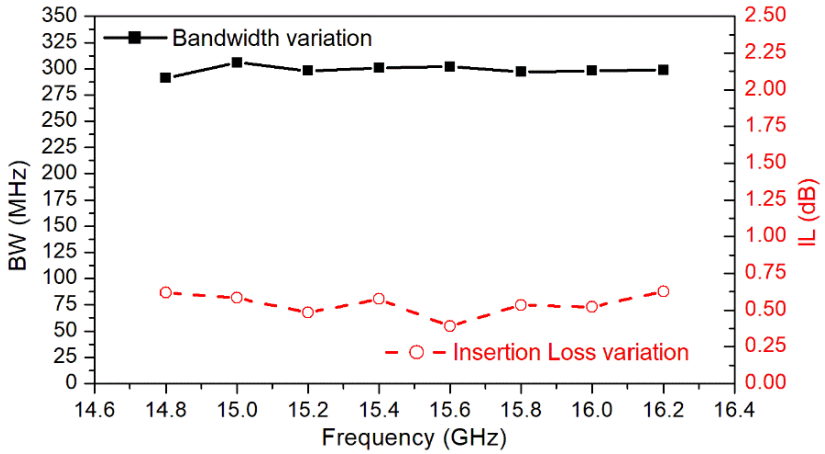

Fig. 4.13: Measured BW and IL Variation over the Tuning Range

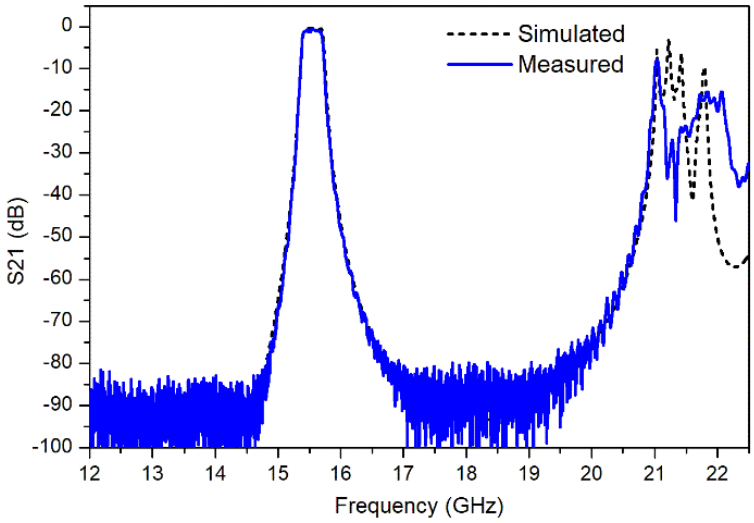

Fig. 4.14(a): Measured Spurious Response of the Tunable Filter at 15.6 GHz

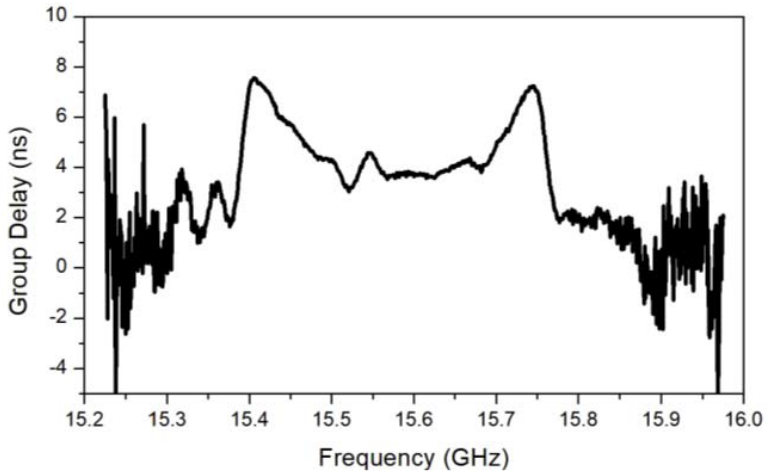

Fig. 4.14(b): Measured Group Delay of the Tunable Filter at 15.6 GHz

Table 4.1: Comparison of Proposed Tunable WG BPF with Existing WG Solutions

Ref.	Tech.	Freq.	Q	Tun. Range	BW and Var.	Tun. Elem. and Mech.
[17]	WG	19.8 GHz	> 6700	200 MHz / (1%)	54 MHz / <±5%	2N+1 / complex
[18]	WG	19.5 GHz	> 4500	340 MHz / (2%)	180 MHz / <±5%	N / robust
[19]	WG	19.5 GHz	> 9000	500 MHz / (3%)	54 MHz / <±5%	N / complex
[24]	WG	21.5 GHz	> 1000	725 MHz / (3%)	350 MHz / <±5%	N / robust
[25]	WG	12 GHz	> 9000	200 MHz / (2%)	60 MHz / <±10%	1 / robust
[26]	WG	11 GHz	> 1400	2.2 GHz / (21%)	516 MHz /<±10%	1 / complex
[27]	WG	12 GHz	> 850	700 MHz / (6%)	200 MHz / <±5%	1 / complex
This work	WG	15.9 GHz	> 5000	2.5 GHz / (15%)	300 MHz / <±5%	1 / robust

4.3 Bandwidth Reconfigurable Filter

With regards to BW reconfigurable high-Q filters, the challenge is to maintain the same center frequency with minimum number of tuning elements as the BW is varied. Reference [14] proposes a 4-pole circular WG cavity filter at K-band which utilizes non-resonating cavities as coupling structures for seamless tuning of inter-resonator and input-output couplings. The filter in [14] is designed at 20 GHz and achieves a BW variation from 54 to 72 MHz. However, the filter utilizes N+1 (where N is the filter order) tuning elements. To reduce the number of tuning elements, reference [36] proposes a 2-pole dual mode circular WG cavity filter at X-band. The filter is designed at 11.2 GHz and achieves a BW variation from 26 to 52 MHz. Though the filter reduces the number of tuning elements required for resonators by 50%, it requires independent tuning elements for each of the couplings.

The proposed High-Q WG filter configuration in this section, aims to drastically reduce the number of tuning elements. The proposed BW reconfigurable filter utilizes only two tuning elements irrespective of the filter order. For the proof of concept, a 4-pole prototype filter is designed, fabricated and tested at Ku-band. The measured BW tunability of the filter is more than 35 % from 225 to 320 MHz. The centre frequency remains un-altered at 13.375 GHz over the BW range.

Fig. 4.15 depicts the 3D model of the proposed BW reconfigurable High-Q WG filter. Inter-resonator and input/output couplings are realized using metal septa located in the E-plane of the WG. BW reconfigurability is achieved by linearly moving the two metal inserts (modified sidewall) referred to as "tuning elements". The linear movements of the two tuning elements provide the flexibility to tune the absolute BW without altering the center frequency of the filter.

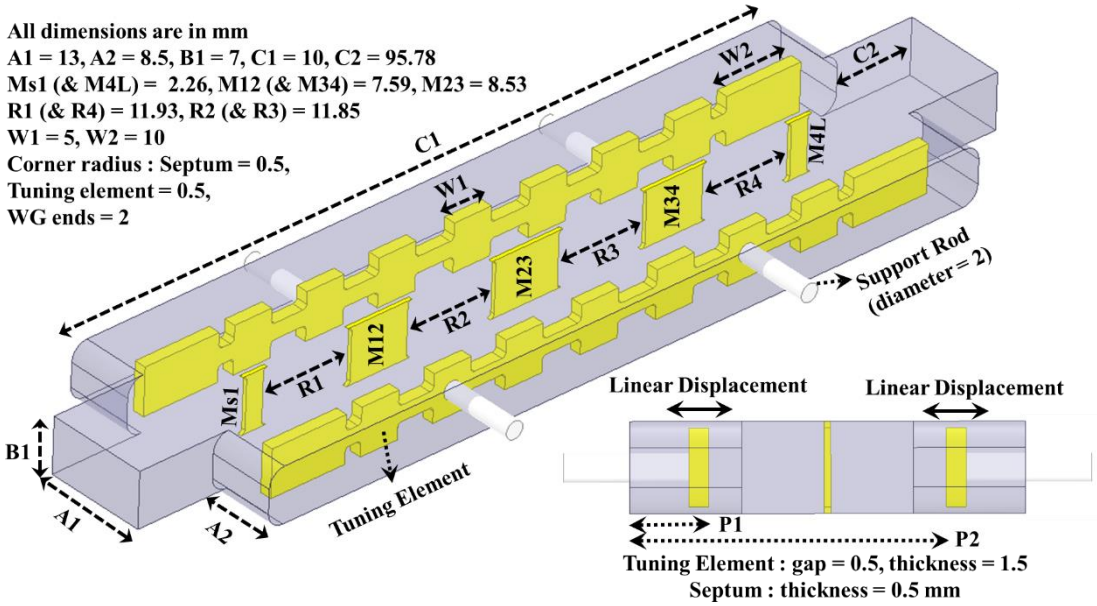

Fig. 4.15: Schematic of the proposed High-Q BW reconfigurable WG filter. Positions P1 and P2 of the tuning elements are altered to tune the BW.

Fig 4.16 depicts an ideal WG cavity to illustrate the variation of the physical coupling co-efficient of an E-plane metal septum as the side walls of the WG cavity are linearly displaced. The linear displacements of the side walls effectively change the location of the metal septum within the WG, and hence change the coupling values which lead to BW variations. As expected, coupling is minimum when the septum is at the center of the WG and coupling increases as the septum approaches either of

the side walls of the cavity. Thus, two tuning elements with linear displacement mechanisms are sufficient to change all the coupling values and hence the BW in the proposed WG filter.

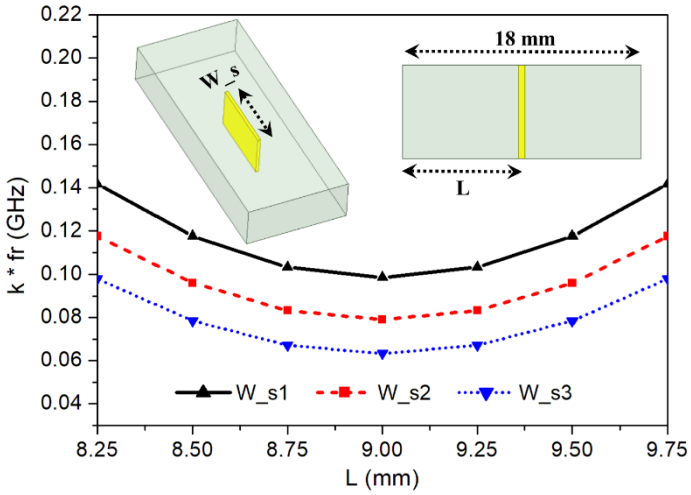

Fig. 4.16: Impact of septum position on the coupling value (k : physical coupling coefficient, fr : resonant frequency, W_s1 < W_s2 < W_s3)

With regards to the impact of resonator loading (i.e. shift in the resonant frequency due to changes in coupling values) Fig. 4.17 depicts the loaded resonant frequency of metal septum versus coupling. It can be seen that the loaded resonance frequency remains uniform over a wide range of coupling values. To highlight this unique feature of septum filters, Fig. 4.17 also depicts the variation of the loaded frequency in case of inductive iris filters. It is noted that the loaded resonance frequency varies significantly in this case with the change in the coupling values.

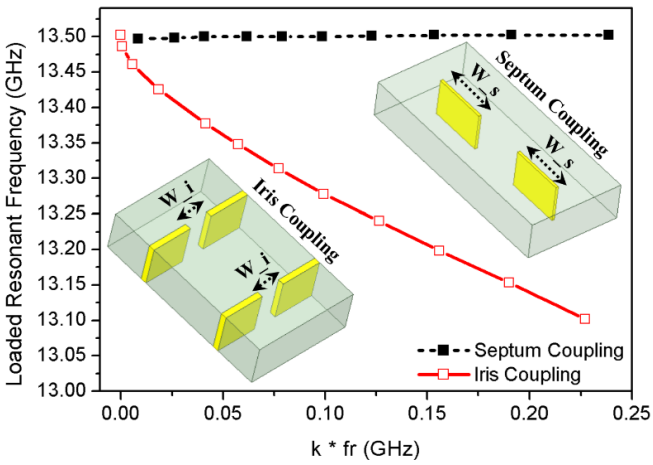

Fig. 4.17: Resonator Loading: Impact of coupling structure on the resonant frequency of a loaded resonator (septum width W_s varied from 25 to 10 mm, iris width W_i varied from 0.5 to 4.25 mm)

Hence, inherently an E-plane metal septum filter is robust to resonator loading impact caused by coupling variations. As a result, no additional tuning elements to correct each of the loaded resonators are required. Thus, the proposed BW reconfigurable filter requires only two tuning elements to tune the BW while maintaining the same center frequency irrespective of the filter order.

For practical implementation, the tuning elements have an air gap of 0.5 mm between top and bottom metal walls. The tuning elements are shaped to push the spurious resonant modes (resulting from air gap) out of the required band [37]. Fig. 4.18 depicts the simulated reflection co-efficient (S_{11}) and transmission co-efficient (S_{21}) of the proposed filter. Insertion loss of the filter varies from 0.25 dB (at 315 MHz) to 0.37 dB (at 210 MHz). The filter is designed using the coupling matrix approach [2] and simulated using a 3D Electro-Magnetic ANSYS HFSS [33].

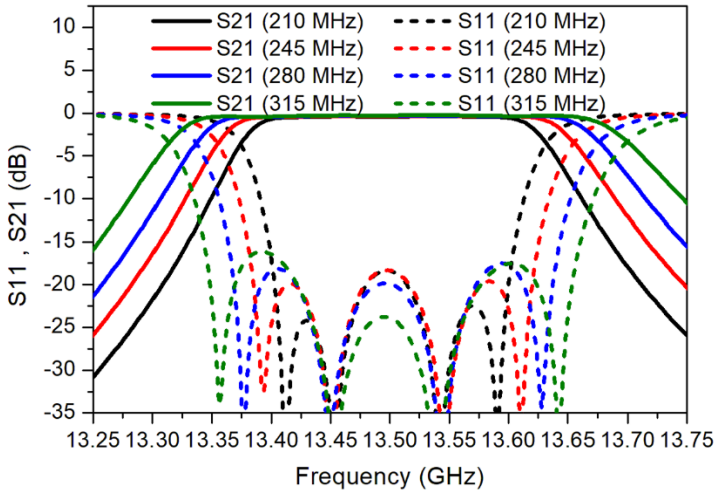

Fig. 4.18: Simulated S_{11} and S_{21}: Referring to Fig. 4.15 (BW in MHz, P1 in mm, P2 in mm) : (210, 6.0, 24.00), (245, 7.0, 24.82), (280, 7.5, 25.14), (315, 8.0, 25.44)

Fig. 4.19 depicts the photograph of the fabricated prototype filter (dis-assembled and assembled). The filter is made from aluminum. M2.5 dowel pins and screws are used for alignment and assembly of the filter. M2 threaded Nylon screws are used as support rods (Fig.4.15). Kapton tape is used at the WG ends to ensure the presence of air gap between tuning elements and WG sides. Compression springs are used over the support rods to precisely adjust the linear displacements of the tuning elements. The measured S_{11} and S_{21} results of the BW reconfigurable prototype filter are depicted in Fig. 4.20. Insertion loss of the filter varies from 0.56 dB (at 320 MHz) to 0.83 dB (at 225 MHz). Measured spurious response of the filter is shown in Fig. 4.21(a). Measured group delay response is shown in Fig. 4.21(b). Table 4.2 compares the proposed BW reconfigurable High-Q filter with other approaches.

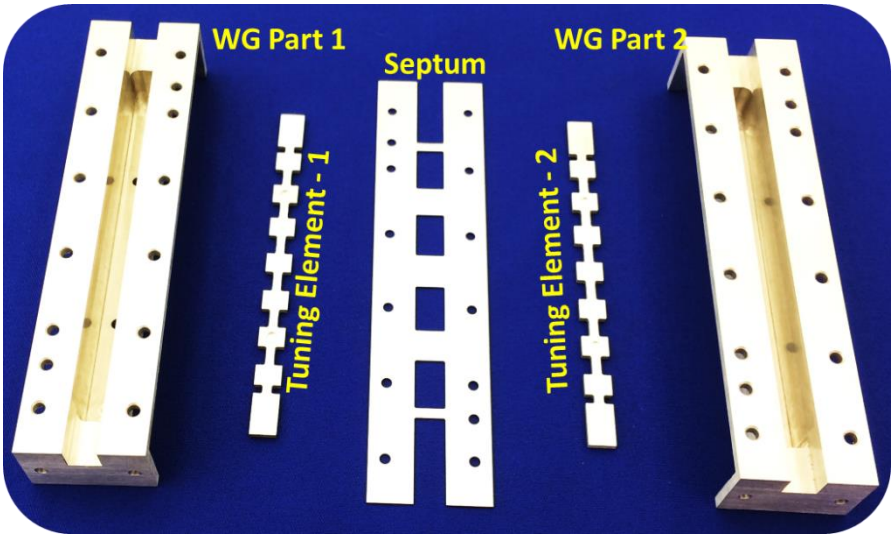

(a) Dis-assembled filter

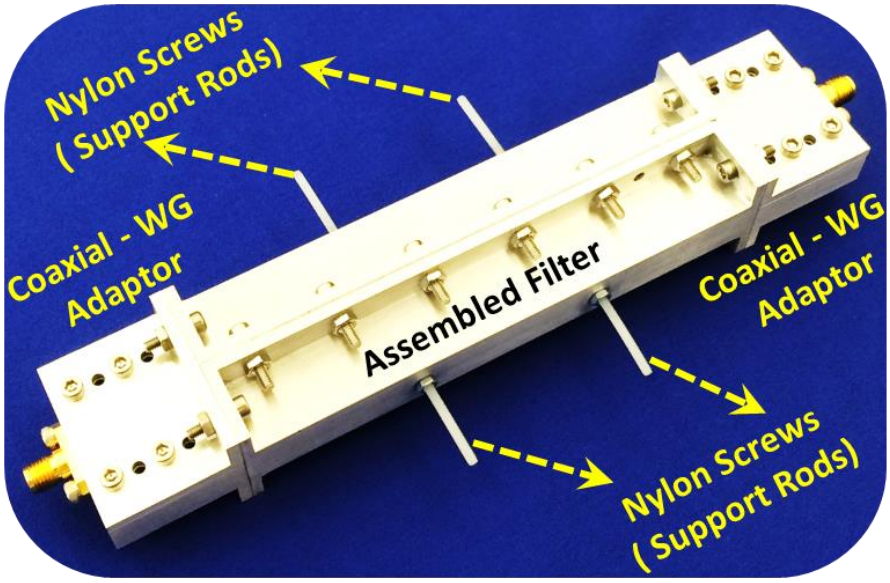

(b) Assembled filter

Fig. 4.19 Photograph of the prototype filter

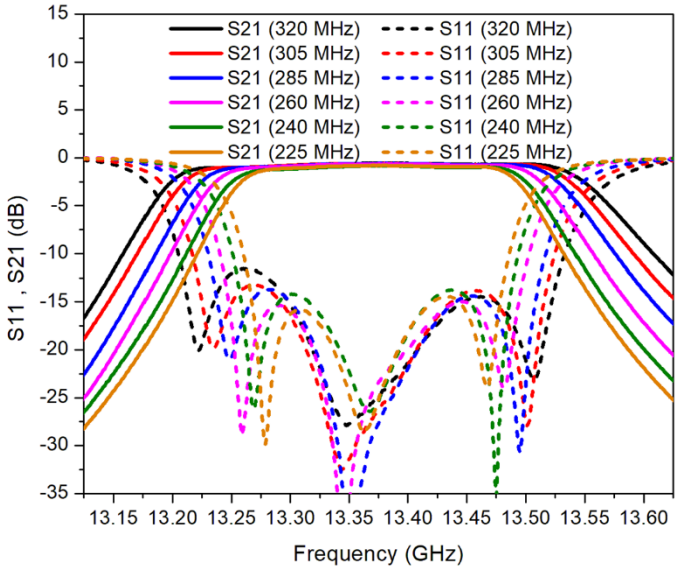

Fig. 4.20: Measured results: reflection co-efficient (S_{11}) and transmission co-efficient (S_{21})

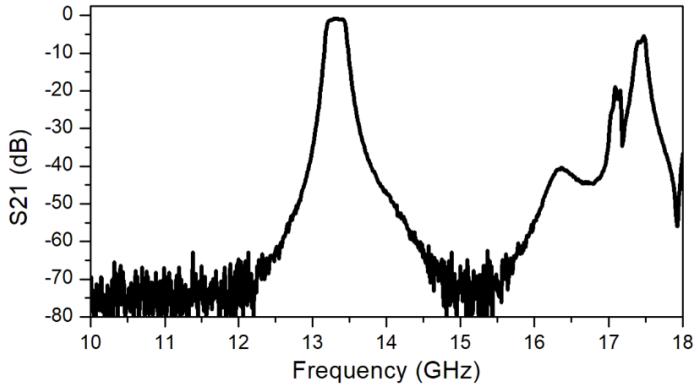

Fig. 4.21(a): Measured results: spurious response

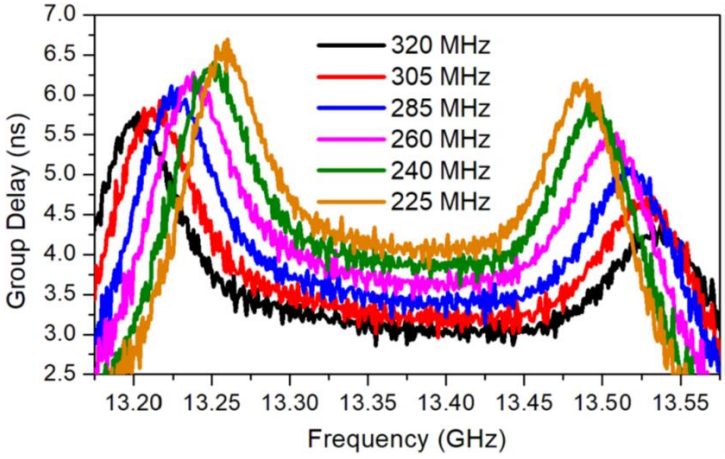

Fig. 4.21(b): Measured results: group delay response

Table 4.2: Comparison of BW Reconfigurable High-Q Filters

Ref.	Tech.	Order (N)	Fc (GHz)	BW var. in MHz	Num. of Tuning
[14]	Circ. WG	4	19.850	54 to 72 (29 %)	5 (N + 1)
[36]	Circ. WG	2	11.200	26 to 52 (67 %)	2 (0.5N + 1)
tw	Rect. WG	4	13.375	225 to 320 (35 %)	2 (ind. of N)

Ref. : reference, tw : this work, Tech. : technology, Fc : centre frequency, var. variation, Num. : number, ind. : independent.

4.4 Frequency Reconfigurable Dual Mode Filter

This section presents a frequency reconfigurable dual-mode WG filter with elliptic response. The proposed filter maintains a constant absolute BW and a constant rejection BW (i.e. constant frequency spacing between transmission zeros) over the tuning range. Furthermore, the filter can be tuned using a single tuning mechanism. A 4th order prototype filter at 11.5 GHz with 50 MHz bandwidth and two symmetric transmission zeros (± 45 MHz) is fabricated and measured. A dual-mode rectangular waveguide cavity is adopted to design the proposed frequency reconfigurable filter with transmission zeros. Such a dual-mode cavity resonator has inherent benefits of realizing transmission zeros using virtual negative coupling through iris coupling structures [2]. Fig. 4.22 depicts the schematic of the proposed 4th order frequency reconfigurable filter with two dual-mode cavities, while Fig. 4.23 depicts the internal dimensions and coupling configuration of the filter. The filter is tuned using a common single tuning mechanism, which linearly displaces the position of metallic tuning element in each cavity, hence effectively tuning the cavity dimension ‘c’ as shown in Fig. 4.22 and Fig. 4.23.

IR Coupling

IR couplings M_{12} and M_{34} are realized using M1.6 mm screws at 45 degrees as shown in Fig. 4.22 and Fig. 4.23. The screw depth controls the coupling strength, while its position (along ‘c’ dimension) determines the flatness of normalized coupling co-efficient, which is essential for maintaining a constant absolute BW [2]. Rectangular slot between the cavities provides the IR coupling M_{23}. The slot position (along ‘c’ dimension) determines the coupling flatness. The circular slot between the cavities provides the IR coupling M_{14} essential for realizing transmission zeros. It is strategically located (position along ‘c’ dimension) to allow for coupling flatness in order to maintain a constant frequency spacing between the transmission zeros over the tuning range.

IO Coupling

IO couplings M_{S1} and M_{4L} are realized using SMA probes. Two degrees of freedom (pin length and probe position along 'c' dimension) enable to realize a constant peak reflection group delay over the tuning range which is essential for maintaining a constant absolute BW [2].

To tune the filter, the tuning element in each cavity is linearly displaced using a common single tuning mechanism. To enable for friction free movement between the tuning element and the cavity walls, an air gap of 0.5 mm is provided (Fig. 4.23). However, such an air gap results in undesired spurious resonance modes within the desired frequency range. Hence, the tuning element is shaped to push the spurious resonance modes outside the frequency band of operation. Dielectric screw (Nylon or PTFE) is used to support the tuning element and connects it to the tuning mechanism.

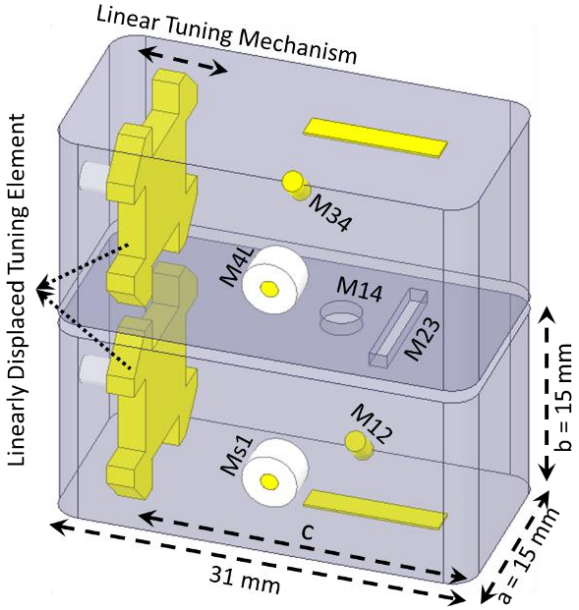

Fig. 4.22: Schematic: Proposed frequency reconfigurable waveguide filter with elliptic response

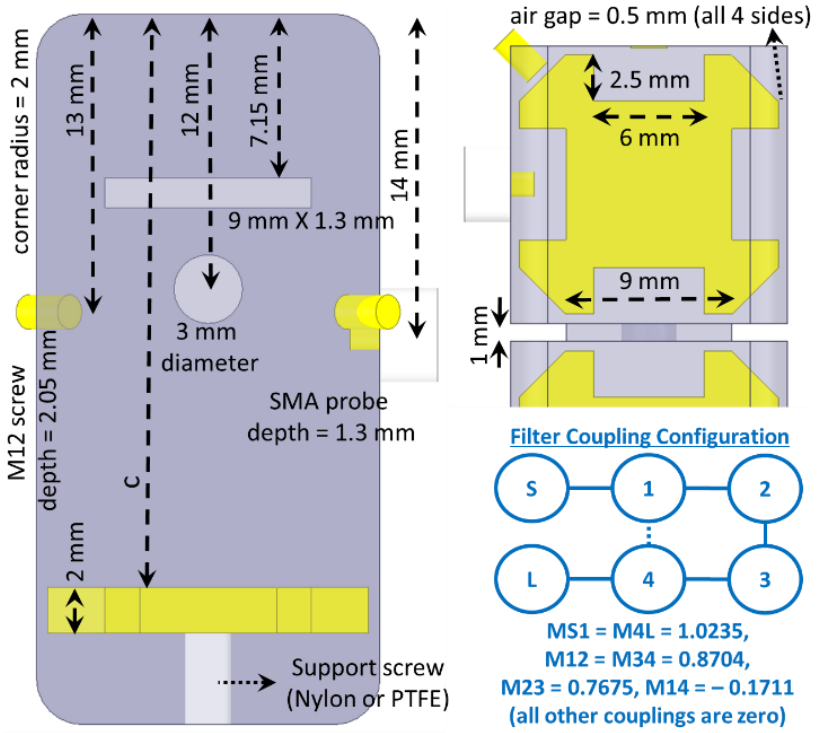

Fig. 4.23: Schematic: Internal dimensions and coupling configuration

Fig. 4.24 and Fig. 4.25 depict the simulated transmission co-efficient (S_{21}) and reflection co-efficient (S_{11}) of the filter as the tuning element is linearly displaced, respectively. The simulated tuning range of the filter is 600 MHz from 11.4 GHz to 12 GHz. Fig. 4.26 plots the absolute BW (S_{11} < -15 dB) over the tuning range, and the variation is within ±1 MHz (between 42 MHz and 44 MHz) over the entire 600 MHz tuning range. Rejection bandwidth is also depicted in Fig. 4.26. It is worth mentioning here that the key feature of the proposed frequency reconfigurable filter is that the rejection BW is nearly constant. As observed in Fig. 4.26, the variation of frequency spacing between the transmission zeros is well within ±2 MHz (between 81.6 MHz and 84.6 MHz) over the entire tuning range. Insertion loss variation is within ±0.05 dB (between 0.79 dB to 0.85 dB) over the tuning range. The simulated Q of the resonator is better than 6000 using aluminum cavity. ANSYS HFSS is used for 3D Electro-Magnetic (EM) simulation [33].

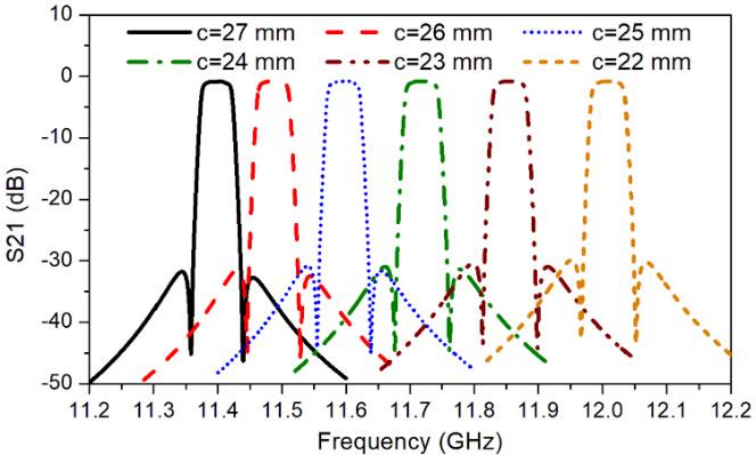

Fig. 4.24: Simulated transmission co-efficient

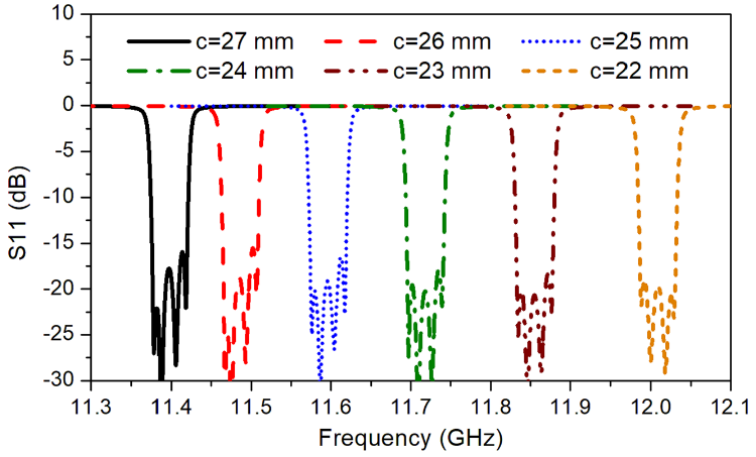

Fig. 4.25: Simulated reflection co-efficient

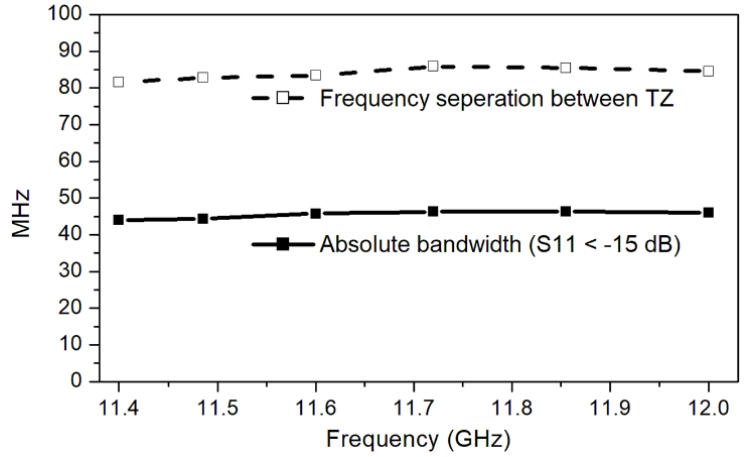

Fig. 4.26: Simulated absolute BW and rejection BW

Fig. 4.27 shows the photograph of the filter parts fabricated using aluminum and the assembled filter. M2.5 screws are used to assemble the filter parts. Silver plated M1.6 screws are used for M_{12} and M_{34} coupling screws. Fig. 4.28 and Fig. 4.29 depict the measured S_{21} and S_{11} of the prototype filter, respectively. The measured tuning range of the filter is 390 MHz from 11.285 GHz to 11.675 GHz. Fig. 4.30 plots the measured absolute BW (S_{11} < -15 dB) over the tuning range, and the variation is within ±1 MHz (between 48 MHz and 50 MHz) over the entire 390 MHz tuning range. The rejection bandwidth is also depicted in Fig. 4.30. The variation of frequency spacing between the transmission zeros is well within ±2 MHz (between 88 MHz and 92 MHz) over the entire tuning range. Insertion loss variation is within ±0.2 dB (between 1.4 dB and 1.8 dB) over the tuning range. Fig. 4.31 shows the measured response over a wide frequency range depicting the spurious separation better than 2 GHz.

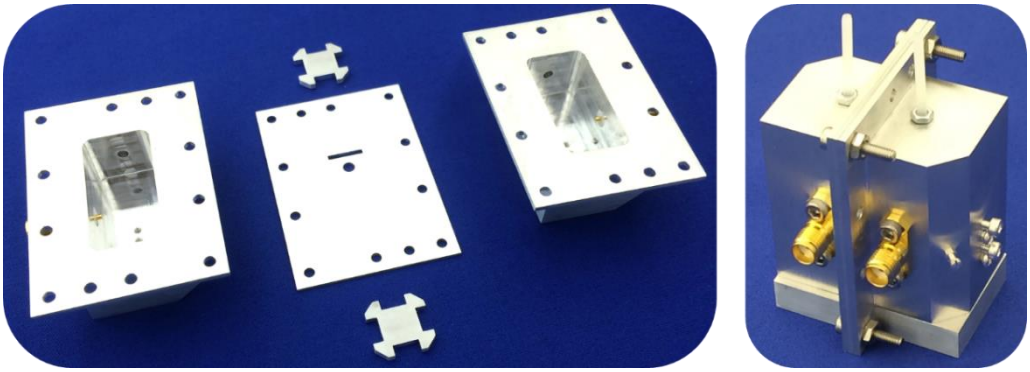

Fig. 4.27: Photograph of prototype filter - fabricated parts and assembled filter

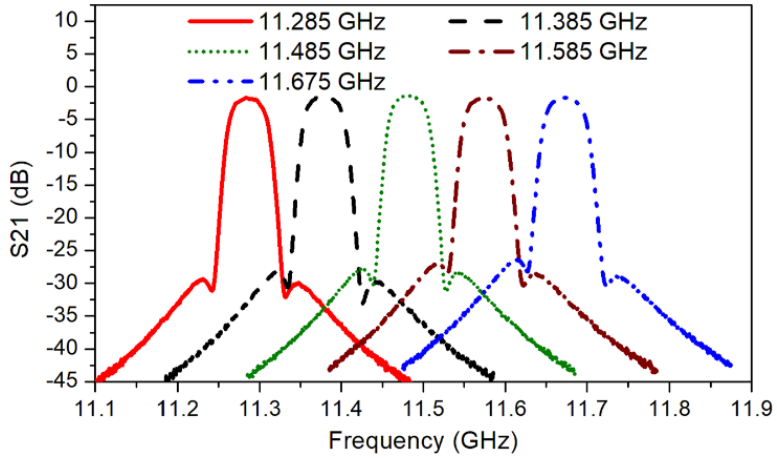

Fig. 4.28: Measured transmission co-efficient

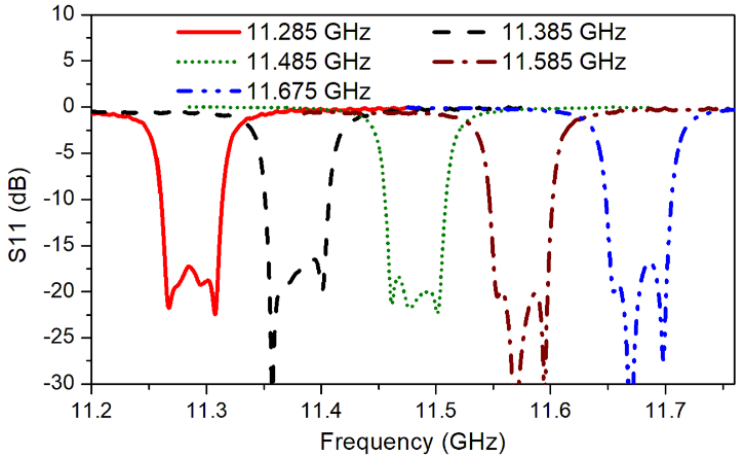

Fig. 4.29: Measured reflection co-efficient

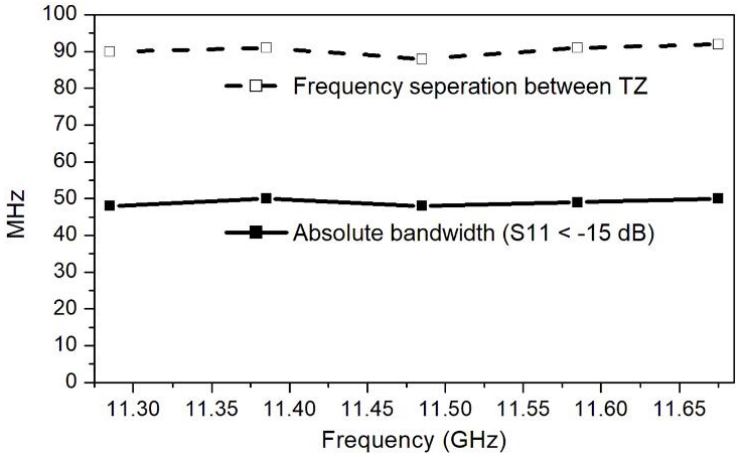

Fig. 4.30: Measured absolute BW and rejection BW

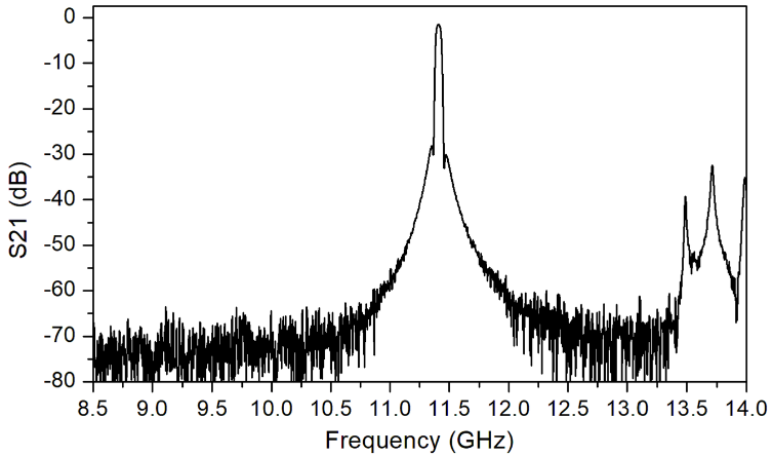

Fig. 4.31: Measured spurious performance

The prototype filter unit is constructed from aluminium cavities and is designed with a bandwidth of 50 MHz, i.e. a fractional bandwidth of 0.43%. With a Q of 6000 the insertion loss of such narrow band filter should not exceed 2 dB over the 50 MHz bandwidth. The higher loss observed in this prototype unit is attributed predominantly to the unintended surface roughness of the middle filter part which incorporates the rectangular and circular slots. In-addition, the usage of Kapton tape to ensure the 0.5 mm air gap between the tuning element and the cavity walls, has also contribute to the increased loss. Certainly, silver plating the filter will help in improving the loss. In addition, an exact assembly workmanship of a tuning mechanism integrated to filter housing will improve insertion loss and minimize deviations from theoretical simulations.

4.5 Conclusion

This chapter has presented three novel filter structures:

- A novel configuration for a High-Q tunable WG filter with a constant absolute BW. The key feature of this filter is that it is tuned by a single tuning element. The variation of the IO coupling and IR coupling of the single septum and double septa filters with filter center frequency has been investigated. The analysis has revealed that double septa with optimized dimensions are optimum to realize a constant absolute BW over a relatively wide tuning range. A detailed design methodology has been presented for proper selection of the optimum offset dimensions of the double septa. An investigation of the shape of the metal insert tuning element on the filter spurious performance has been also presented. Measured results are presented for a Ku-band tunable filter achieving a constant absolute BW over a tuning range of 15%. The filter promises to be useful in emerging 5G millimeter-wave applications where the filter size is very small to accommodate many mechanical tuning elements.
- A novel configuration of a BW reconfigurable WG filter that uses only two tuning elements irrespective of the filter order. The proposed filter configuration demonstrates that it can achieve relatively wide BW variations without deviating the center frequency. A four-pole prototype filter is designed, fabricated, and tested at the Ku-band. The measured BW tunability of the filter is nearly 35% from 225 to 320 MHz at 13.375 GHz. To the best of our knowledge, this is the only BW reconfigurable filter that can be tuned with only two tuning elements regardless of the filter order.
- A novel configuration for a high-Q dual-mode frequency reconfigurable waveguide filter with elliptic response. The filter maintains a constant absolute bandwidth and a constant rejection

bandwidth (frequency spacing between transmission zeros) over the tuning range. The key additional feature of this filter is that it is tuned by a single tuning mechanism, which linearly displaces the tuning element. In-addition, the proposed design methodology can be scaled to realize higher order filters with additional transmission zeros (e.g. an 8th order filter with 4 transmission zeros). The proposed filter promises to be useful in a wide range of telecommunication applications including flexible payload in aerospace applications.

Chapter 5
Tunable Coaxial Filters

5.1 Introduction

This chapter presents two novel filter configurations:

- A novel configuration for a high-Q tunable coaxial filter employing λ/2 resonators, which is tuned by a single rotational tuning element. The proposed filter has low variations in the absolute BW and insertion loss (IL) over a relatively wide tuning range. A prototype four-pole filter is developed at 2.5 GHz with a fractional BW of 4% to verify the concept. The measured tuning range of the filter is 20%, within which the BW variation is better than ±10% and IL variation is better than 0.05 dB. The proposed concept is easily expandable to filters with higher order. Furthermore, the concept is adopted to design a tunable diplexer which can be tuned using a single tuning mechanism. The proposed High-Q tunable filter is promising for use in the frequency-agile communication architecture at the cellular base-station and aerospace applications.
- A novel configuration for a High-Q coaxial tunable filter using λ/4 resonators, employing a single rotational mechanism to tune the filter, while achieving a constant absolute bandwidth. A prototype filter is designed for the proof of concept, with a bandwidth of 1.5% demonstrating a bandwidth variation of less than 700 KHz over a tuning range from 685 MHz to 770 MHz. The proposed design methodology can be scaled to realize higher order filters. The proposed filter promises to be useful in a wide range of telecommunication applications including flexible payload in aerospace applications.

5.2 Frequency Reconfigurable λ/2 Resonator Filter

Typically, λ/4 resonators are predominantly used in realizing coaxial filters owing to superior spurious performance, which is nearly at three times the frequency of operation [2], [12], [13], [19], [20] and [25]. Such a filter can be mechanically tuned by varying the capacitance between metallic post and filter housing as depicted in Fig. 5.1(a). However, one of the major issues with such a topology is that for a given linear movement the frequency shift achieved by each loaded resonator is different due to different loading. This inevitably requires an independent tuning element for each resonator.

The proposed λ/2 resonator with elliptic casing depicted in Fig. 5.1(b) addresses this crucial issue by de-coupling the loading mechanism with tuning mechanism. It provides flexibility to achieve independent capacitance variation and hence same frequency shift for each of the loaded resonator. Electric field distribution within the resonator at extreme rotation angles is depicted in Fig. 5.1(c) and Fig. 5.1(d). As seen from Fig. 5.2(a), the axes ratio determines the frequency tuning range for a fixed post length. The ratio of minor axis to major axis of an ellipse is referred to as "axes ratio" within this thesis. Simulated Q is better than 4800 over the entire tuning range using aluminum for post and elliptic cavity as shown in Fig. 5.2(b).

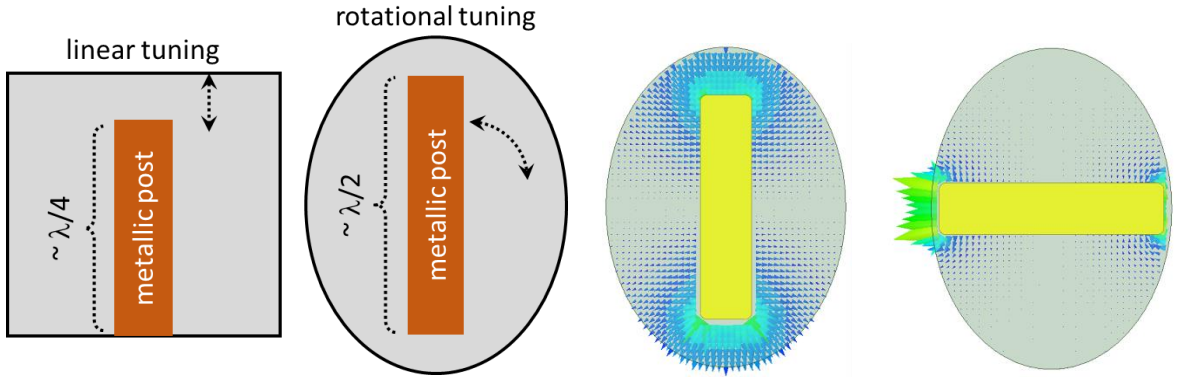

(a) (b) (c) (d)

Fig. 5.1: Coaxial Resonator: (a) Conventional λ/4 Resonator with Linear Tuning, (b) Proposed λ/2 Resonator with Rotational Tuning, (c) Electric Field Distribution at 0 deg, (d) Electric Field Distribution at 90 deg

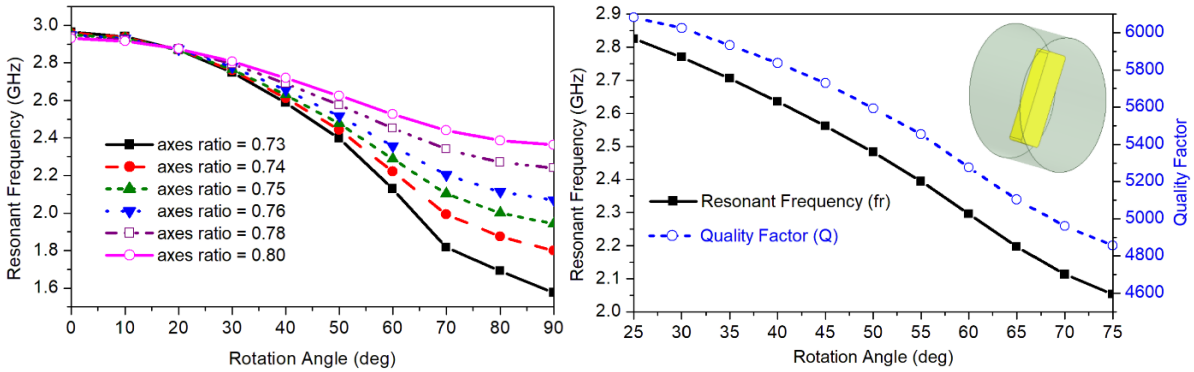

(a) (b)

Fig. 5.2: Proposed Resonator: (a) Impact of Axes Ratio on Tuning Range, (b) Resonant Frequency and Quality factor with Rotation Angle

IR Coupling

As discussed in section 4.1, one of the important criteria to be satisfied while designing tunable filters with constant absolute BW is that the $k_{ij}f_r$ product should be maintained constant over the tuning range [2],[34]. In the proposed filter, an elliptic iris opening is utilized to realize the required IR coupling. An elliptic iris has two degrees of freedom, namely, major axis and minor axis. Fig. 5.3(a) plots the family of $k_{ij}f_r$ product by parametrically varying axes ratio for a fixed major axis (= 25 mm). It can be observed that an axes ratio of 0.85 provides a constant $k_{ij}f_r$ product over the tuning range. Fig. 5.3(b) plots the family of $k_{ij}f_r$ product by parametrically varying major axis for a fixed axes ratio (= 0.85). Hence, by adopting an appropriate axes ratio, the criteria of constant $k_{ij}f_r$ product can be achieved. The value of IR coupling itself can then be controlled by selecting a suitable major axis.

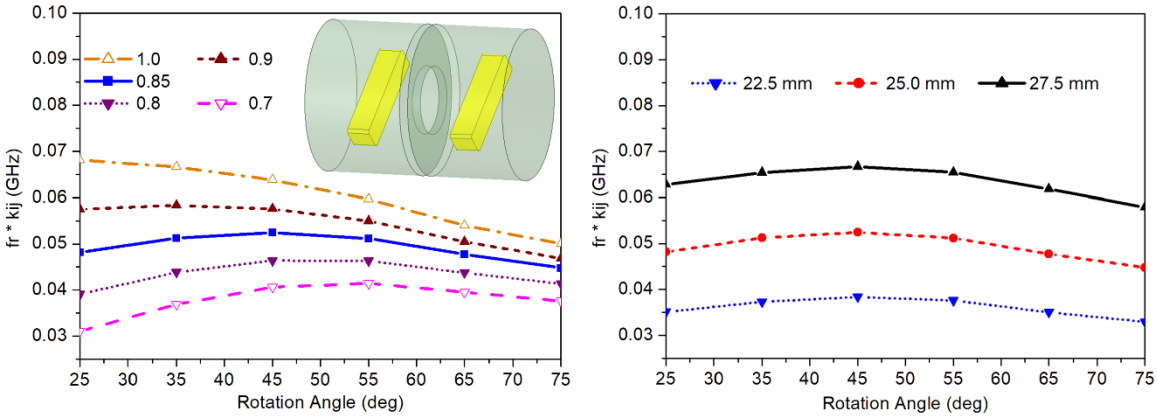

(a) (b)

Fig. 5.3: IR coupling with Elliptic Iris: (a) Axes Ratio Variation, (b) Major Axis Variation

IO Coupling

The other important criteria to be satisfied while designing tunable filters with constant absolute BW is, a constant peak reflection group delay w.r.t to f_r over the tuning range [2],[34]. In the proposed filter, a shaped metallic probe is utilized to realize the required IO coupling. The shaped probe has three degrees of freedom namely probe angle, gap and the position. To start with, the probe position and gap are varied to realize the desired IO coupling at the centre of the tuning range. Following which, the probe is gradually extended on circular arcs on either side to realize the desired IO couplings over the entire tuning range. Fig. 5.4 plots the reflection group delay realized using the shaped probe over the tuning range.

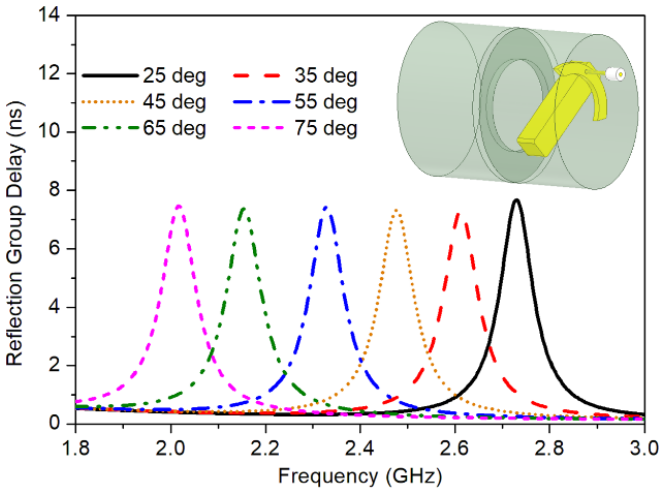

Fig. 5.4: IO Coupling with Shaped Probe

One of the important practical challenges in designing a tunable filter with single tuning mechanism is to absorb the impact of loading on the resonant frequency of each resonator. A widely adopted approach is to re-adjust the resonator dimensions such that all of the loaded resonators resonate at the same frequency [2]. Such an approach can be effectively utilized for a fixed frequency design but cannot absorb the loading impact on the resonators over the entire tuning range in a tunable filter. This is the primary reason which mandates the requirement of an independent tuning mechanism for each resonator in the reported High-Q tunable filters [12]–[21]. In other words, the tuning elements for the resonators have to be adjusted by different amount for each resonator at each frequency. This is also the primary reason for using different ramp (or slope) for each of the resonator tuning element in the reported tunable coaxial filter [25]. The issue of resonator loading becomes even more prominent as the tuning range increases.

Resonator Loading

Hence, one of the research goals is to find a robust solution to absorb the crucial impact of resonator loading. This important practical issue is effectively addressed in the proposed resonator, which provides the flexibility to realize independent capacitance variation for each of the loaded resonator at each frequency over the entire tuning range. Two methodologies can be adopted in the proposed resonator to effectively absorb the impact of resonator loading over the entire tuning range: fixed screw approach and generic polygon approach. A sophisticated method to address the same would be to utilize a generic polygon-based cavity (instead of elliptic cavity) which would provide higher degrees of freedom in designing the resonator cavity as shown in Fig. 5.5. However, a much simpler and effective

approach (which is also adopted for our hardware prototype filter) is to insert fixed screws in the elliptic cavity to provide independent capacitance variation for each of the loaded resonator at each frequency over the entire tuning range. Furthermore, the fixed screw approach is a robust approach to deal with fabrication and assembly tolerances.

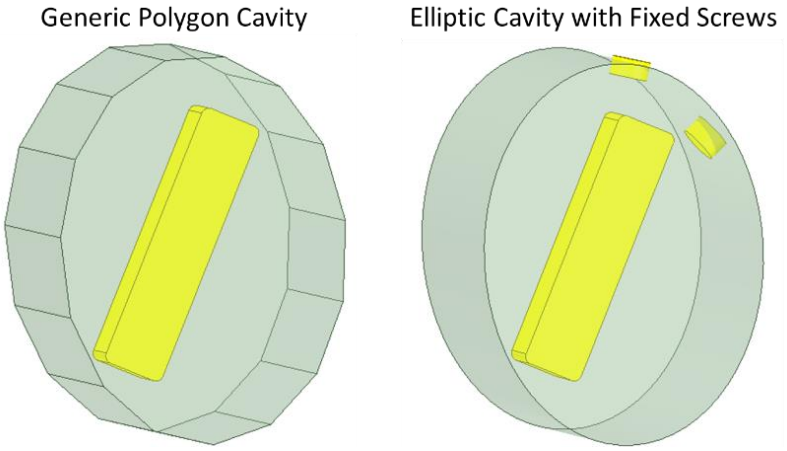

Fig. 5.5: Resonator Loading: Generic Polygon and Fixed Screw

For prototyping, a 4th order Chebyshev tunable coaxial filter is designed at 2.5 GHz with a fractional BW of 4% (100 MHz). Fig. 5.6(a) depicts the internal 3D model of the proposed tunable filter. The required IR couplings are realized using elliptic iris openings between successive resonators. The required IO coupling is realized using a shaped probe connected to SMA connector as shown in Fig. 5.6(b). Tuning mechanism is realized using a PTFE (or plastic) rod along the axis of the filter. The half-wavelength resonator posts are mounted on the PTFE rod. On rotating the rod, the resonator posts rotate, which varies the capacitance between the post and the elliptic casing, thus changing the frequency response of the filter. It is worth mentioning here that the IR coupling using elliptic iris provides the necessary opening for the tuning rod along the axis of the filter, there by significantly simplifying the tuning mechanism. To absorb the impact of resonator loading, fixed screws are adopted within the elliptic cavity in the prototype filter. Fixed screws t1 to t4 enable the resonant frequency of loaded resonators to overlap with each other over the entire tuning range. Fig. 5.7 plots the resonant frequencies, with and without the fixed screws. It can be observed that when screws are not employed (Fig. 5.7(a)) the loading impact is absorbed only at the center of tuning range. Whereas, by employing fixed screws (Fig. 5.7(b)) the loading impact can be absorbed over the entire tuning range.

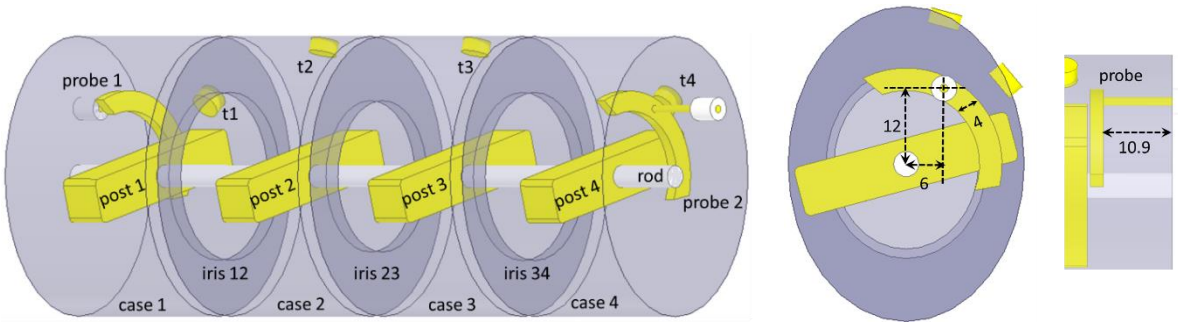

(a) (b)

Fig. 5.6: Tunable Coaxial Filter Prototype: (a) Schematic 3D Model, (b) IO Coupling Details

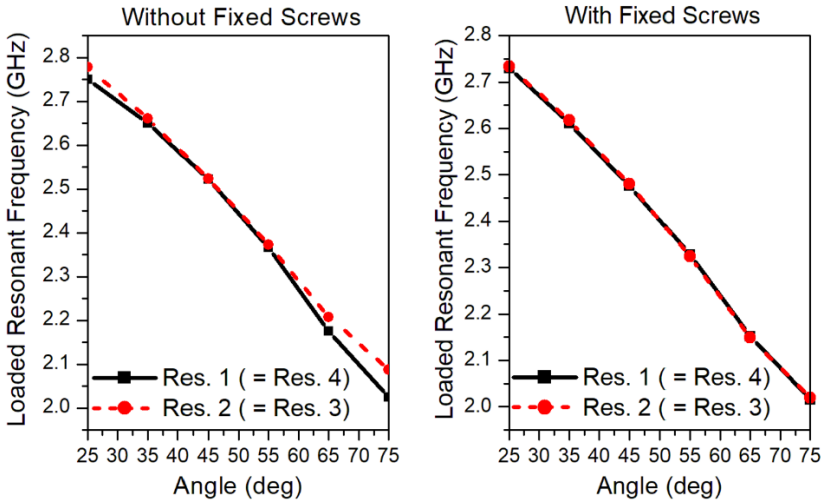

(a) (b)

Fig. 5.7: Resonator Loading: (a) Without Fixed Screws, (b) With Fixed Screws

The prototype filter is designed using the coupling matrix approach and simulated using HFSS [2],[33]. Fig. 5.8 depicts the simulated transmission co-efficient (S_{21}) and reflection co-efficient (S_{11}) of the filter as the tuning rod is rotated. Tuning range achieved by the filter is around 700 MHz from 2.035 GHz to 2.735 GHz. Fig. 5.9 depicts the absolute BW and IL over the tuning range. BW variation is within ±10% (min. = 85.6 MHz, max. = 103.3 MHz). The filter exhibits a peak IL better than 0.15 dB with a loss variation 0.02 dB.

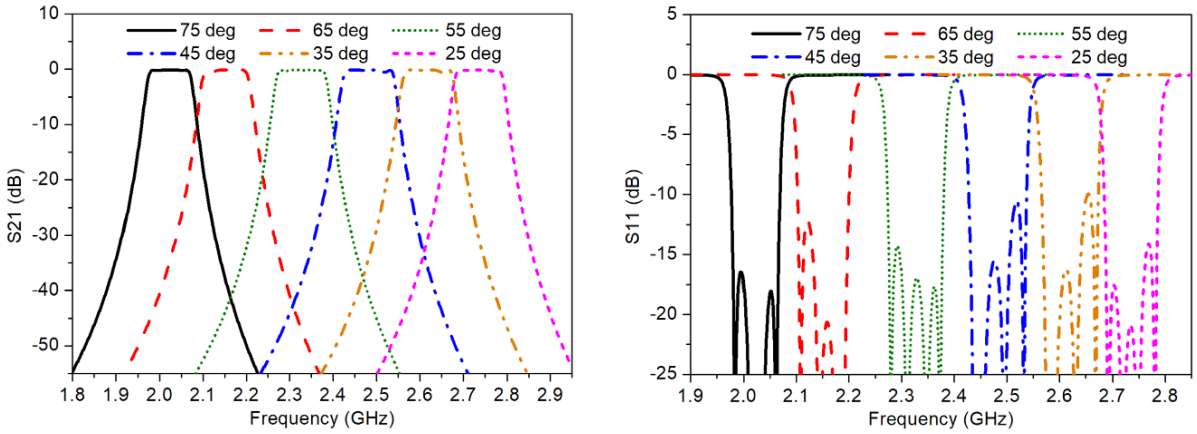

(a) (b)

Fig. 5.8: EM Simulated Response: (a) S_{21} (b) S_{11}

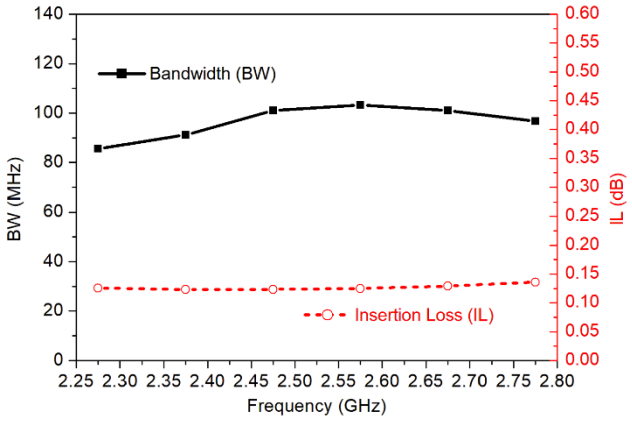

Fig. 5.9: Simulated BW and IL over the Tuning Range

Fig. 5.10 shows the hardware parts of the fabricated prototype. Filter casing, iris openings and resonator posts are fabricated using aluminum. The input-output circular-shaped probe is fabricated using copper and is mounted to SMA connector using silver epoxy. The tuning rod is made from rigid plastic. Two compatible ball bearings are used to support the tuning rod and to facilitate friction free rotation. Silver plated M5 screws (t1, t2, t3 and t4 in Fig. 5.6(a)) are used for one-time filter tuning and fixed thereafter. The housing cases are assembled using M4 screws, and two M4 dowel pins are used for fine alignment between each section. Fig. 5.10(b) shows the photograph of the assembled filter with control system.

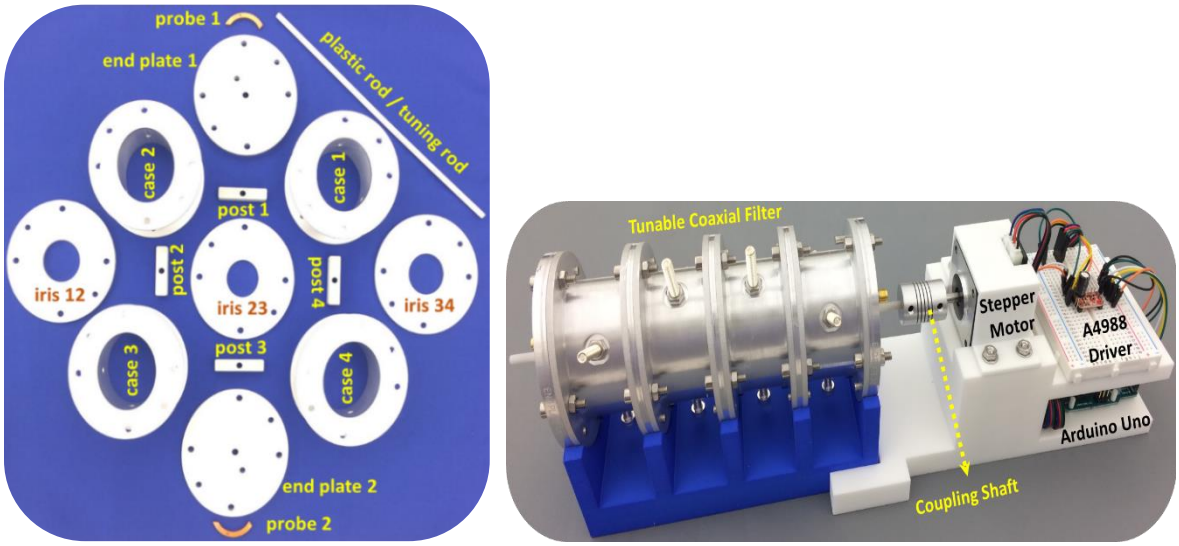

(a) (b)

Fig. 5.10 Fabricated Prototype: (a) Hardware Parts (b) Assembled Tunable Filter

A stepper motor-based control system is implemented to mechanically tune the proposed tunable coaxial filter. Alternatively, a servo motor can also be used since the application does not require complete 360 degree rotation. However, a stepper motor is adopted for simplicity and for precise control of step angle through micro-stepping. NEMA 17 bipolar stepper motor is used which has a step angle of 1.8 degree and holding torque of 26 Ncm. The motor is controlled using A4988 chip on an Arduino Uno platform [38]. A4988 is a stepper motor driver from Allegro Microsystem which has provisions for micro-stepping up to 1/16th of a step angle [39]. An open source “Processing” software is used to develop a GUI (Graphical User Interface) for the control system [40]. The GUI enables the user to precisely tune the coaxial filter. An added feature to control the frequency step size (of A4988 driver) is also implemented within the GUI. The software interacts with the Arduino Uno platform via serial port of a computer. A shaft coupling is used to integrate the plastic tuning rod (4 mm diameter) with the stepper motor shaft (5 mm diameter). Fig. 5.11 shows the photograph of the measurement setup.

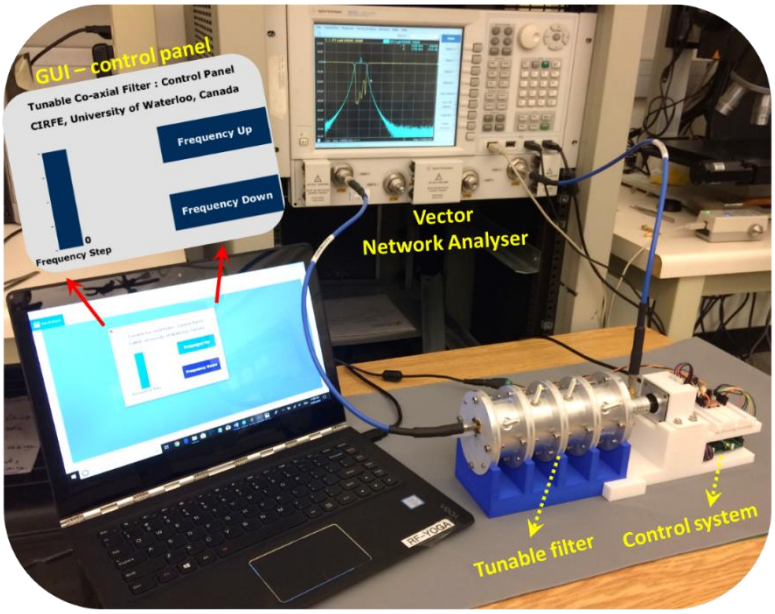

Fig. 5.11: Measurement Setup

Fig. 5.12 depicts the measured S_{21} and S_{11} of the tunable coaxial filter as the tuning rod is rotated. Fig. 5.13(a) depicts the measured absolute BW and IL over the tuning range. The measured tuning range achieved by the filter is 500 MHz from 2.275 GHz to 2.775 GHz. The measured BW variation is within ±10% (min. = 96.1 MHz, max. = 116.9 MHz) over the tuning range. Measured peak IL is better than 0.4 dB with a loss variation of 0.05 dB over the tuning range. Fig. 5.13(b) depicts the measured spurious response of the tunable coaxial filter. As expected, the spurious transmission is around twice the frequency of operation. However, the spurious response can further be improved by adopting a stepped-impedance variation of the metallic post [41].

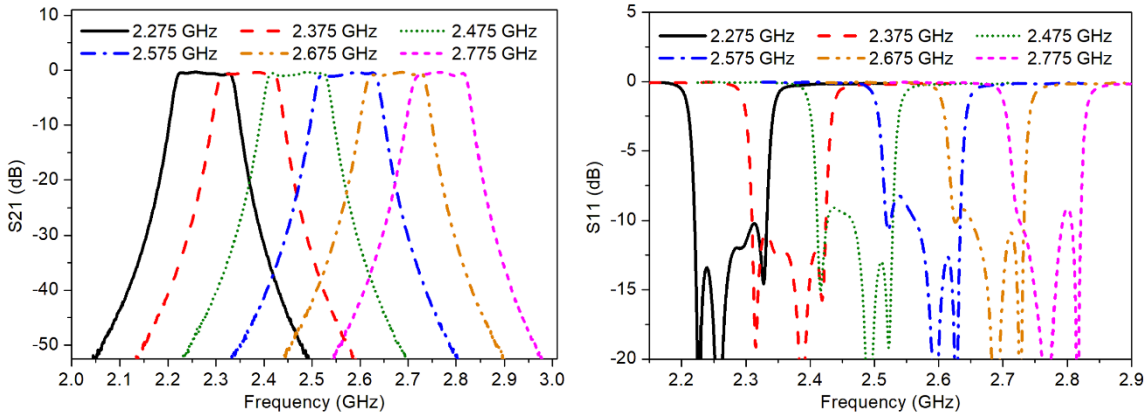

(a) (b)

Fig. 5.12: Measured Response: (a) S_{21} (b) S_{11}

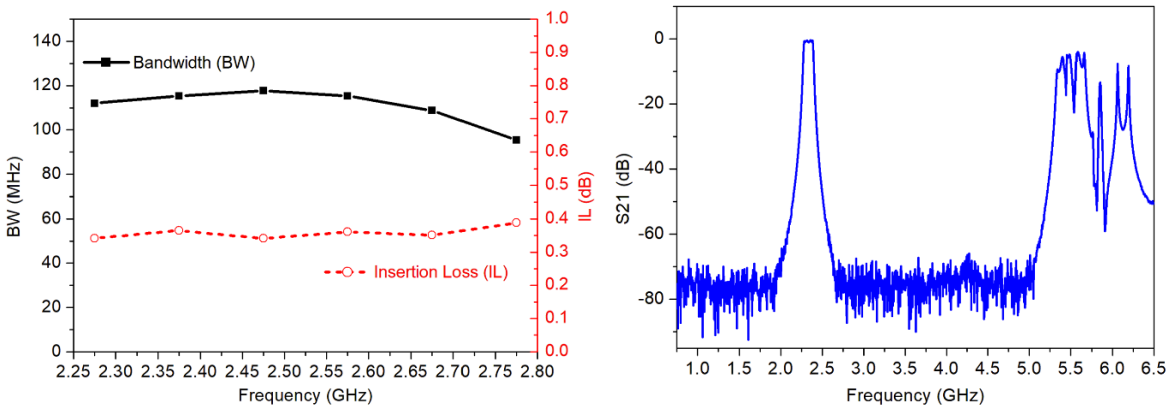

(a) (b)

Fig. 5.13: Measured results (a) BW and IL (b) Spurious Performance

It is important to note that though the prototype has some minor deviations from the simulated response, it is indeed very promising as a proof of concept. The deviations in frequency and tuning range is attributed to inexact assembly of tuning rod supported on ball-bearings in the filter housing. An exact assembly workmanship will significantly minimize these deviations. The higher measured IL is attributed to the rigid commercial plastic rod used for the prototype. Usage of low loss rigid dielectric material (like rexolite or ceramic) for tuning rod will minimize the deviation in IL. In-addition, silver plating of metallic posts will further improve IL of the filter. It is worth mentioning here that the methodology used for the design of the proposed tunable filter is easily scalable, i.e., the tuning mechanism is independent of the filter order. It is also worth mentioning here that by reducing the frequency mismatch between the resonators (caused by resonator loading) to within a fraction of BW, it is possible to further improve the return loss over the tuning range. This can be achieved by incorporating additional fixed screws. Since, the philosophy adopted in this work was rapid prototyping for the proof of concept, hence rigorous optimization with additional fixed screws to improve the return loss was not carried in the prototype. However for the sake of completeness, Fig. 5.14 shows the tunable filter with additional fixed screws and the corresponding improved S_{11}.

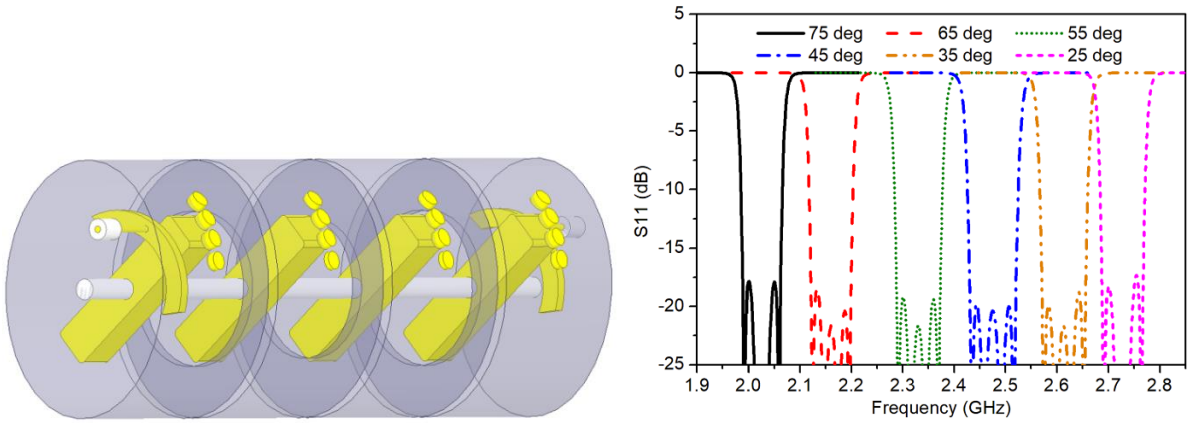

(a) (b)

Fig. 5.14: Enhancing Return Loss : (a) Additional Fixed Screws, (b) Improved S_{11}

It is also worth mentioning here that, in addition to tunable filter applications, the proposed concept also promises to be useful in reducing the production cost and delivery schedule of communication systems that usually use identical filters (or diplexers) with the exception of filter's centre frequency. The production cost can be significantly reduced by fabricating identical filter units ahead of time that can be easily reconfigured during the final production phase to fit the required frequency plan, offering a competitive delivery schedule. The proposed concept is easily expandable to filters with higher order. Furthermore, the proposed concept can be adopted to design a tunable diplexer which can be tuned using a single tuning mechanism. Table 5.1 compares the proposed tunable coaxial BPF with existing solutions in coaxial technology.

Table 5.1: Comparison of Proposed Tunable Coaxial BPF with Existing Coaxial Solutions

Ref.	Tech.	Freq.	Q	Tun. Range	BW and Var.	Tun. Elem. and Mech.
[12]	coaxial	2.5 GHz	> 2250	400 MHz / (16%)	30 MHz / <±5%	N / robust
[13]	coaxial	3.6 GHz	> 5650	430 MHz / (12%)	75 MHz / <±5%	N / robust
[19]	coaxial	4.8 GHz	> 460	2.8 GHz /(1.8:1)	not constant	N / complex
[20]	coaxial	4.8 GHz	> 300	1.5 GHz /(1.4:1)	not constant	N / complex
[25]	coaxial	2 GHz	> 2000	360 MHz / (18%)	25 MHz / <±5%	2*N-1 / complex
tw	coaxial	2.5 GHz	> 4850	500 MHz / (20%)	100 MHz /<±10%	1 / robust

tw : this work

The proposed tunable filter concept can be adopted in designing a tunable diplexer, which can be tuned using a single tuning mechanism by rotating a common tuning rod for both filters. One might think that a tunable filter with a wider tuning range itself can be potentially used for both the upper and lower frequency bands of the tunable diplexer, where the starting orientation of metallic posts in one filter is aligned differently from the other filter. However, such a diplexer would have varying frequency separation over the tuning range. This is because, referring to Fig. 5.2, the frequency variation of the tunable filter with respect to the rotation angle is not perfectly linear. Though the linearity of tuning mechanism would not impact the operation of the tunable filter itself, it does impact the frequency separation in a tunable diplexer if the same filter is used for both bands.

To address this issue, two separate tunable filters are used, each dedicated to upper and lower bands, thus enabling same frequency separation as the diplexer is tuned using a common tuning rod. The prototype tunable filter is used for the higher frequency band. Another fourth-order Chebyshev tunable coaxial filter with a BW of 120 MHz is designed for the lower frequency band, which has a tuning range of 700 MHz from 1.79 to 2.49 GHz. Fig. 5.15 shows the 3-D model of the tunable diplexer using separately designed filters for upper and lower bands. The diplexer has a common tuning rod, and hence can be tuned using a single rotating mechanism. Figs. 5.16 and 5.17 show the simulated responses of the tunable diplexer at either end of the tuning range. It can be observed that the tunable diplexer now maintains a consistent frequency separation between the frequency bands over the tuning range. The diplexing junction is a co-axial T-junction where the lengths are designed based on the phase match condition. The phase change is reasonably low over the entire frequency band, and hence the junction provides a reasonably good return loss over the frequency band. Further improvement in return loss for the diplexer unit can be achieved by rigorous optimization of junction parameters namely: junction lengths, input couplings of higher and lower band filters (only those toward junction), and the resonator centre frequencies. In applications requiring independent frequency control for the filters, a tunable diplexer with two tuning mechanisms, each dedicated to a filter, can also be realized. Similarly, the proposed tunable filters can be effectively utilized in designing tunable multiplexers, when using a separate rotary mechanism for each channel.

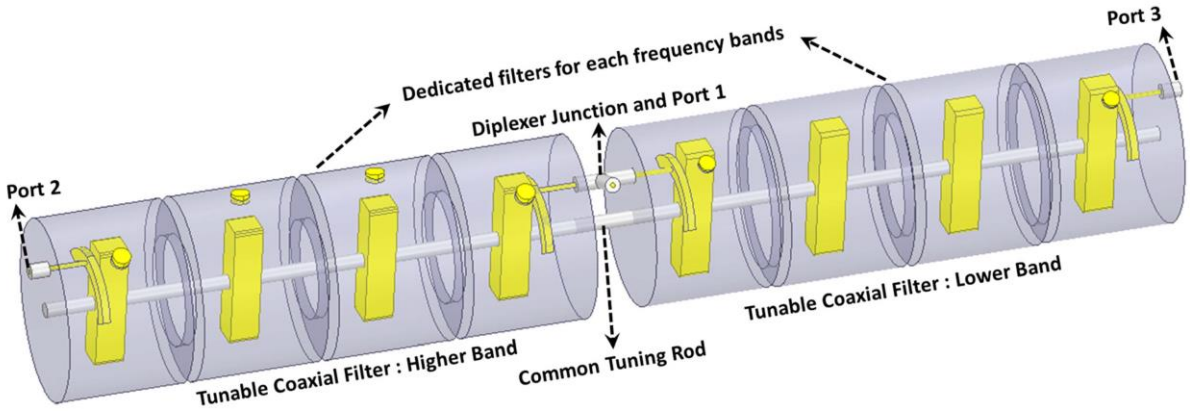

Fig. 5.15: 3-D model of a tunable diplexer using dedicated filters at each frequency band

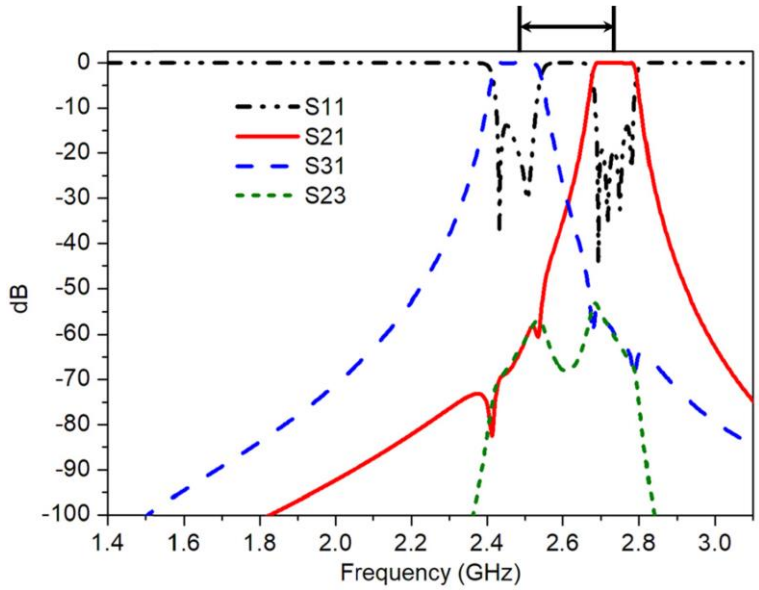

Fig. 5.16: Simulated results of the tunable diplexer: tuning rod is at 25 degrees.

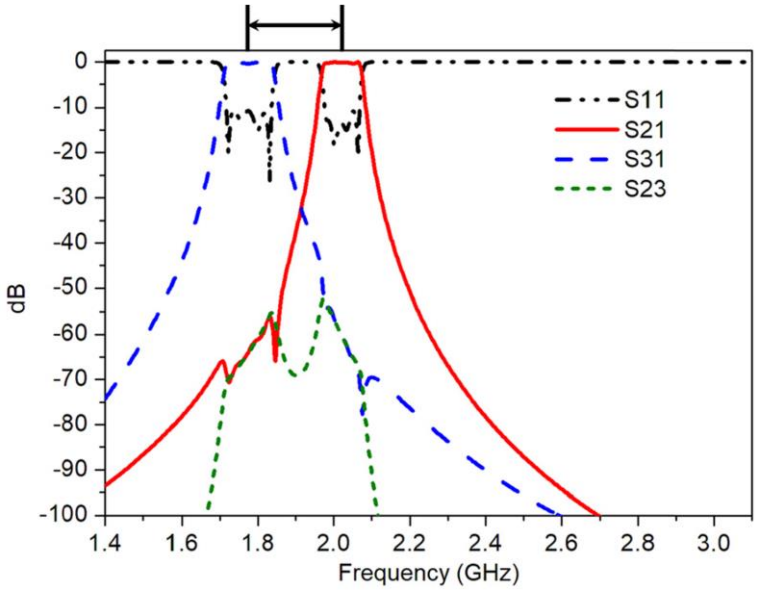

Fig. 5.17: Simulated results of the tunable diplexer: tuning rod is at 75 degrees.

5.3 Frequency Reconfigurable λ/4 Resonator Filter

This section describes a High-Q tunable coaxial filter which employs a single rotational mechanism to tune the filter, while using fixed λ/4 resonators. A prototype filter is designed for the proof of concept, which has a tuning range of 11.6% from 685 MHz to 770 MHz, over which bandwidth variation is within 10.5±0.7 MHz. Unlike the filter presented in section 5.1, the proposed tunable filter employs a fixed resonator posts (height = 75 mm, diameter = 22.5 mm) over which elliptic metallic tuning elements are rotated as shown in Fig. 5.18. As the tuning rod (made from dielectric material) is rotated, the air gap between resonator post and elliptic tuning element as well as air gap between elliptic tuning element and top plate get altered, which tunes the frequency response of the tunable filter as shown in Fig. 5.19. Fig. 5.20 depicts the variation of resonant frequency and unloaded Quality factor (Qu) of the proposed resonator as the elliptic metallic tuning element is rotated from 0 to 90 degrees. Aluminum is employed in the design.

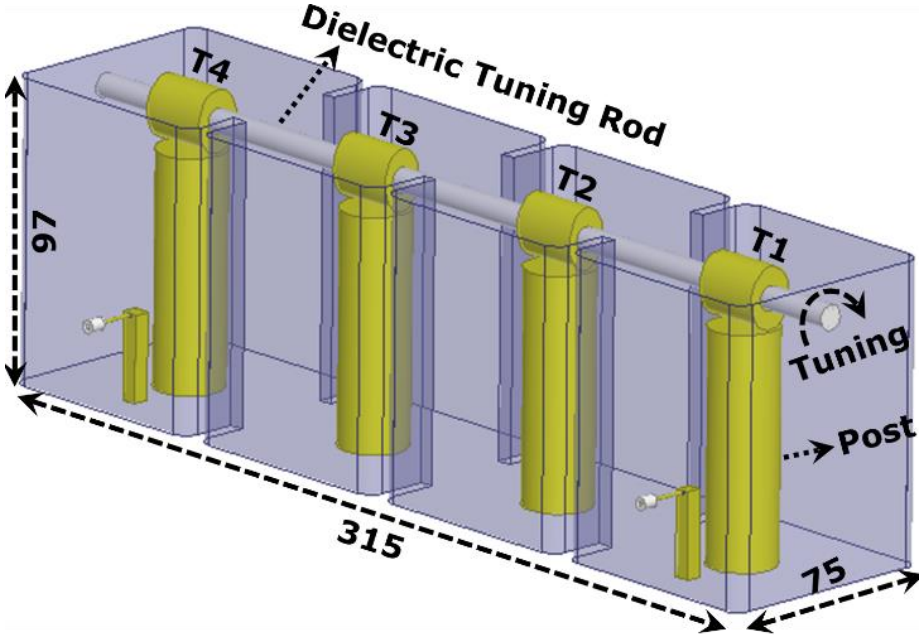

Fig. 5.18: Schematic: Proposed Coaxial Tunable Filter [post height = 75, post diameter = 22.5, iris thickness = 5, iris 12 = iris 34 = 36.9, iris 23 = 32.7, loop coupling (lc) height = 28, lc width = 5, lc position = 12.5, semi major axis (T1 and T4) = 10.05, semi minor axis (T1 and T4) = 7.91, semi major axis (T2 and T3) = 9.96, semi minor axis (T2 and T3) = 7, tuning rod diameter = 8, interface = SMA, all dimensions are in mm]

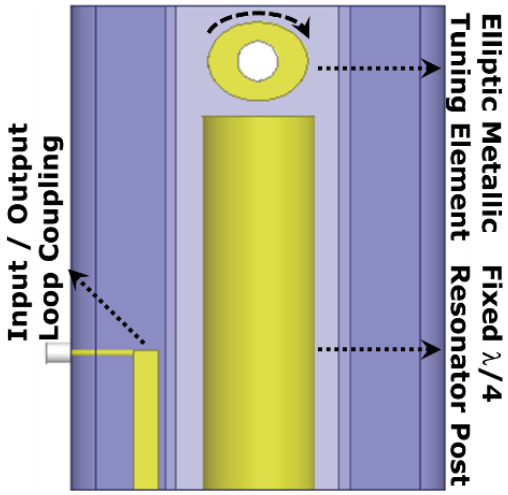

Fig. 5.19: Schematic: Front View of the Proposed Coaxial Tunable Filter [depicting the air gap between tuning element and resonator post, and the air gap between tuning element and top plate]

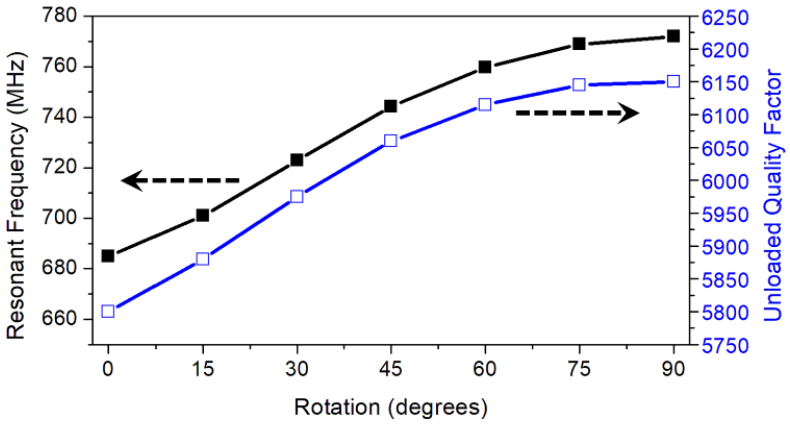

Fig. 5.20: Resonant Frequency and Unloaded Quality Factor

IR Coupling

A requirement on the IR coupling for realizing tunable filters with constant absolute bandwidth is that the product of physical coupling co-efficient (k_{ij}) and the resonant frequency (f_r) must be constant over the tuning range. In the proposed filter, vertical irises depicted in Fig. 5.15 are employed to realize the IR couplings between the resonators since they are relatively simple to fabricate. Thickness of the irises are 5 mm. The iris opening between resonators 1 and 2 (same as between resonators 3 and 4) is 36.9 mm. The iris opening between resonators 2 and 3 is 32.7 mm. Fig. 5.21 depicts the $k_{ij}f_r$ product for the IR couplings.

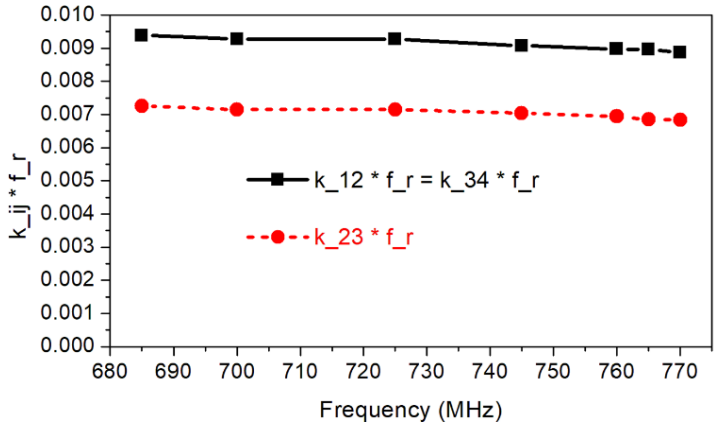

Fig. 5.21: Inter-Resonator Couplings over the Tuning Range

IO Coupling

A requirement on the IO coupling for realizing tunable filters with constant absolute bandwidth is that the reflection group delay (τ_{S11}) must be constant over the tuning range. In the proposed filter, loop coupling depicted in Fig. 5.19 is employed to realize the IO couplings. The center conductor of the

SMA connector touches the loop coupling post (which has a width of 5 mm and a height of 28 mm) at a distance of 12.5 mm. Fig. 5.22 depicts the reflection group delay (τ_{S11}) over the tuning range.

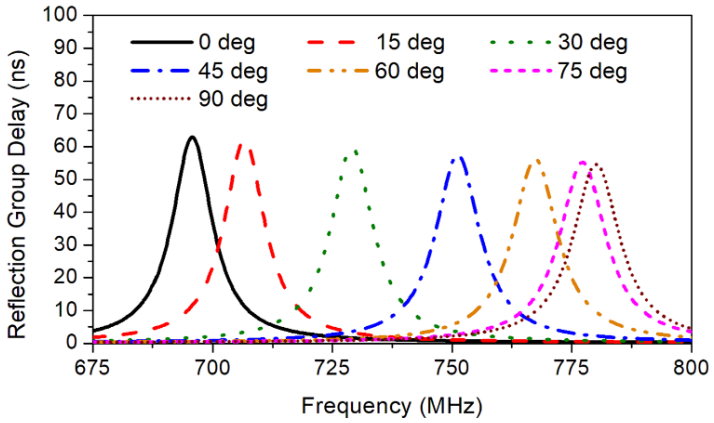

Fig. 5.22: Input-Output Couplings over the Tuning Range

The filter is tuned by a single rotating mechanism. By rotating the dielectric rod shown in Fig. 5.18, all the elliptic metallic tuning elements (T1, T2, T3 and T4) rotate thus altering the capacitive air gaps. This tunes the frequency response of the filter. The major axis and the minor axis of the elliptic metallic tuning elements are modified to absorb the resonator loading [42]. Fig. 5.23 and Fig. 5.24 depict the simulated transmission co-efficient (S_{21}) and the reflection co-efficient (S_{11}) of the proposed tunable filter, as the filter is tuned by rotating the dielectric rod, respectively. The tuning range of the filter is from 685 MHz to 770 MHz. Absolute bandwidth (S_{11} < -15 dB) and insertion loss over the tuning range is depicted in Fig.5.25. The bandwidth variation over the tuning range is within 10.5±0.7 MHz. Coupling matrix-based design methodology is adopted [2]. ANSYS HFSS is used for 3D Electro-Magnetic (EM) simulations [33].

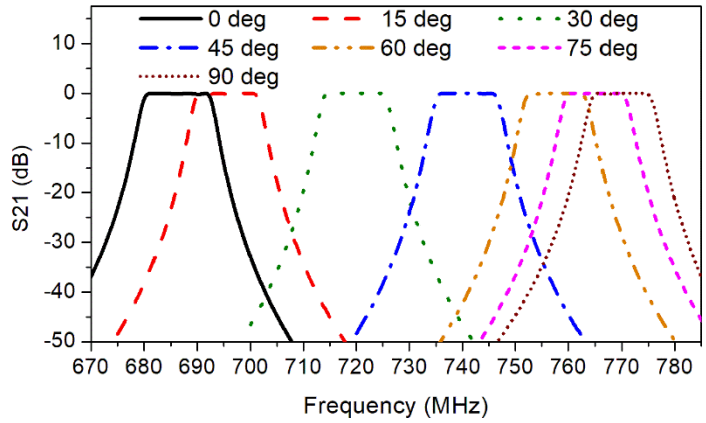

Fig. 5.23: Simulation: Transmission Co-efficient

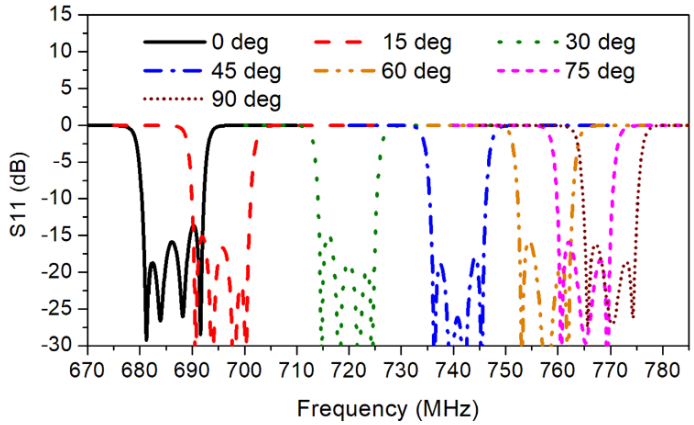

Fig. 5.24: Simulation: Reflection Co-efficient

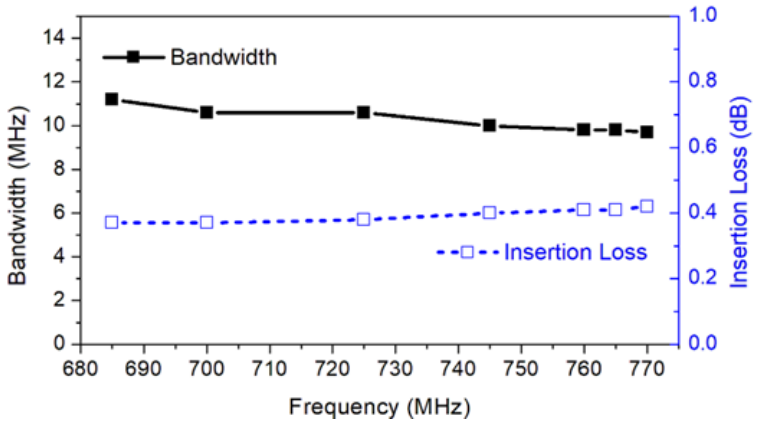

Fig. 5.25: Simulation: Bandwidth and Insertion Loss

Fig. 5.26 shows the photograph of the filter parts fabricated using aluminum and the assembled filter. M5 screws are used to assemble the filter parts. Fig. 5.27 and Fig. 5.28 depict the measured S_{21} and S_{11} of the prototype filter, respectively. The measured tuning range of the filter is 80 MHz from 680 MHz to 760 MHz. Fig. 5.29 plots the measured absolute bandwidth (S_{11} < -15 dB) over the tuning range, and the variation is within 11.2±1 MHz over the entire 80 MHz tuning range. Insertion loss variation is within 0.85±0.05 dB over the tuning range. Table 5.2 presents a comparison of the proposed tunable coaxial filter and other high-Q tunable coaxial filters which maintain a constant absolute BW over the tuning range.

Fig. 5.26: Fabrication - Photograph of the Tunable Filter

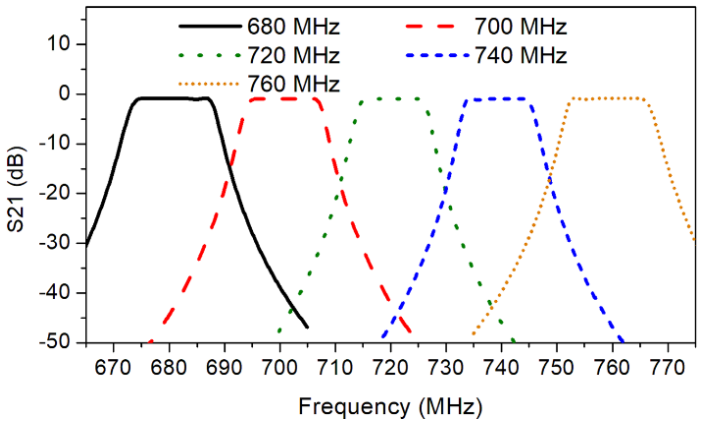

Fig. 5.27: Measurement - Transmission Co-efficient

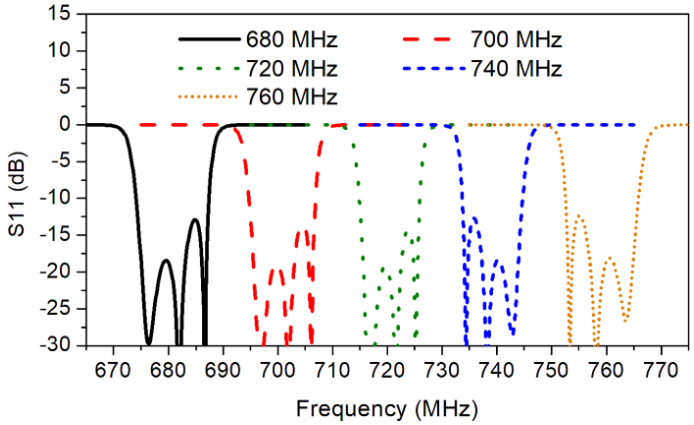

Fig. 5.28: Measurement - Reflection Co-efficient

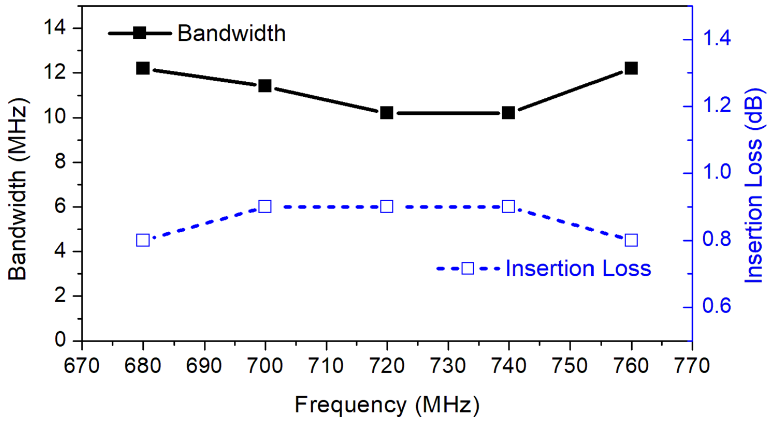

Fig. 5.29: Measurement - Bandwidth and Insertion Loss

Table 5.2: Comparison of High-Q Tunable Coaxial Filters

	Res.	Freq.	Tuning Range	Qu	BW and var.	Tun. Elem. and Mech
[12]	λ / 4	2.5 GHz	400 MHz (16 %)	> 2250	30 MHz < ±5 %	N / robust
[13]	λ / 4	3.6 GHz	430 MHz (12 %)	> 5650	75 MHz < ±5 %	N / robust
[25]	λ / 4	2 GHz	360 MHz (18 %)	> 2000	25 MHz NA	2N-1 / complex
[42]	λ / 2	2.5 GHz	500 MHz (20 %)	> 4850	100 MHz < ±10 %	1 / robust
This work	λ / 4	727.5 MHz	85 MHz (11.6 %)	> 5800	10.5 MHz < ±6.6 %	1 / robust

Res.: Resonator, Freq.: Frequency, var.: variation, Elem.: Element, λ: wavelength, N: order of the filter,

5.4 Conclusion

This chapter has presented two novel filter structures:

- A novel configuration for a high-Q tunable coaxial filter capable of maintaining a constant absolute BW over the tuning range. The proposed filter is tuned by a single tuning element. A prototype at 2.5 GHz is fabricated to verify the concept. The proposed filter is promising to be adopted in the frequency-agile communication architecture at the cellular base-station and aerospace applications, which require a high-Q tunable filter with minimum tuning elements. In addition to the tunable filter applications, the proposed design also promises to be useful in reducing the production cost and the delivery schedule of communication systems that usually use identical filters with the exception of the center frequency. The production cost can be significantly reduced by fabricating identical filter units ahead of time that can be easily reconfigured during the final production phase to fit the required frequency plan, thus offering a competitive delivery schedule. To our knowledge, this is the first coaxial type filter that can be tuned by a single tuning element with minimum variations in absolute BW and IL over the tuning range. The proposed concept is easily expandable to filters with a higher order. Furthermore, the proposed concept can be adopted to design a tunable diplexer, which can be tuned using a single tuning mechanism.
- A High-Q coaxial tunable filter, which employs a single rotational mechanism to tune the filter, while using fixed $\lambda/4$ resonators. The filter maintains a constant absolute BW over the tuning range. The proposed design offers the flexibility to adjust the major and minor axes of individual elliptic metallic tuning elements on a single rotary mechanism to properly absorb the resonator loading over the tuning range. A prototype 4th order filter is designed and realized for the proof of concept. The proposed design methodology can be scaled to realize higher order filters. Moreover, it can be used to design tunable diplexers, where the two channel filters can be tuned by the same single rotational mechanism.

Chapter 6
Conclusion and Future Work

6.1 Conclusion

The focus of the research had been on developing novel architectures for realizing High-Q tunable BPF using minimum number of tuning elements yet maintaining constant absolute bandwidth over the tuning range. Section 4.1 presented a novel configuration for a high-Q tunable waveguide (WG) filter with a constant absolute bandwidth (BW). The key feature of this filter is that it is tuned by a single tuning element. The theory of coupling behavior of single septum and double septa to achieve constant absolute BW is explored. The tuning mechanism of the proposed filter is explained with measurement results presented for a Ku-band tunable WG filter designed at 15 GHz with a 2% BW to achieve 15% tuning range. BW variation is observed to be within ±5% while the center frequency is tuned from 14.65 to 17.15 GHz. The filter promises to be useful in emerging 5G millimeter-wave applications, where the filter size is very small to accommodate many mechanical tuning elements. Furthermore, the proposed design methodology is scalable, i.e., the tuning mechanism is independent of the filter order. [44], [51].

Section 4.2 presented a novel configuration of a BW reconfigurable WG filter that uses only two tuning elements irrespective of the filter order. The proposed filter configuration demonstrates that it can achieve a relatively wide BW variations without deviating the center frequency. A 4 pole prototype filter is designed, fabricated and tested at Ku-band. The measured BW tunability of the filter is nearly 35 % from 225 to 320 MHz at 13.375 GHz. To our knowledge, this is the only BW reconfigurable filter that can be tuned with only two tuning elements regardless of the filter order [49].

Section 4.3 presented a frequency reconfigurable dual-mode WG filter with elliptic response. The proposed filter maintains a constant absolute BW and a constant rejection BW (i.e. constant frequency spacing between transmission zeros) over the tuning range. Furthermore, the filter can be tuned using a single tuning mechanism. A 4^{th} order prototype filter at 11.5 GHz with 50 MHz bandwidth and 2 symmetric transmission zeros (± 45 MHz) is fabricated and measured [46].

Section 5.1 demonstrated the feasibility of realizing a high-Q $\lambda/2$ resonator based tunable coaxial filter, which is tuned by a single rotational tuning element irrespective of the filter order. The proposed filter has low variations in the absolute BW and insertion loss (IL) over a relatively wide tuning range. A prototype four-pole filter is developed at 2.5 GHz with a fractional BW of 4% to verify the concept.

The measured tuning range of the filter is 20%, within which the BW variation is better than ±10% and IL variation is better than 0.05 dB. The proposed concept is easily expandable to filters with higher order. Furthermore, the concept is adopted to design a tunable diplexer which can be tuned using a single tuning mechanism. The proposed high-Q tunable filter is promising for use in the frequency-agile communication architecture at the cellular base-station and aerospace applications [45], [52].

Section 5.2 presented a novel configuration High-Q coaxial tunable filter which employs a single rotational mechanism to tune the filter, while using fixed λ/4 resonators. A prototype filter is designed for the proof of concept, which has a tuning range of 11.6% from 685 MHz to 770 MHz, over which bandwidth variation is within 10.5±0.7 MHz. In-addition, the proposed design methodology can be scaled to realize higher order filters. The proposed filter promises to be useful in a wide range of telecommunication applications including flexible payload in aerospace applications [47].

6.2 Future Work

Further research in the future is required in following aspects:

- Enhancing the tuning range of the frequency reconfigurable BPF to around 100 %, while maintaining constant absolute BW and using single tuning element, in both waveguide and coaxial guide technologies.
- Exploring the architecture to introduce transmission zeros in frequency reconfigurable coaxial BPF, while maintaining constant absolute BW and using single tuning element.
- Exploring the architectures to realize frequency reconfigurable Dielectric Resonator BPF, while maintaining constant absolute BW and using single tuning element.

Bibliography

[1] H. Arslan, *Cognitive Radio, Software Defined Radio, and Adaptive Wireless Systems*, Springer, 2007.

[2] R. J. Cameron, C. M. Kudsia, and R. R. Mansour, *Microwave Filters for Communication Systems: Fundamentals, Design and Applications*, Wiley, 2nd ed., 2018.

[3] R. D. Gaudenzi, “Challenges in Future Satellite Communications”, *IEEE Communication Theory Workshop*, May 15 2018.

[4] Flexible Payloads, *Airbus*, https://www.airbus.com

[5] Future Trends For The Space Market, *Thales*, March 2018, https://www.thalesgroup.com

[6] Robotic Refueling Mission, *NASA Satellite Servicing Projects Division*, https://sspd.gsfc.nasa.gov/rrm_tools.html

[7] Caleb Henry, “Why Intelsat’s going with life extension over refueling”, *Spacenews*, July, 2018, https://spacenews.com

[8] Electric propulsion satellites, *Airbus*, https://www.airbus.com

[9] R. R. Mansour, F. Huang, S. Fouladi, W. D. Yan and M. Nasr, "High-Q tunable filters: challenges and potential" in *IEEE Microw. Mag.*, vol. 15, no. 5, pp. 70-82, Aug. 2014.

[10] D. Peroulis, E. Naglich, M. Sinani and M. Hickle, "Tuned to Resonance" in *IEEE Microw. Mag.*, vol. 15, no. 5, pp. 55-69, July-Aug. 2014.

[11] Fengxi Huang, Siamak Fouladi Azarnaminy, Mitra Nasresfahani, and Raafat R. Mansour, “Three dimensional tunable filters with an absolute constant bandwidth and method”, *US 2016/0049710 A1*, 2016.

[12] S. Fouladi, F. Huang, W. D. Yan, and R. R. Mansour, "High-Q Narrowband Tunable Combline Bandpass Filters Using MEMS Capacitor Banks and Piezomotors," in *IEEE Trans. Microw. Theory Techn.*, vol. 61, no. 1, pp. 393-402, Jan. 2013.

[13] M. A. Iskander, N. Mitra , and R. R. Mansour, "A constant-Q tunable combline bandpass filter using angular tuning technique," *44th European Microw. Conf.*, Rome, 2014.

[14] C. Arnold, J. Parlebas and T. Zwick, "Reconfigurable Waveguide Filter with Variable Bandwidth and Center Frequency," in *IEEE Trans. Microw. Theory Techn.*, vol. 62, no. 8, pp. 1663-1670, Aug. 2014

[15] S. Nam, B. Lee, C. Kwak, and J. Lee, "A New Class of K-Band High-Q Frequency-Tunable Circular Cavity Filter," in *IEEE Trans. Microw. Theory Techn.*, vol. 66, no. 3, pp. 1228-1237, March 2018

[16] S. Nam, B. Lee, C. Kwak and J. Lee, "Contactless Tuning Plunger and its Application to K-Band Frequency-Tunable Cavity Filter," in *IEEE Trans. Microw. Theory Techn.*, vol. 67, no. 7, pp. 2713-2719, July 2019

[17] W. D. Yan and R. R. Mansour, "Tunable Dielectric Resonator Bandpass Filter With Embedded MEMS Tuning Elements," in *IEEE Trans. Microw. Theory Techn.*, vol. 55, no. 1, pp. 154-160, Jan. 2007

[18] F. Huang, S. Fouladi and R. R. Mansour, "High-Q Tunable Dielectric Resonator Filters Using MEMS Technology," in *IEEE Trans. Microw. Theory Techn.*, vol. 59, no. 12, pp. 3401-3409, Dec. 2011

[19] Xiaoguang Liu, L. P. B. Katehi, W. J. Chappell and D. Peroulis, "A 3.4 – 6.2 GHz Continuously tunable electrostatic MEMS resonator with quality factor of 460–530," *IEEE MTT-S Int. Microw. Symp. Dig.*, Boston, MA, 2009, pp. 1149-1152.

[20] S. J. Park, I. Reines, C. Patel and G. M. Rebeiz, "High-Q RF-MEMS 4–6-GHz Tunable Evanescent-Mode Cavity Filter," in *IEEE Trans. Microw. Theory Techn.*, vol. 58, no. 2, pp. 381-389, Feb. 2010

[21] L. Pelliccia, F. Cacciamani, P. Farinelli and R. Sorrentino, "High-Q Tunable Waveguide Filters Using Ohmic RF MEMS Switches," *IEEE Trans. Microw. Theory Techn.*, vol. 63, no. 10, Oct. 2015

[22] M. A. Kunes and G. G. Connor, "A Digitally Controlled Tunable High Power Output Filter For Space Applications," *19th European Microw. Conf., London*, UK, 1989

[23] A. Périgaud et al., "Continuously Tuned Ku-Band Cavity Filter Based on Dielectric Perturbers Made by Ceramic Additive Manufacturing for Space Applications," in *Proceedings of the IEEE*, vol. 105, no. 4, pp. 677-687, April 2017

[24] P. Aurélien, V. Serge, D. Nicolas, B. Stéphane, T. Olivier, and L. Carpentier, "Continuously Tunable X-Band Filter Using a 3D Spiral Ribbon," *IEEE MTT-S Int. Conf. on Numerical Electromagnetic and Multiphysics Modeling and Optimization (NEMO)*, Reykjavik, 2018

[25] M. Hoeft, A. Kronberger, and O. Bartz, "Tunable Bandpass Filters for Multi-Standard Applications," *German Microw. Conf.*, Hamburg, Germany, 2008

[26] Jia Sheng Hong, *Microstrip Filters for RF/Microwave Applications*, 2nd ed., John Wiley and Sons, Inc., New Jersey, 2011.

[27] G. Matthaei, L. Young, and E. M. T. Jones, *Microwave Filters, Impedance Matching Networks and Coupling Structures*, Norwood, MA, USA, Artech House 1980.

[28] A. Atia, A. Williams and R. Newcomb, "Narrow-band multiple-coupled cavity synthesis," in *IEEE Transactions on Circuits and Systems*, vol. 21, no. 5, pp. 649-655, September 1974.

[29] J. B. Ness, "A unified approach to the design, measurement, and tuning of coupled-resonator filters," in *IEEE Transactions on Microwave Theory and Techniques*, vol. 46, no. 4, pp. 343-351, April 1998.

[30] H. Jia and R. R. Mansour, "An Efficient Technique for Tuning and Design of Wideband Filters," 2018 *IEEE/MTT-S International Microwave Symposium - IMS*, Philadelphia, PA, 2018.

[31] C. A. Balanis, *Advanced Engineering Electromagnetics*, 2nd ed. Hoboken, NJ, USA, Wiley 2012.

[32] J. W. Bandler, R. M. Biernacki, S. H. Chen, P. A. Grobelny, R. H. Hemmers, "Space mapping technique for electromagnetic optimization", *Transactions on Microwave Theory and Techniques*, vol. 42, pp. 2536-2544, Dec. 1994.

[33] ANSYS HFSS, http://www.ansys.com/products/electronics/ansys-hfss

[34] N. Zahirovic, S. Fouladi, R. R. Mansour and M. Yu, "Tunable suspended substrate stripline filters with constant bandwidth," *2011 IEEE MTT-S International Microwave Symposium*, Baltimore, MD, 2011.

[35] R. R. Mansour and A. Zybura, "Superconducting millimeter-wave E-plane filters," in *IEEE Transactions on Microwave Theory and Techniques*, vol. 39, no. 9, pp. 1488-1492, Sep 1991.

[36] U. Rosenberg et al., "Novel remote controlled dual mode filter providing flexible re-allocation of center frequency and bandwidth," *IEEE MTT-S Int. Microw. Symp. Dig.*, San Francisco, CA, 2016.

[37] B. Gowrish and R. R. Mansour, "Design Methodology of a Tunable Waveguide Filter With a Constant Absolute Bandwidth Using a Single Tuning Element," in *IEEE Trans. Microw. Theory Techn.*, vol. 66, no. 12, pp. 5632-5639, Dec. 2018.

[38] Massimo Banzi and Michael Shiloh, Getting Started with Arduino, Maker Media, Inc, 3rd ed., 2014.

[39] Data sheet, A4988: DMOS Microstepping Driver, Allegro Microsystem.

[40] Processing software, https://processing.org

[41] Hui-Wen Yao, K. A. Zaki, A. E. Atia, and T. Dolan, "Improvement of spurious performance of combline filters," *1997 IEEE MTT-S International Microwave Symposium*, Denver, CO, USA, 1997.

[42] G. Basavarajappa and R. R. Mansour, "Design Methodology of a High- Q Tunable Coaxial Filter and Diplexer," in *IEEE Transactions on Microwave Theory and Techniques*, vol. 67, no. 12, pp. 5005-5015, Dec. 2019.

[43] Y. Yu *et al.*, "Radio Frequency Magnet-Free Circulators Based on Spatiotemporal Modulation of Surface Acoustic Wave Filters," in *IEEE Transactions on Microwave Theory and Techniques*, vol. 67, no. 12, pp. 4773-4782, Dec. 2019.

[44] Gowrish B. and R. R. Mansour, "A Tunable Waveguide Filter Designed with a Constantan Absolute Bandwidth Using a Single Tuning Element," 2018 IEEE/MTT-S International Microwave Symposium - IMS, Philadelphia, PA, 2018.

[45] Gowrish B. and R. R. Mansour, "A Tunable Coaxial Filter with Minimum Variations in Absolute Bandwidth and Q Using a Single Tuning Element," 2019 IEEE MTT-S International Microwave Symposium (IMS), Boston, MA, USA, 2019.

[46] Gowrish B. and R. R. Mansour, " A Dual-Mode Frequency Reconfigurable Waveguide Filter with a Constant Frequency Spacing between Transmission Zeros," 2020 IEEE MTT-S International Microwave Symposium (IMS), Los Angeles, CA, USA, 2020.

[47] Gowrish B. and R. R. Mansour, " A Tunable Quarter-wavelength Coaxial Filter With Constant Absolute Bandwidth Using a Single Tuning Element," under review, IMS 2021.

[48] Gowrish B. and R. R. Mansour, "A High-Q Quadruple-Mode Rectangular Waveguide Resonator," in IEEE Microwave and Wireless Components Letters, vol. 29, no. 5, pp. 324-326, May 2019.

[49] Gowrish B. and R. R. Mansour, "A Novel Bandwidth Reconfigurable Waveguide Filter for Aerospace Applications," in IEEE Microwave and Wireless Components Letters, vol. 30, no. 6, pp. 577-580, June 2020.

[50] Gowrish B., Shiban K. Koul and R. R. Mansour, " Transversal Coupled Triple Mode Spherical Resonator-based Band Pass Filters," under review, IEEE Microwave and Wireless Components Letters.

[51] Gowrish B. and R. R. Mansour, "Design Methodology of a Tunable Waveguide Filter With a Constant Absolute Bandwidth Using a Single Tuning Element," in IEEE Transactions on Microwave Theory and Techniques, vol. 66, no. 12, pp. 5632-5639, Dec. 2018.

[52] Gowrish B. and R. R. Mansour, "Design Methodology of a High- Q Tunable Coaxial Filter and Diplexer," in IEEE Transactions on Microwave Theory and Techniques, vol. 67, no. 12, pp. 5005-5015, Dec. 2019.

[53] Gowrish B. and R. R. Mansour, " An Efficient EM-Based Synthesis Technique for Single-Band and Dual-Band Waveguide Filters," under review, IEEE Transactions on Microwave Theory and Techniques.

[54] Gowrish B. and R. R. Mansour, "Design Methodology of a Tunable Waveguide Filter With a Constant Absolute Bandwidth Using a Single Tuning Element," in IEEE Transactions on Microwave Theory and Techniques, vol. 66, no. 12, pp. 5632-5639, Dec. 2018.

[55] Gowrish B. and R. R. Mansour, "Design Methodology of a High- Q Tunable Coaxial Filter and Diplexer," in IEEE Transactions on Microwave Theory and Techniques, vol. 67, no. 12, pp. 5005-5015, Dec. 2019.

[56] Gowrish B. and R. R. Mansour, " An Efficient EM-Based Synthesis Technique for Single-Band and Dual-Band Waveguide Filters," under review, IEEE Transactions on Microwave Theory and Techniques.

Appendix A
Publications

Conferences

1. Gowrish B. and R. R. Mansour, "A Tunable Waveguide Filter Designed with a Constantan Absolute Bandwidth Using a Single Tuning Element," 2018 IEEE/MTT-S International Microwave Symposium (IMS), Philadelphia, PA, 2018.
2. Gowrish B. and R. R. Mansour, "A Tunable Coaxial Filter with Minimum Variations in Absolute Bandwidth and Q Using a Single Tuning Element," 2019 IEEE MTT-S International Microwave Symposium (IMS), Boston, MA, USA, 2019.
3. Gowrish B. and R. R. Mansour, " A Dual-Mode Frequency Reconfigurable Waveguide Filter with a Constant Frequency Spacing between Transmission Zeros," 2020 IEEE MTT-S International Microwave Symposium (IMS), Los Angeles, CA, USA, 2020.
4. Gowrish B. and R. R. Mansour, " A Tunable Quarter-wavelength Coaxial Filter With Constant Absolute Bandwidth Using a Single Tuning Element," 2021 IEEE MTT-S International Microwave Symposium (IMS), Atlanta, GA, USA, 2021.

Short Papers / Letters

1. Gowrish B. and R. R. Mansour, "A High-Q Quadruple-Mode Rectangular Waveguide Resonator," in IEEE Microwave and Wireless Components Letters, vol. 29, no. 5, pp. 324-326, May 2019.
2. Gowrish B. and R. R. Mansour, "A Novel Bandwidth Reconfigurable Waveguide Filter for Aerospace Applications," in IEEE Microwave and Wireless Components Letters, vol. 30, no. 6, pp. 577-580, June 2020.
3. Gowrish B., Shiban K. Koul and R. R. Mansour, " Transversal Coupled Triple Mode Spherical Resonator-based Band Pass Filters," early access, IEEE Microwave and Wireless Components Letters.
4. Gowrish B. and R. R. Mansour, " A Tunable Quarter-wavelength Coaxial Filter With Constant Absolute Bandwidth Using a Single Tuning Element," early access, IEEE Microwave and Wireless Components Letters.

Journals / Transactions

1. Gowrish B. and R. R. Mansour, "Design Methodology of a Tunable Waveguide Filter With a Constant Absolute Bandwidth Using a Single Tuning Element," in IEEE Transactions on Microwave Theory and Techniques, vol. 66, no. 12, pp. 5632-5639, Dec. 2018.
2. Gowrish B. and R. R. Mansour, "Design Methodology of a High- Q Tunable Coaxial Filter and Diplexer," in IEEE Transactions on Microwave Theory and Techniques, vol. 67, no. 12, pp. 5005-5015, Dec. 2019.

Patent Applications

1. Tunable Bandpass Filter With Constant Absolute Bandwidth Using Single Tuning Element, Gowrish B. and Raafat R. Mansour, Patent application: US 16/228,587; Dec 21, 2017.
2. Tunable Filter With Minimum Variations In Absolute Bandwidth And Insertion Loss Using A Single Tuning Element, Gowrish B. and Raafat R. Mansour, Patent application: US 16/713,198; Dec 21, 2018.
3. A Quarter Wavelength Tunable Coaxial Filter With Minimum Variations in Absolute Bandwidth and Insertion Loss Using a Single Tuning Element, Gowrish B. and Raafat R. Mansour, Patent application: US 63141480; Jan 26, 2021.